XNICE: A SYSTEM FOR ASSESSING NETWORK IDENTIFICATION PERFORMANCE

T. G. Barker

S-CUBED
Division of Maxwell Laboratories, Inc.
P.O. Box 1620
La Jolla, CA 92038-1620

May 1996

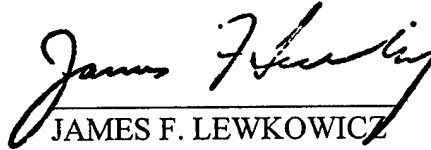*19970303 062*

Final Report
19 August 1993-1 May 1996

SPONSORED BY
Advanced Research Projects Agency (DoD)
Nuclear Monitoring Research Office
ARPA ORDER No. 0325

MONITORED BY
Phillips Laboratory
CONTRACT No. F19628-93-C-0177

The views and conclusions contained in this document are those of the authors and should not be interpreted as representing the official policies, either express or implied, of the Air Force or U.S. Government.

This technical report has been reviewed and is approved for publication.

DELAINE R. REITER
Contract Manager
Earth Sciences Division

JAMES F. LEWKOWICZ
Director
Earth Sciences Division

1. AGENCY USE ONLY *(Leave blank)*	2. REPORT DATE May 1996	3. REPORT TYPE AND DATES COVERED Final (19 Aug 1993–1 May 1996)

4. TITLE AND SUBTITLE	5. FUNDING NUMBERS
Xnice: A System for Assessing Network Identification Performance	Contract No: F19628-93-C-0177 PE 62301E PR NM 93 GA GM WU AN
6. AUTHOR(S) T. G. Barker	

7. PERFORMING ORGANIZATION NAME(S) AND ADDRESS(ES)	8. PERFORMING ORGANIZATION REPORT NUMBER
S-CUBED, A Division of Maxwell Laboratories, Inc. P.O. Box 1620 La Jolla, CA 92038-1620	SSS-FR-95-15215

9. SPONSORING/MONITORING AGENCY NAME(S) AND ADDRESS(ES)	10. SPONSORING/MONITORING AGENCY REPORT NUMBER
Phillips Laboratory 29 Randolph Road Hanscom AFB, MA 01731-3010 Contract Manager: James Lewkowicz/GPE	PL-TR-96-2087

11. SUPPLEMENTARY NOTES

12a. DISTRIBUTION/AVAILABILITY STATEMENT	12b. DISTRIBUTION CODE
Approved for public release; distribution unlimited	

13. ABSTRACT *(Maximum 200 words)*

This report describes a computer system for evaluating the ability of a network to detect and identify seismic sources. The program, called Xnice, for Network Identification Capability Evaluation running under an X-windows interface, has a complete graphics interface for setting the parameters of simulations and evaluating the results. The performance of both regional and teleseismic discriminants can be easily examined. We describe here the use of the program, including a manual, as well as several applications.

14. SUBJECT TERMS		15. NUMBER OF PAGES
Seismic Seismic Networks Discrimination Comprehensive Test Ban Treaty Nuclear Explosion		138
		16. PRICE CODE

17. SECURITY CLASSIFICATION OF REPORT	18. SECURITY CLASSIFICATION OF THIS PAGE	19. SECURITY CLASSIFICATION OF ABSTRACT	20. LIMITATION OF ABSTRACT
Unclassifed	Unclassifed	Unclassifed	SAR

Table of Contents

List of Illustrations

List of Illustrations (Continued)

List of Illustrations (Continued)

List of Tables

1. Introduction

An essential part of monitoring a comprehensive test ban treaty is the evaluation of the performance of the monitoring network. Previous programs have focused on the ability of networks to detect seismic sources but have not been able to evaluate the identification performance of the network. The computer program Xnice, for <u>N</u>etwork <u>I</u>dentification <u>C</u>apability <u>E</u>valuation running under an <u>X</u>-windows interface, has been for this purpose. The program simulates the detection, location and identification of populations of events recorded on regional and teleseismic networks using a Monte Carlo approach. This approach allows one to isolate the effects of source type, propagation path, and choice of discriminants on the discrimination process. In addition, discriminant performance and network thresholds of detection, location and identification are assessed.

Xnice generates the parameters of a sequence of events and computes the ground motions from the events at the stations of the network. The features of the ground motions used for discrimination are then measured, and discrimination scores are assigned to each event. From a suite of events, the performance of the network and the discriminants can be assessed. The program has the capability to compute signals from earthquakes, quarry blasts and both overburied and normally buried explosions.

Development of Xnice began with the program Nice described in Barker and Rodi (1986). Although the core routines for telesesmic analysis remain in Xnice, the current programs are far more capable and user-friendly. Among the enhancments to Xnice are the following:

1. A theoretical and practical means for modeling regional ground motions that include, in a simple way with few parmeters, the effects of source type, source emplacement materials, source depth, and of propagation on all regional phases.

2. A means for modeling regional identification performance, including the Lg spectral slope, Pn and Pg spectral slopes, Lg/P ratio, and Mo:ML, and a means for forming scores of identification performance.

3. A means for interactively calibrating a network and source/propagation parameters used in a netowrk simulation.

1

4. Establishment of a database of station (noise, down time, etc.) and propagation parameters that have formats compatible with the detection program NetSim.

5. Development of an extensive set of interactive methods for setting up simulations and for examining the results as 2D plots or contour map plots.

6. The incorporation of a modular design that easily allows inclusion of additional source types, seismic phases and non-seismic signals (infrasonic and hydroacoustic).We give an overview of the program in the main body of the report, referring the reader to appendices in which details of computational methods and program usage are included as Unix-style "man" pages for programs and files. Following the overview, we describe simulations in three geographic areas: (1) California-Nevada, (2) central Europe and (3) the Middle East.

In the study of the California-Nevada region, we simulate earthquakes and explosions used in Woods, *et al.* (1993) in their investigations of the efficacy of the M_L:M_0 discriminant in that region. Using propagation and source excitation parameters used by Barker, *et al.* (1994) for the western U.S., the simulations show that this discriminant is effective, as did Woods, *et al.* Central Europe was chosen for study because there are numerous investigations into the propagation properties of regional phases there. We investigate the Lg/P ratio, Lg spectral ratio, M_L:M_0 and depth by travel times discriminants. In the simulations, the Lg/P discriminant is effective, consistent with observations by Bennett, *et al.* (1992) and Wuster (1993). Lg spectral slope appears less effective. Investigation of populations of M_L:M_0 for the different source types indicate that this would be a good discriminant, but this is difficult to quantify without good long-period noise estimates (which are currently unavailable). Using preliminary estimates of parameters for the Middle East, we simulated events there and find the Lg/P discriminant to be less effective than in central Europe, due both to earth structure and earthquake stress drop differences between the two regions.

2

2. Description of Xnice

2.1 Introduction

Xnice is comprised of four modules. The user communicates with the modules through the X interface, which also coordinates the modules. A flow chart of the program is shown in Figure 1. The modular design allows one to examine independently the effects of the seismic source, the wave propagation, the seismic network operation (location and detection) and discrimination rules on identification of events. The parameters of each module can be verified by direct comparison with observations.

Xnice plots allows the user to examine a realization of the seismic events and details of the discrimination results. In addition, a link to the plotter package GMT provides map drawings. The appendices of this report describe the methods, files and programs in detail. Further details on regional propagation modeling can be found in Barker, *et al.* (1994).

2.2 Events Module

The **events** module computes the source properties of a sequence of events which are realizations of probability distributions derived from observations of the source region. The distributions of earthquakes describe the epicenter, depth, moment, focal plane orientation and recurrence interval of the events. The program computes source parameters for earthquakes, overburied and normally buried explosions and quarry blasts. The parameters are chosen to be consistent with standard testing and quarrying practices (see Barker, *et al.*, 1994). Nuclear explosions are specified by their yield, and in the case of overburied explosions, also by their depth of burial (a standard value of scaled depth of burial is assumed for normally buried explosions). Quarry blasts are specified by their total yield. The results of the **events** module are written to a catalogue of events. Seismicity (natural and artificial) levels, depth and epicenter distributions are specified by files, which the user chooses with the X interface. The results of the **events** run can be viewed with a plotting module, which plots cumulative and incremental seismicity, event locations, depths and source sizes. The program can be run in two modes of operation: (1) a sequence of events with the random distributions discussed

3

XNICE

X windows users's interface

```
events  →  synwave  →  analyst  →  examine  →  GeoSys
```

events → synwave: Source parameters

synwave → analyst: Waveforms, arrivals

analyst → examine: Network bulletin

examine: Interactive graphics

GeoSys: Maps

events:

Earthquakes:

Recurrence rates, epicentral, depth and focal mechanism distributions.

Artificial Seismicity:

Location, depth, yield distributions

synwave:

Local propagation
Regional Propagation
Teleseismic propagation
Instrument responses
Noise levels
Station locations

analyst:

Station locations
Detection rules
Location rules
Focal mechanism rules

Figure 1.

4

above, or (2) a fixed event occurring on a uniform grid of latitude and longitude. The second mode is used to generate contour maps of network detection and identification performance. The events bulletin can also be examined in lists of the bulletin which appear on the screen on demand ("pop-ups").

2.3   Synwav Module

The **synwav** module is a synthetic seismogram package. It reads the events catalogue generated by the **events** module and station locations and detection level parameters from a station file and computes synthetic teleseismic body wave (P, pP and S phases) and fundamental-mode surface wave seismograms for the network, and amplitudes of regional phases (Pn, Pg, Sn, Sg, Lg) at a set of prescribed frequencies. Discrimination methods use measurements of peak amplitude, spectral amplitude, period and travel time, which the program models by incorporating the most important physical effects. The signals depend upon the source spectrum (which depends on the moment), instrument response, source depth, anelastic attenuation, and, for surface waves, dispersion. The amplitude depends upon on source strength, radiation pattern, geometric spreading and anelastic attenuation. The signals are measured for amplitude, period and travel time after which random noise is added to the measurements. Signals which do not meet a specified signal-to-noise ratio are classified as non-detections. An arrival bulletin is then written to a file. The parameters of wave propagation can be regionalized and verified by comparison with observations. The user specifies the bulletin names and propagation files through the X interface. The arrival bulletins can be examined in pop-up lists.

2.4.   Analyst Module

The **analyst** module reads the arrival bulletin made by the synwav module and does calculations based upon network analysis. The calculations include assignment of discrimination scores, network averaged m_b, M_s and regional magnitudes, such as $m_b(Lg)$. The analyst module computes the scores for these teleseismic discriminants: epicentral location, depth by pP, depth by travel times and ratio of m_b to M_s. We have now included regional

discriminants based on spectral amplitudes and slopes used in discriminants such as the ratio of high to low frequency Lg. The program uses teleseismic rules similar to those of AFTAC for censoring bad data (rejection of signals based on signal-to-noise ratios and number of quadrants reporting) and for assigning discrimination scores, which indicate the degree of confidence to which the event can be considered an earthquake. The results of the calculations by the **analyst** module are written to a discrimination bulletin file.

2.5. Examine Module

The **examine** module makes lists and plots which allow the user to examine interactively the discrimination bulletin and the identification performance of the network. An X interface allows the user to view not only the overall performance, but also features of the process which contributed to the performance. For example, one may determine the identification rate as a function of m_b. In addition, discrimination bulletins can be compared with this module. Thus, the results of a Monte Carlo simulation can be compared with a bulletin derived directly from observations so that the program can be calibrated for a particular seismic area and network. An extensive menu of plots and lists are available to the user through the X interface.

2.6. Evswan Module

The **evswan** combines the **events, synwav** and **analyst** modules into one module. This combination eliminates considerable overhead and duplication and greatly reduces input/output operations. It thus requires much less computer time than running the three modules separately.

3. Simulations

In this section, we describe simulations for three areas: the western U.S., central Europe and the Middle East. In addition, we have compared the detection thresholds of earthquakes for $m_b(Lg)$ and M_s with those from simulations we have done with program NetSim. Due to differences in the way regional phases and surface waves are modeled in the programs, the results are not precisely the same, but are close enough to conclude that they are giving the same answers. We examine the detection thresholds for the three areas and show results that Xnice gives that cannot be obtained by NetSim. These results include the effects of source type and depth on detection and the identification performance of the recording networks.

3.1 Simulation of $M_L : M_0$ for Earthquakes and Explosions

Woods, *et al.* (1993) have compiled local magnitudes (M_L) and moments (M_0) for earthquakes in southern California and Nevada and nuclear explosions at NTS. Their data, which came from a variety of studies, show that the ratio $M_L : \log(M_0)$ is an effective discriminant for events spanning a wide range of magnitudes (from 2 to above 6), as can be seen on Figure 2. This figure was made by us from data transmitted to us by B. Woods. The two straight lines in the figure are linear fits to the earthquake and explosion populations. The lines have the formulas:

$$M_L = -6 + \frac{2}{3}\log(M_0) \text{ for earthquakes and} \tag{1}$$

$$M_L = -5.2 + \frac{2}{3}\log(M_0) \text{ for explosions.} \tag{2}$$

As a check on the modeling capabilities of Xnice, we gathered the pertinent data for the region and made simulations for the network in the study by Woods, *et al.* (1993). The network is listed in Table 1:

Earthquake and Explosion ML vs Moment
Woods, Kedar, and Helmberger (1993)
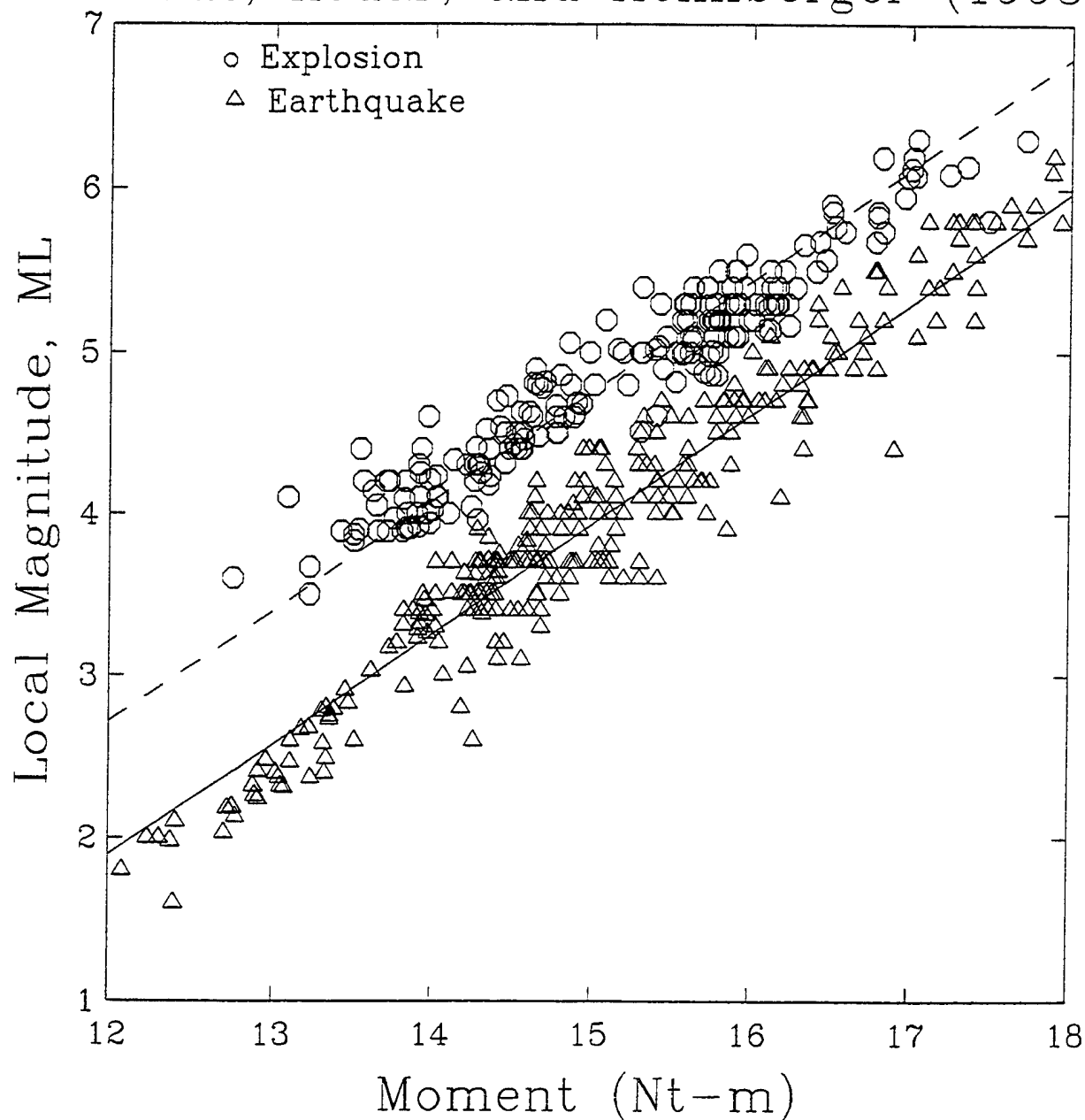
Figure 2.   Values of M_L versus $\log(M_0)$ for earthquakes and explosions in the southwestern U.S., from Woods, *et al.* (1993. The straight lines are from linear regressions of the data.

Table 1
Station Locations

Station	Latitude	Longitude
BKS	36.50	-122.30
STAN	36.31	-122.21
SBC	34.72	-119.76
ISA	35.66	-118.47
PAS	34.56	-118.22
GOL	39.70	-105.37
SVD	34.54	-117.13
PFCA	33.61	-116.46

The majority of earthquakes in the study were the main shock and aftershocks of the M_L = 4.9 event in Pasadena (12/3/88), the M_L = 4.6 event at Joshua Tree (4/23/92) and aftershocks of the M_L = 7.1 Landers earthquake (6/28/92). In addition, events at Lee Vining (m_b = 5.0, 10/24/90) and Little Skull Mountain (m_b = 5.7, 6/29/92) were part of the data set. In the simulation, a set of earthquakes in the vicinity of each of these five events were included. Values of $\log(M_0)$ were uniformly distributed between 13 and 18 N-m. In addition, we included both overburied (dob = 500m) and normally buried events with yields ranging from 0.01 to 1000 KT located on NTS. We used the regional propagation path properties derived for the western U.S. by Barker, *et al.* (1994). The results of the simulation are shown in Figure 3, on which M_L is plotted versus $\log(M_0)$ The events of the three source types are indicated by symbols on the figure and dashed lines show the linear fits to the data (equations 1 and 2, above). We see that the simulations follow the data well, and that in particular the population of earthquakes separate from the explosions. The data trends, scatter and absolute value follow the data. An exception is that the values of M_L are smaller for the earthquake simulations than for the data for large events. The slope of magnitudes versus moment curve decreases for larger moments for the simulated earthquakes primarily because the source corner frequency shifts to below the M_L bandwidth (around 1 Hz). The 'saturation" of M_L with moment has been widely observed, and it is not clear why it is not observed for this data compilation.

woods
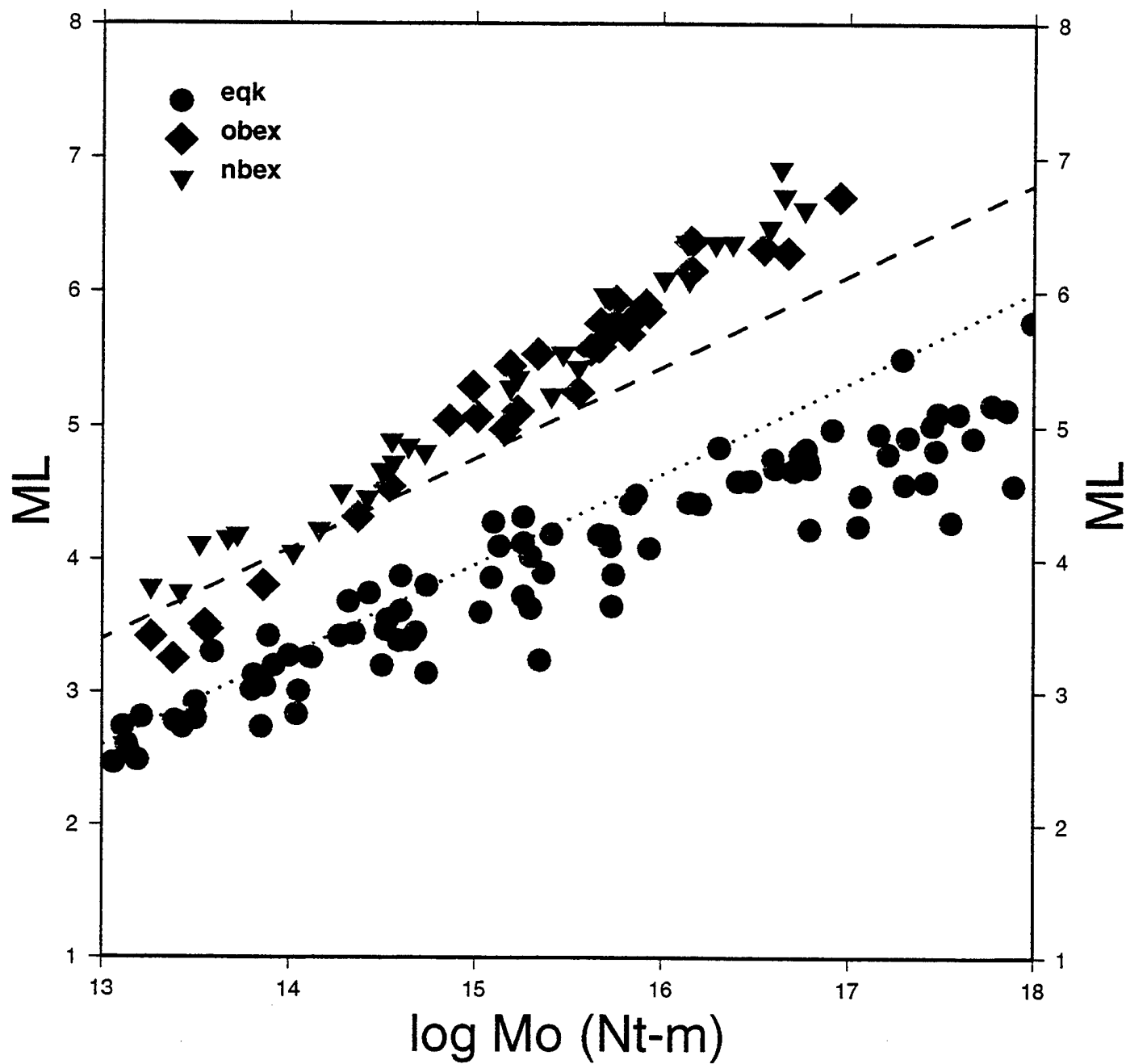
Figure 3. Values of M_L versus $\log(M_0)$ from an Xnice simulation of earthquakes and explosions in the southwestern U.S. The dashed lines are from linear regressions of the data in Woods, *et al.* (1993) (Figure 2).

3.2. Simulations for Central Europe

The purpose of the calculations described in this section is to exercise Xnice in Europe where there are regional propagation data and discrimination results. We have synthesized the results of the following studies: Bouchon, et al. (1990), Isrealsson and Carter (1991), Schulte-Pelkum (1993), Shih, et al. (1994), Zielhaus and Nolet (1994), Kramme, et al. (1995) and Campillo, et al. (1985). The regional propagation parameters are in the following table (see file descriptions for regional parameters in Appendix C for the meaning of the symbols):

Table 2
Regional Propagation and Exicitation Parameters for Central Europe

Phase	Q_0	η	n	S	c_0^{exp}	c_1^{exp}	c_0^{vf}	c_1^{vf}
Lg	500.	0.45	0.833	-20.5	-0.4	-1.1	2.6	-1.1
Pg	750.	0.68	0.833	-21.2	0.8	-0.1	4.0	-1.5
Pn	1000.	0.80	0.833	-21.2	2.2	-1.0	4.0	-1.5

The values of Lg attenuation were found in several of the papers referenced above. The explosion and vertical force excitation levels were found from synthetic seismogram calculations as described in Barker, et al. (1994) using the earth structure from Lomax and Sneider (1994) (Figure 4). The above parameters were used throughout the region except along the Teisseyre-Tornquist Zone (TTZ), which has been observed to block regional phases (Schweitzer, 1995). This is modeled by a zone 100 km wide in which the values of Q_0 are reduced to 10% of the values in the table. For teleseismic phases (P, pP and S), we use travel time and amplitude curves which are taken from tables in Veith and Claussen (1972). The tables are in the same format as those used by NetSim, but include values for a sequence of source depths so that depth can be determined from travel times.

The stations used were the Conference on Disarmament WP224 primary (Alpha) and secondary (Beta) networks (shown on Figure 5). Also shown on the figure is the TTZ. Station parameters (noise spectra, location, down times) were taken from the NetSim/Xnice database (McLaughlin, et al., 1995),

11
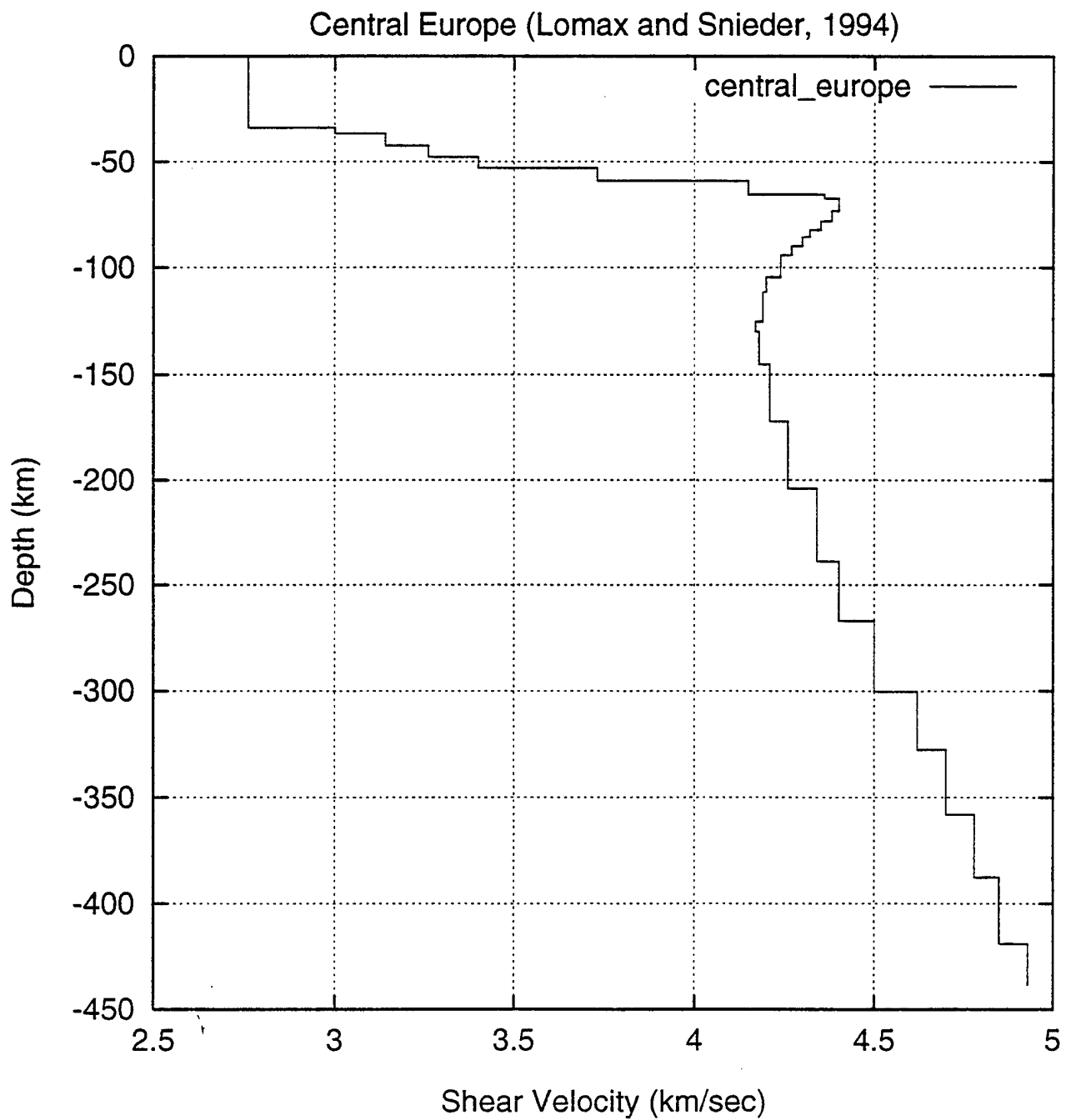
Figure 4.   Shear wave velocity structure for central Europe from Lomax and Snieder (1994.

wp224: Alpha + Beta Stations
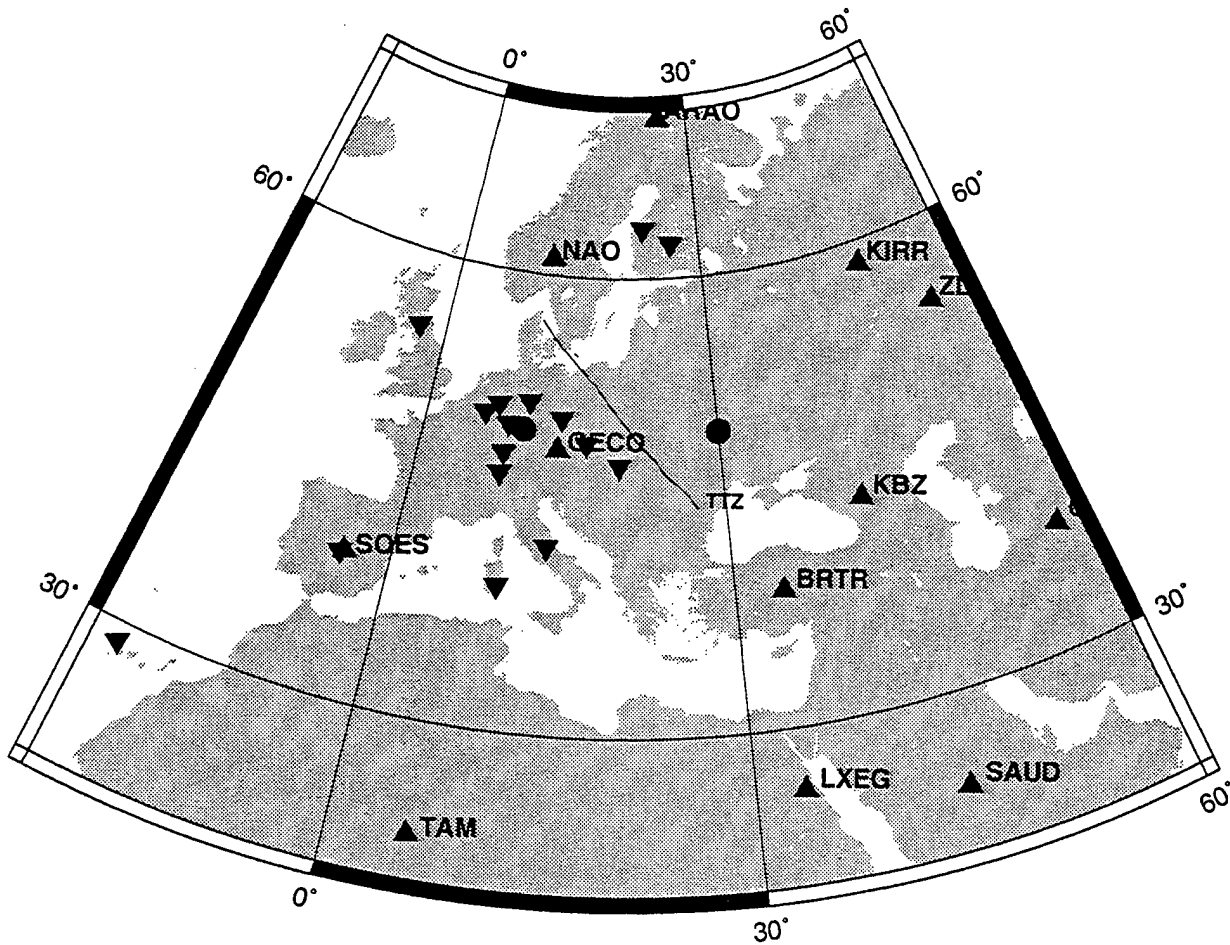
Figure 5.   Map of central Europe showing the Conference on Disarmament WP224 primary (Alpha) and secondary (Beta) networks. Also shown is the Teisseyre-Tornquist Zone (TTZ).

where available. When noise estimates were unavailable at a station, the parameters of the nearest available station or the station judged to be most like it (with regard to distance from the ocean, etc.) was used. The fraction of down time was set to a value of 0.10 for all stations. Using the parameters in the above table, we generated a suite of events with four source types (earthquakes, overburied explosions, normally buried explosions and quarry blasts). The events used the standard source parameters described in Appendix A. In keeping with the results of Kvamme, *et al.*, 1995, the average earthquake stress drop was set to the relatively low value of 2 Mpa (20 bars). Earthquake depths were in the range 10 to 20 km while normally overburied explosions were set at 500 m. Figures 6 and 7 show contour plots of the $m_b(Lg)$ detection threshold in the region for earthquakes and overburied explosions, respectively, using Alpha stations alone. The detection criteria are those used by GSETT (see Appendix B). These plots were made by choosing the Discrimination Plot and Contour Plot entries from the Plots menu, selecting $m_b(Lg)$ threshold as the Plot Variable from the Discrimination Plot popup window with the A condition set to GSE detection and the B condition set to All Events Occurring. The plots shown in this report were made by pushing the GMT plot "Yes" button, which spawns the GMT plot program (done because this package makes postscript files which can be incorporated into reports). A comparable plot also appears in the Xnice canvas. Note that the detection threshold is higher for earthquakes than overburied explosions. This is because (1) the GSE detection criteria are criteria for location using regional or teleseismic P waves (Appendix B) and (2) the ratio of Lg to P energy is higher for earthquakes. Thus, at a given $m_b(Lg)$, the P waves are smaller for earthquakes or, put another way, the inferred threshold is higher.

Another way to view detection threshold is using the distribution of events at particular source locations. We consider two source regions: 50N by 10E and 50N by 30E (also shown on Figure 5). The first source region is near European Alpha stations as well as a large group of Beta stations. The second source region is not near any stations.

In Figure 8, we show the incremental fraction of events at 50N by 10E detected by the Alpha stations as a function of $m_b(Lg)$. Quarry blasts and normally buried explosions are also included in these populations. These

mb(Lg) detection thresholds (GSE criteria)
earthquakes
wp224 network
cntrl_eur.eqk.mblg_det_thresh

Figure 6.   Contour plot of the m_b(Lg) detection threshold for earthquakes using Alpha stations alone.

mb(Lg) detection thresholds (GSE criteria)

overburied explosions
wp224 network

cntrl_eur.obex.mblg_det_thresh
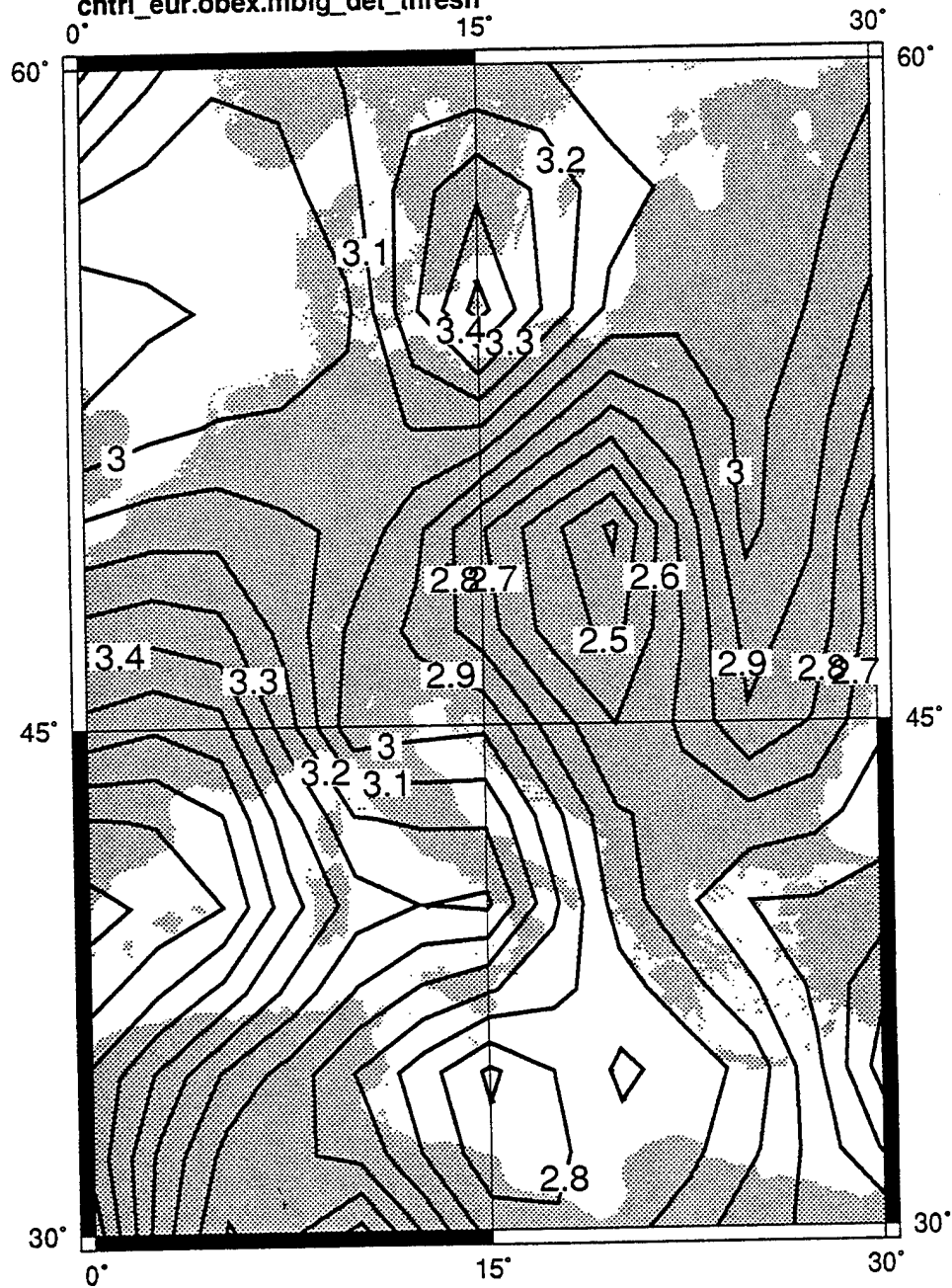
Figure 7.   Contour plot of the m_b(Lg) detection threshold for overburied explosions, using Alpha stations alone.

A conditions:

Class c14: GSE detection

areas: eur.50x10.2

mb range: 0.05 to 6.22

Ms range: 0.00 to 3.89

depth range: -157.47 to 337.99

first year and number of years: 81 1

B conditions:

Class c16: occurring

areas: eur.50x10.2

mb range: 0.05 to 6.22

Ms range: 0.00 to 3.89

depth range: -157.47 to 337.99

first year and number of years: 81 1
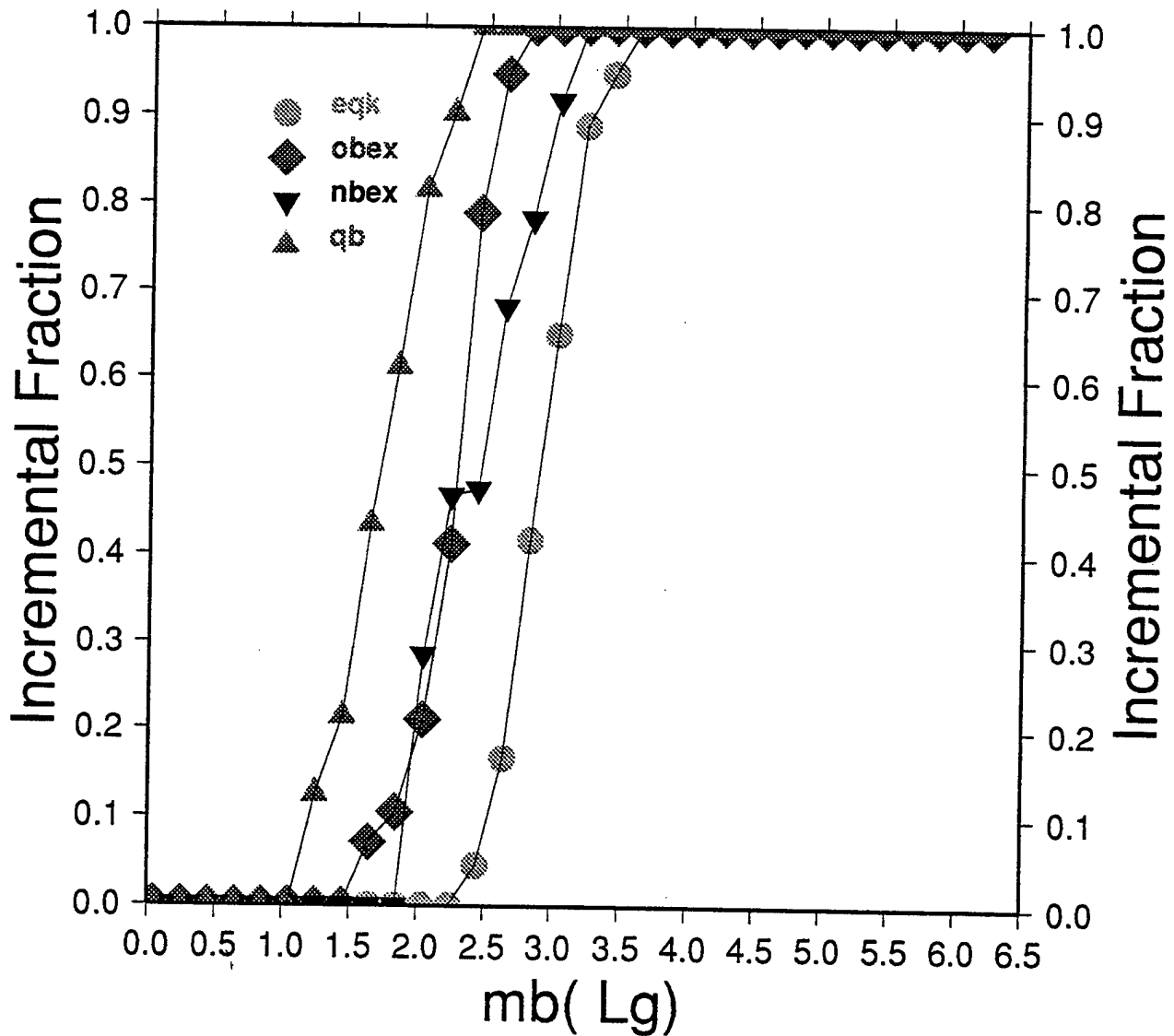
Figure 8.   The incremental fraction of events at 50N by 10E detected by the
Alpha stations as a function of m_b(Lg).

plots were made by choosing the Discrimination Plot and XY Plot entries from the Plots menu, choosing Incremental Fraction as the Y Variable and $m_b(Lg)$ as the X Variable with the A condition set to GSE detection and the B condition set to All Events Occurring. There are several things to note from this figure. First, as seen in the contour maps, the detection threshold (the m_b at which the incremental fraction is 0.9) is higher for earthquakes than overburied explosions and the other sources. In Figure 9, the detections are shown as a function of moment. In this case, the quarry blasts have the highest threshold since the finite duration of the source has the effect of lowpass filtering the source spectrum (Barker, *et al.*, 1994), reducing the m_b (amplitude near 1 Hz) relative to the moment. The detection curves at 50N by 30E, shown in Figure 10, illustrate the increase in threshold due to being farther from most of the stations in the network.

Thresholds are traditionally deduced from data by fitting (using maximum likelihood or other means) the observed cumulative distribution of events to a Gaussian distribution. The target Gaussian joint distribution is the product of conditional distributions, one of which is the distribution of events with magnitudes. For earthquakes, this is usually based on a Poisson process (the standard "b-value" model). For the populations shown in Figures 5 and 6, we have instead used a uniform distribution of source sizes (yields for explosions, moments for earthquakes) for ease of comparison between sources. In addition, we compare incremental, rather than cumulative, distributions because the distributions give the pleasing result of a constant value of one above a certain magnitude, indicating complete detection or identification above that magnitude. Figures 11 and 12 shows the effect of including the Beta stations on contours of detection threshold for earthquakes and overburied explosions. The thresholds are reduced significantly.

We have thus far focused on detection levels. In the following, we change focus to identification levels and examine the identification performance of three regional discriminants: Lg/P ratio, Lg spectral slope and $M_L:M_0$ and the teleseismic discriminant based on depth by travel time. We have not investigated the performance of the $M_s:m_b$ discriminant because reliable long period noise estimates are currently not available except at a few stations.

18

Discrimination bulletin: eur.50x10.2.unf

network: wp224

A conditions:	B conditions:
Class c14: GSE detection	Class c16: occurring
areas: eur.50x10.2	areas: eur.50x10.2
mb range: 0.00 to 6.21	mb range: 0.00 to 6.21
Ms range: 0.00 to 3.90	Ms range: 0.00 to 3.90
depth range: -294.94 to 230.96	depth range: -294.94 to 230.96
first year and number of years: 81 1	first year and number of years: 81 1
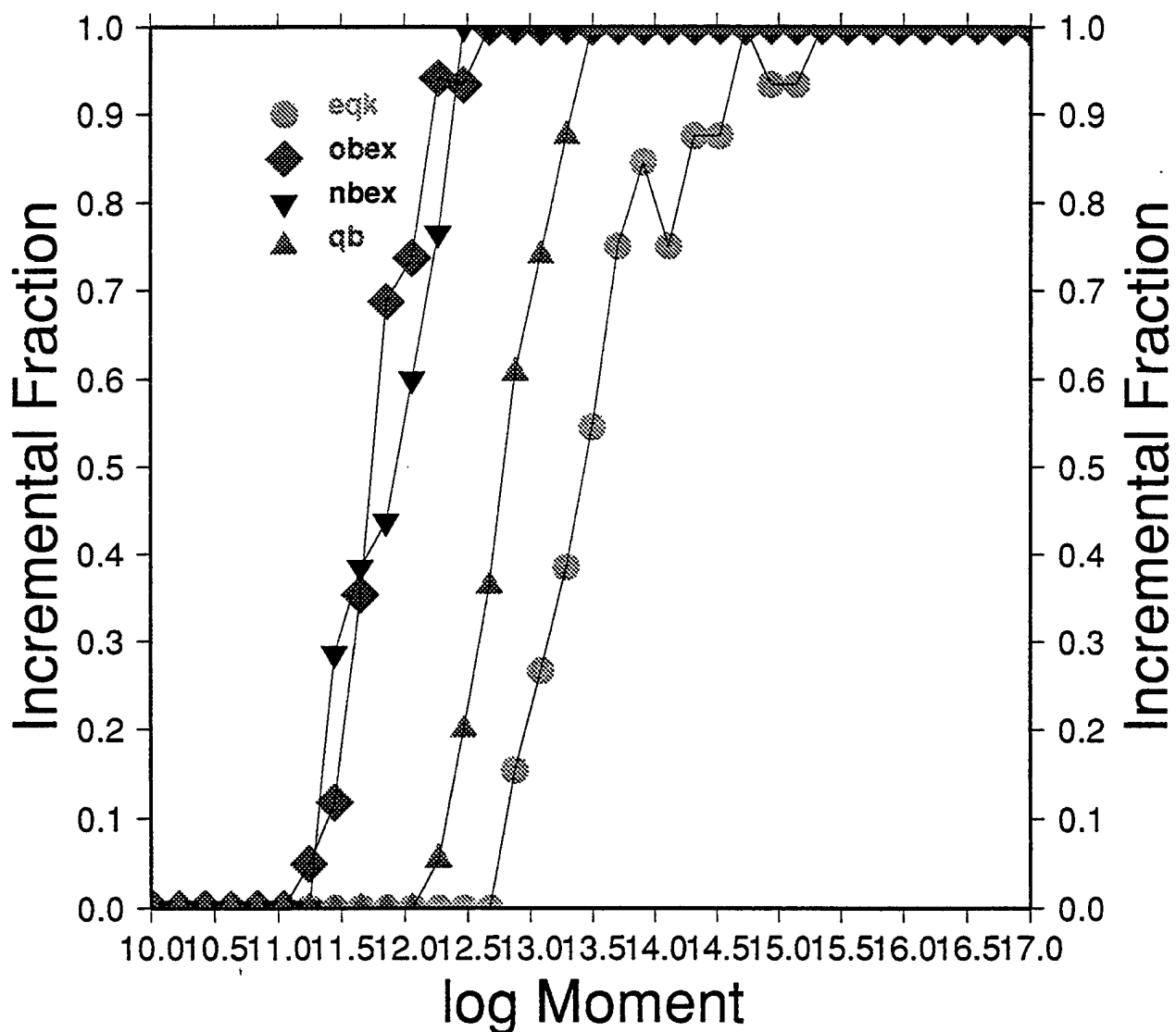
Figure 9.   The incremental fraction of events at 50N by 10E detected by the Alpha stations as a function of moment.
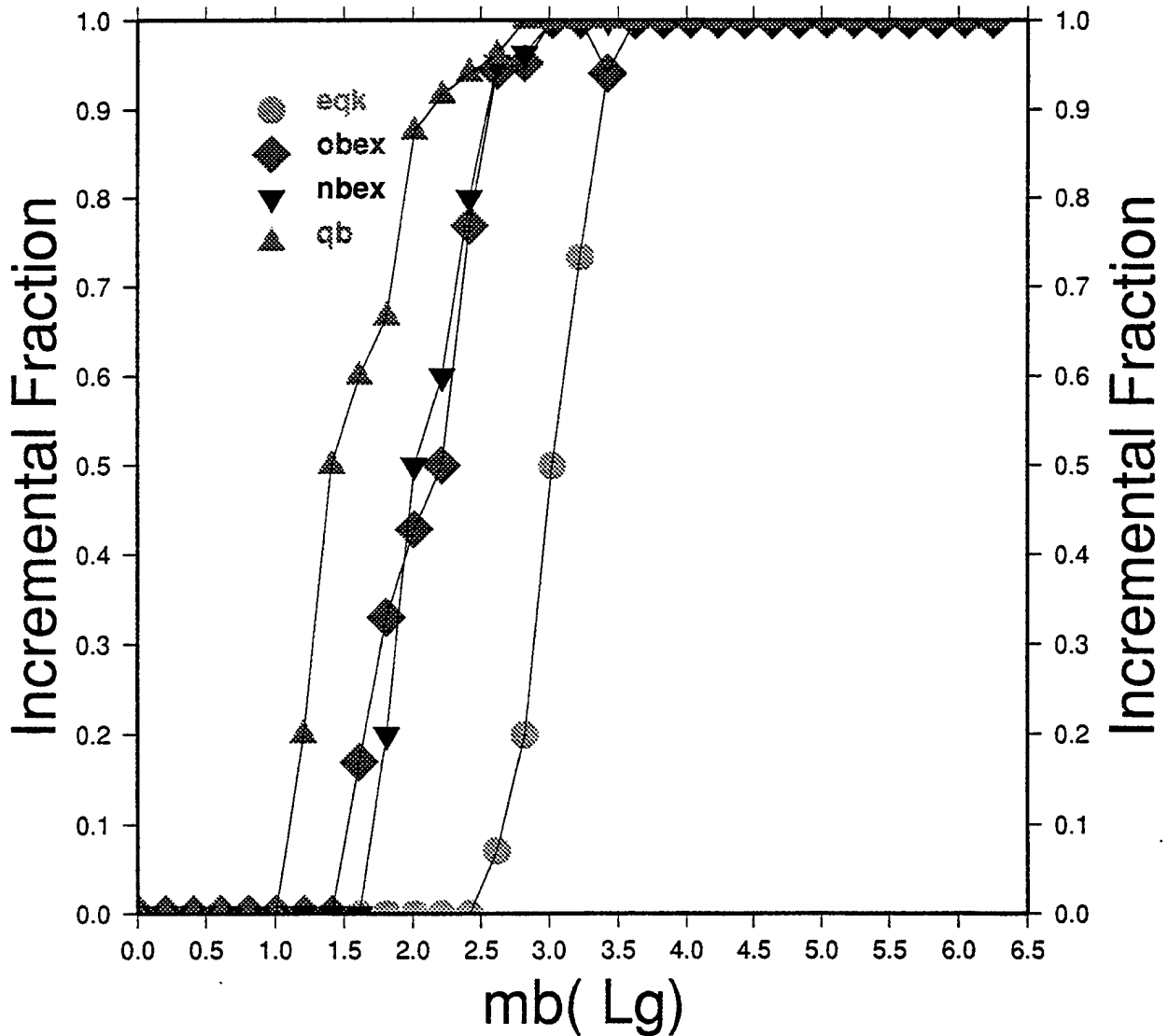
Figure 10. The incremental fraction of events at 50N by 30E detected by the Alpha stations as a function of m_b(Lg).

mb(Lg) detection thresholds (GSE criteria)

earthquakes
wp224 Alpha + proposed Beta stations
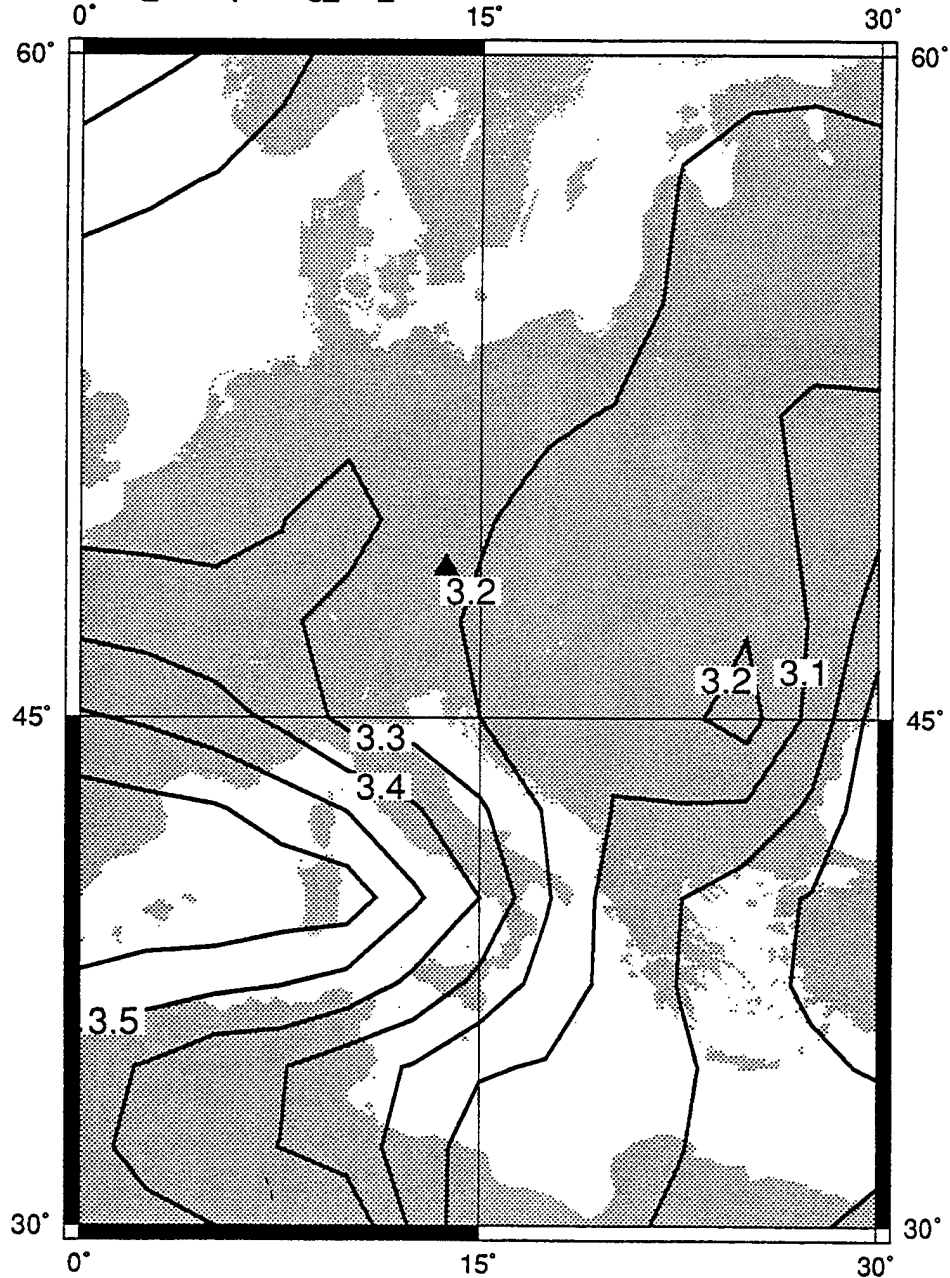cntrl_eur.beta.eqk.mblg_det_thresh
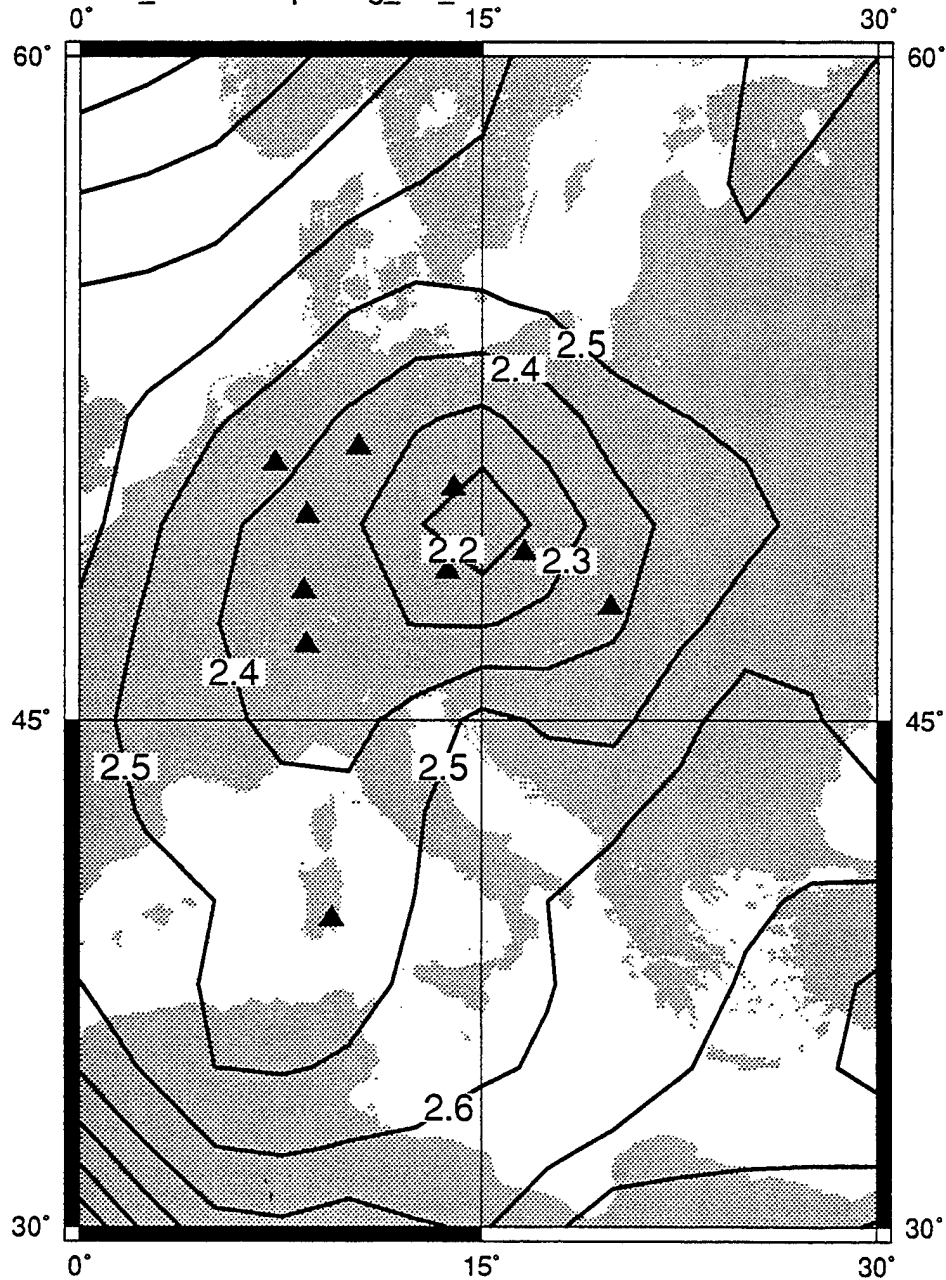
Figure 11.   Contour plot of the m_b(Lg) detection threshold for earthquakes using Alpha and Beta stations.

mb(Lg) detection thresholds (GSE criteria)

overburied explosions
wp224 Alpha + proposed Beta stations
cntrl_eur.beta.obex.mblg_det_thresh
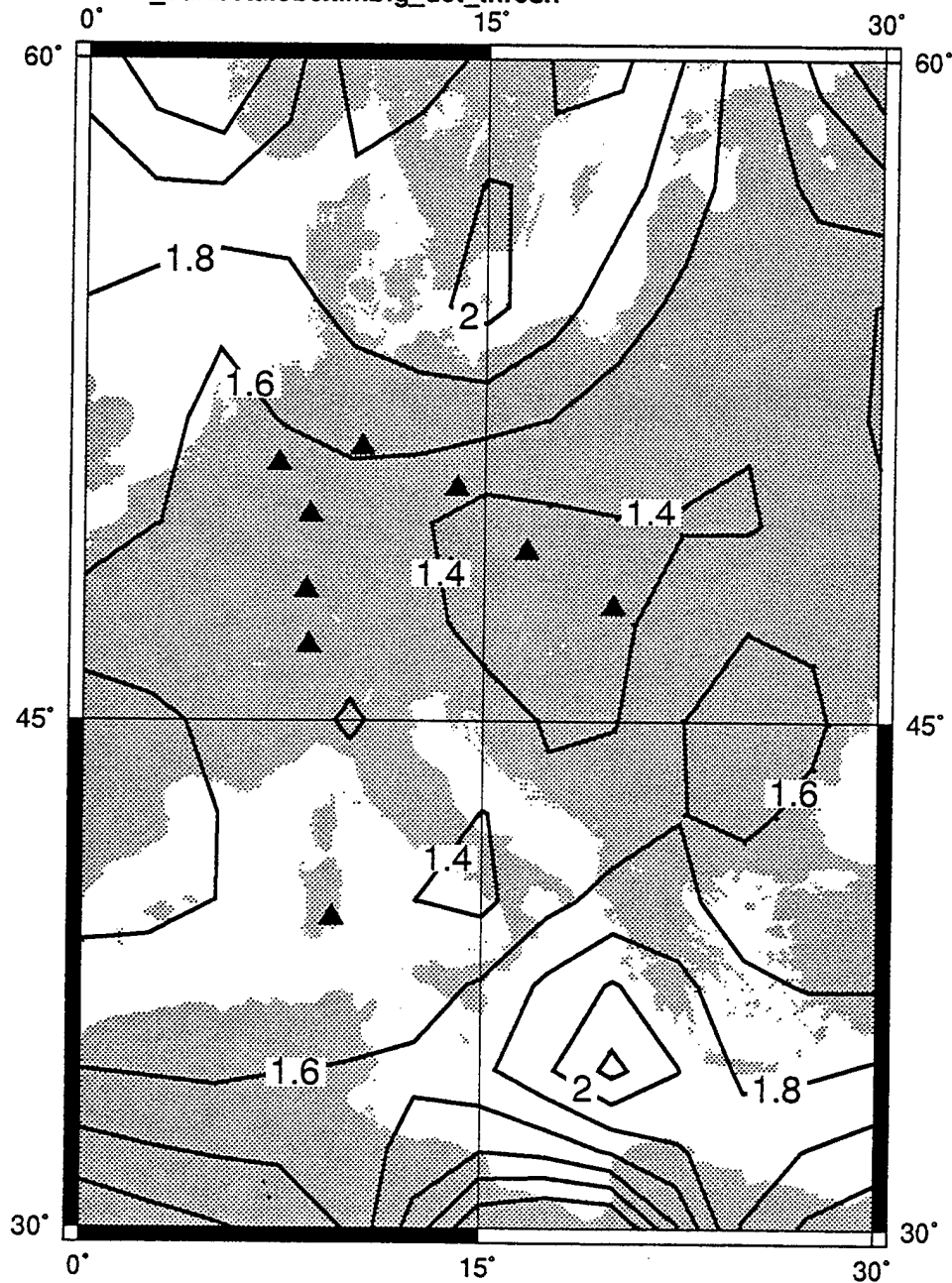
Figure 12. Contour plot of the mb(Lg) detection threshold for overburied explosions, using Alpha and Beta stations.

Long-period noise levels are quite variable and the results for M_S detection and therefore $M_S:m_b$ are very sensitive to these levels.

Figure 13 shows values of Lg/P versus m_b for events at 50N by 10E. P amplitudes are the larger of Pn and Pg. (The data points for the different are much easier to distinguish on the original color plots generated by Xnice since they are color coded). All values are corrected for propagation. It can be seen in the figure that log(Lg/P) exceeds a value of about 0.2 for earthquakes and is less than -0.2 for the other sources. The separation improves at higher magnitudes, due primarily to better resolution of signal amplitudes. Figure 14 shows the incremental fraction of events which have been assigned a score of 1, the most earthquake-like score (see Appendix A) according to the Lg/P discriminant. No explosion sources have a score of 1 while all earthquakes above $m_b \sim 3.5$ have a score of 1. Figure 15 shows the incremental fraction of events with a score of 2 or higher (a score of 2 is less earthquake-like than a score of 1, and scores of 3 and 4 are explosion-like). All the explosion sources have a score of 2 or more above an $m_b(Lg)$ of about 2.5, with quarry blasts having the lowest threshold and normally buried explosions the highest. About 15% of the earthquakes have some explosion-like Lg/P ratios near $m_b=5$, but none above that magnitude.

Contours of the identification threshold for the Lg/P discriminant are shown for earthquakes in Figure 16. As with the discrimination thresholds, distributions of the incremental fraction of events that were classified as earthquakes were generated and fit to a Gaussian distributions. The contour variable is the $m_b(Lg)$ at which the Gaussian distribution equals 0.9. For the Alpha stations alone, the thresholds vary between 3.3 and 3.6. The inclusion of the Beta stations (Figure 17) reduces the threshold by about 0.7 magnitude units, particularly where the Beta stations are concentrated. Figure 18 shows contours of the percentage of earthquakes identified as such by the Lg/P discriminant. In continental Europe, the percentages are 95% or more, while the values are around 75% in the Mediterranean Sea. Contours of the percentage of overburied explosions identified as explosion-like by the Alpha stations are shown in Figure 19. The percentages are greater than 95% in most of the study area except in the Mediterranean Sea.

Discrimination bulletin: eur.50x10.2.unf
network: wp224

A conditions:

Class c16: occurring

areas: eur.50x10.2

mb range: 0.05 to 6.22

Ms range: 0.00 to 3.89

depth range: -157.47 to 337.99

first year and number of years: 81 1
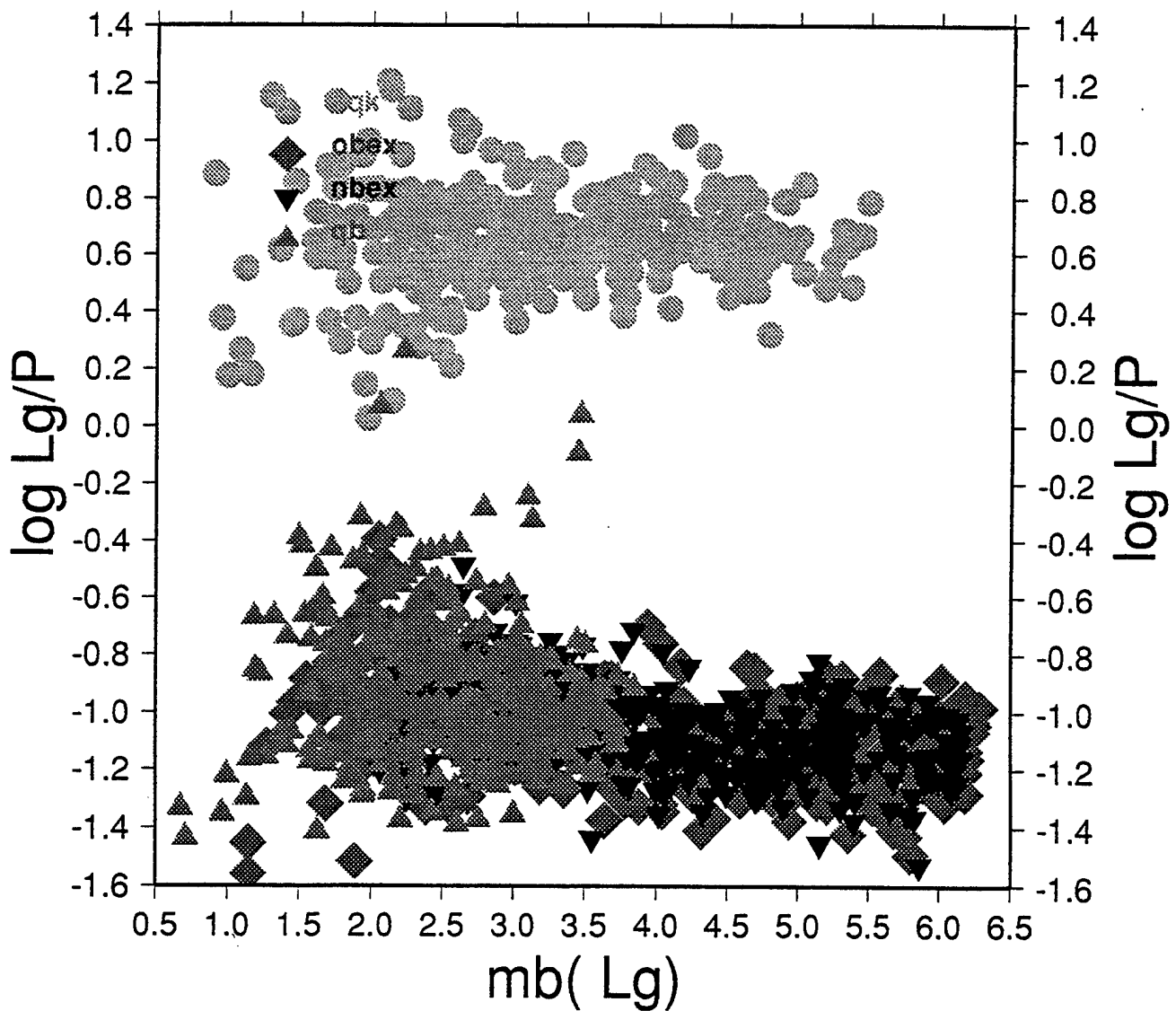
Figure 13.   Values of Lg/P versus m_b for events at 50N by 10E. P amplitudes
are the larger of Pn and Pg.

A conditions:

Class c8: 1's by spec'd discriminant

Discriminants

   Lg/Pg at one Hz

areas: eur.50x10.2

mb range: 1.42 to 5.28

Ms range: 0.00 to 3.90

depth range: -156.81 to 281.59

first year and number of years: 81 1

B conditions:

Class c15: occurring

areas: eur.50x10.2

mb range: 1.42 to 5.28

Ms range: 0.00 to 3.90

depth range: -156.81 to 281.59

first year and number of years: 81 1
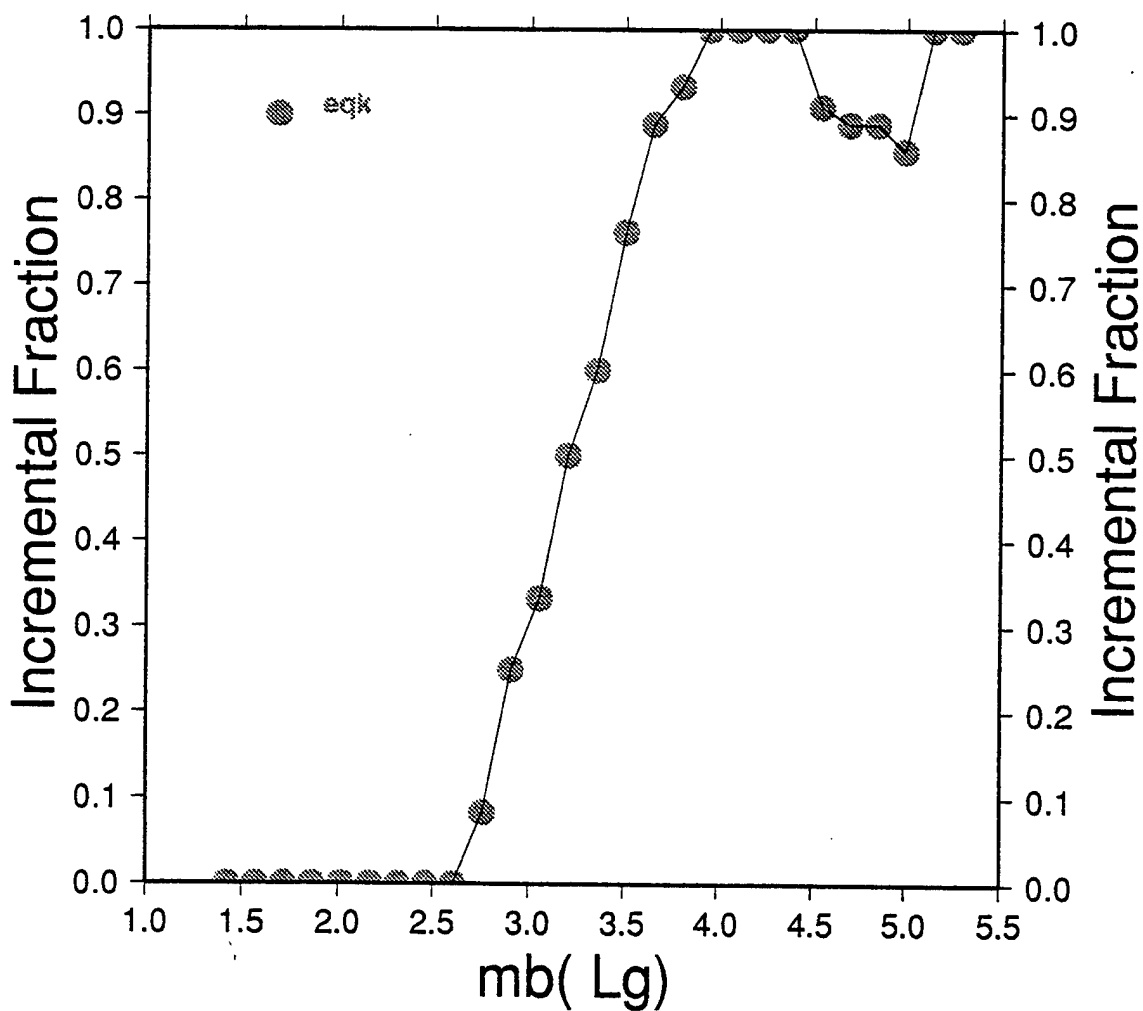
Figure 14. Incremental fraction of events at 50N by 10E which have been assigned a score of 1, the most earthquake-like score according to the Lg/P discriminant.

25

Discrimination bulletin: eur.50x10.2.unf

network: wp224

A conditions:

Class c11: 2 or higher by spec'd discriminant

Discriminants	**B conditions:**
Lg/Pg at one Hz	**Class c16: occurring**
areas: eur.50x10.2	areas: eur.50x10.2
mb range: 0.05 to 6.22	mb range: 0.05 to 6.22
Ms range: 0.00 to 3.89	Ms range: 0.00 to 3.89
depth range: -157.47 to 337.99	depth range: -157.47 to 337.99
first year and number of years: 81 1	first year and number of years: 81 1
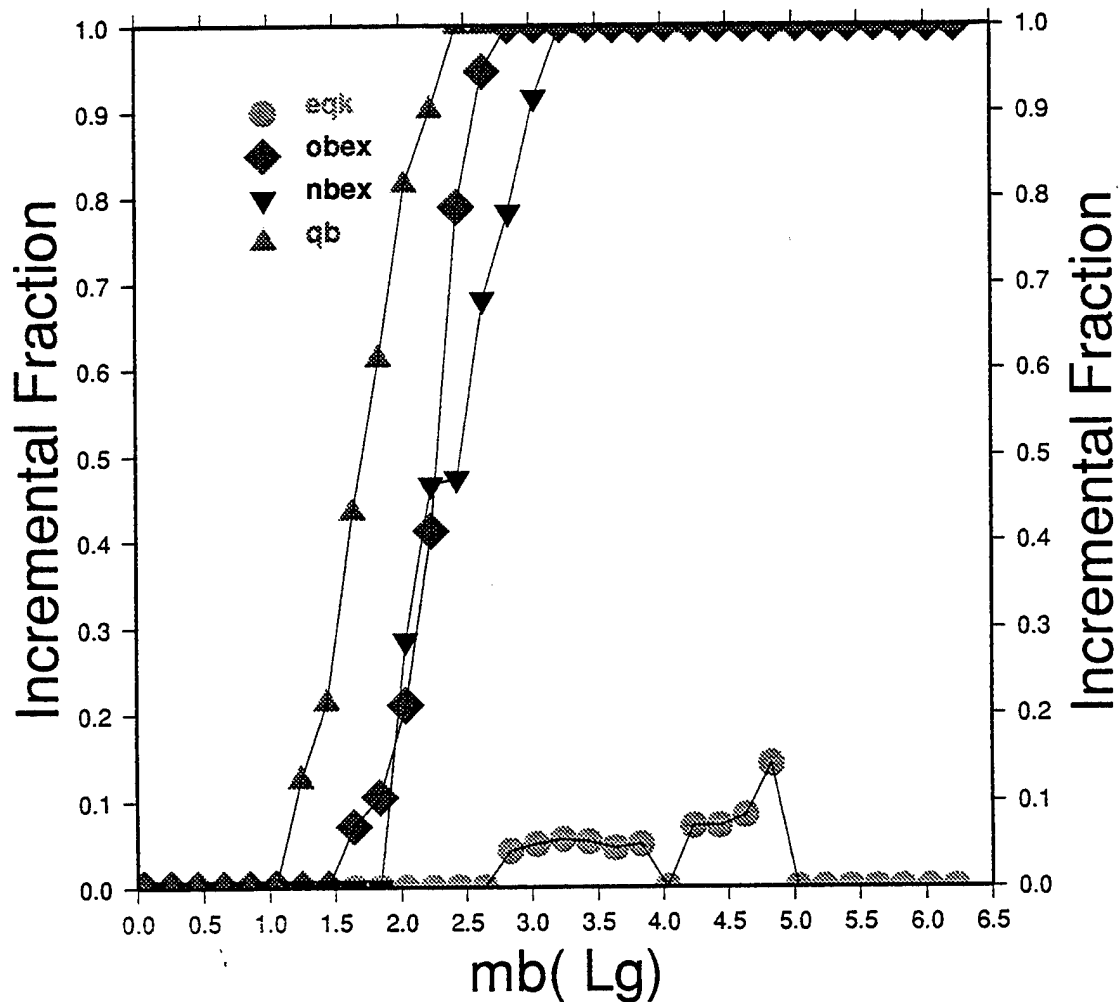
Figure 15. The incremental fraction of events at 50N by 10E with a score of 2 or higher (a score of 2 is less earthquake-like than a score of 1, and scores of 3 and 4 are explosion-like).

26

mb(Lg) identification thresholds for Lg/P

earthquakes
wp224 network
cntrl_eur.idbyLgP
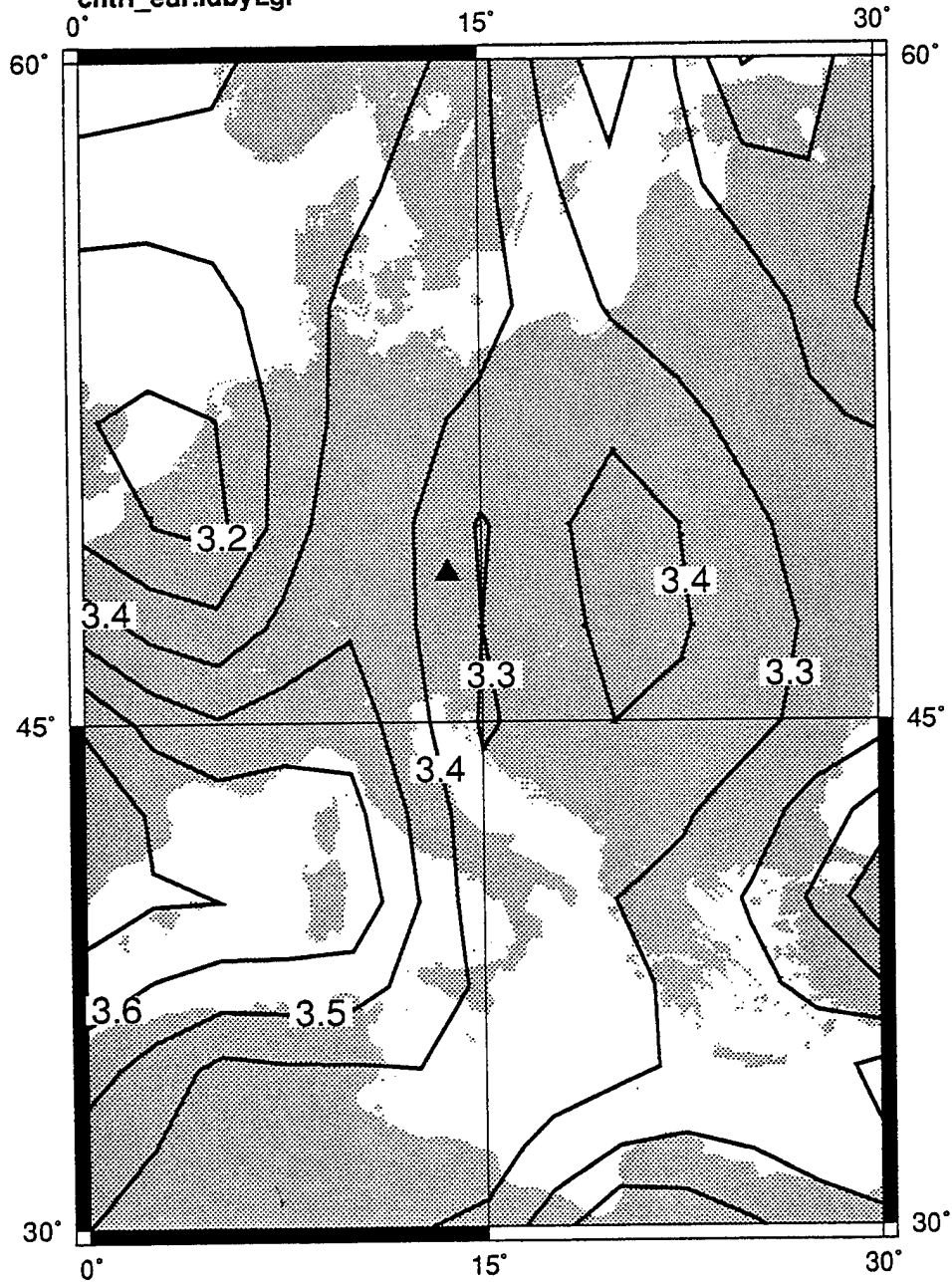
Figure 16. Contours of the identification threshold for the Lg/P discriminant are shown for earthquakes (Alpha stations alone).

mb(Lg) identification thresholds for Lg/P earthquakes
wp224 Alpha + proposed Beta stations
cntrl_eur.beta.eqk.idbyLgP
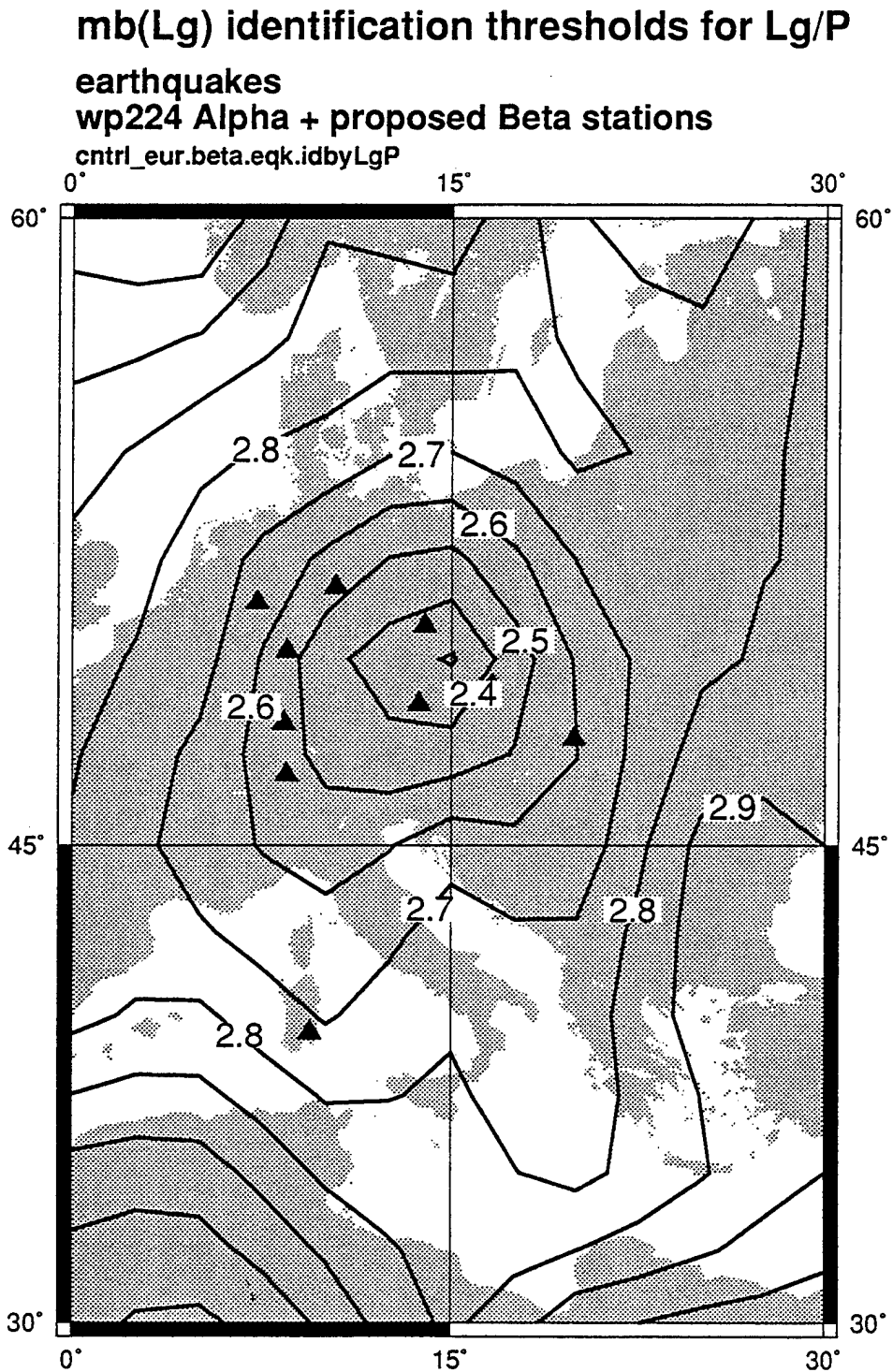
Figure 17. Contours of the identification threshold for the Lg/P discriminant are shown for earthquakes (Alpha and Beta stations).

Percentage of events identified by Lg/P at mb(Lg)=3.5

earthquakes
wp224 network

cntrl_eur.eqk.idbyLgP_at3.5
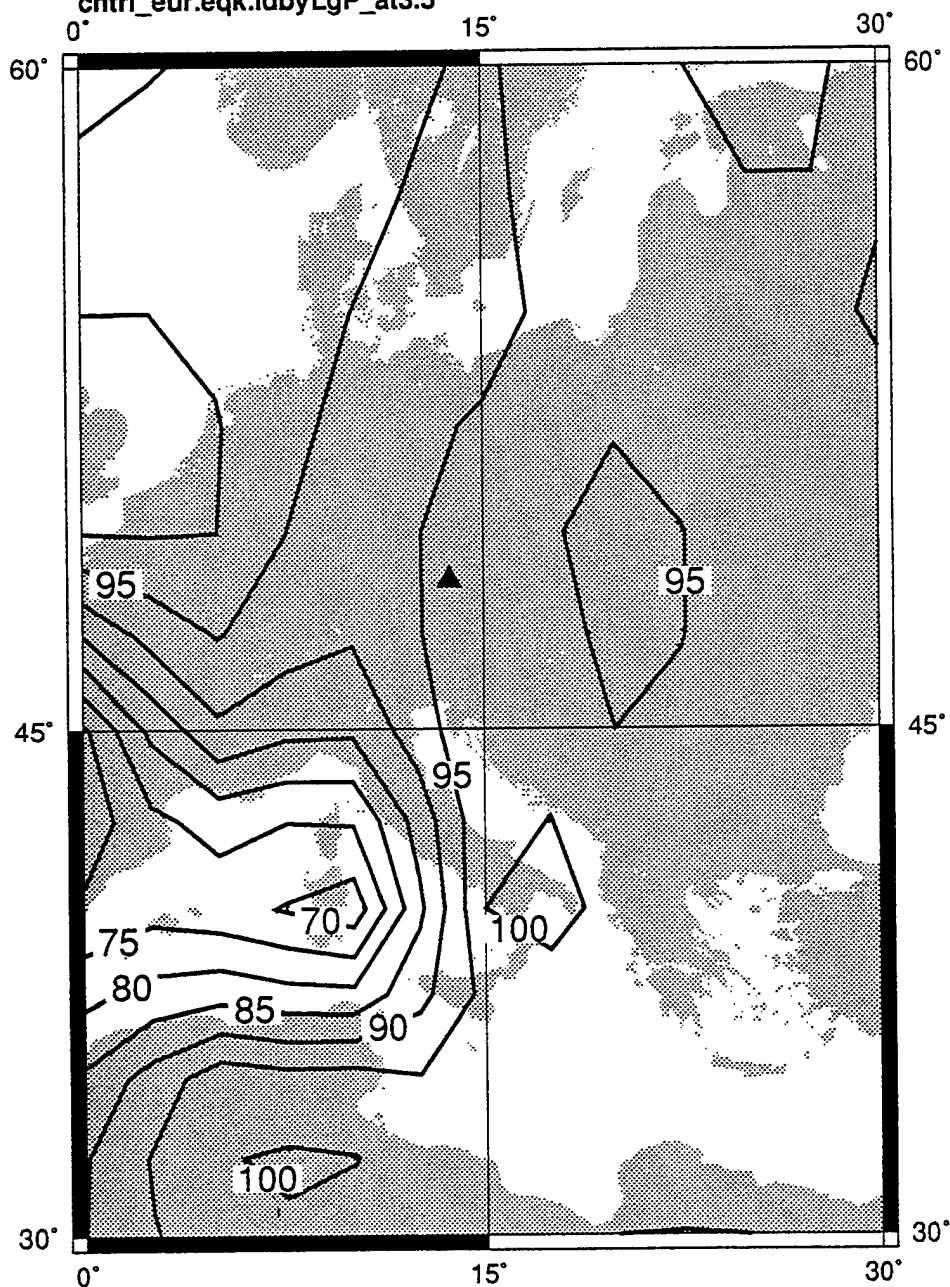
Figure 18.   Contours of the percentage of earthquakes identified as such by the Lg/P discriminant (Alpha stations alone).

Percentage of explosion-like events by Lg/P at mb(Lg)=3.5

overburied explosions
wp224 network

cntrl_eur.obex.idbyLgP_at3.5
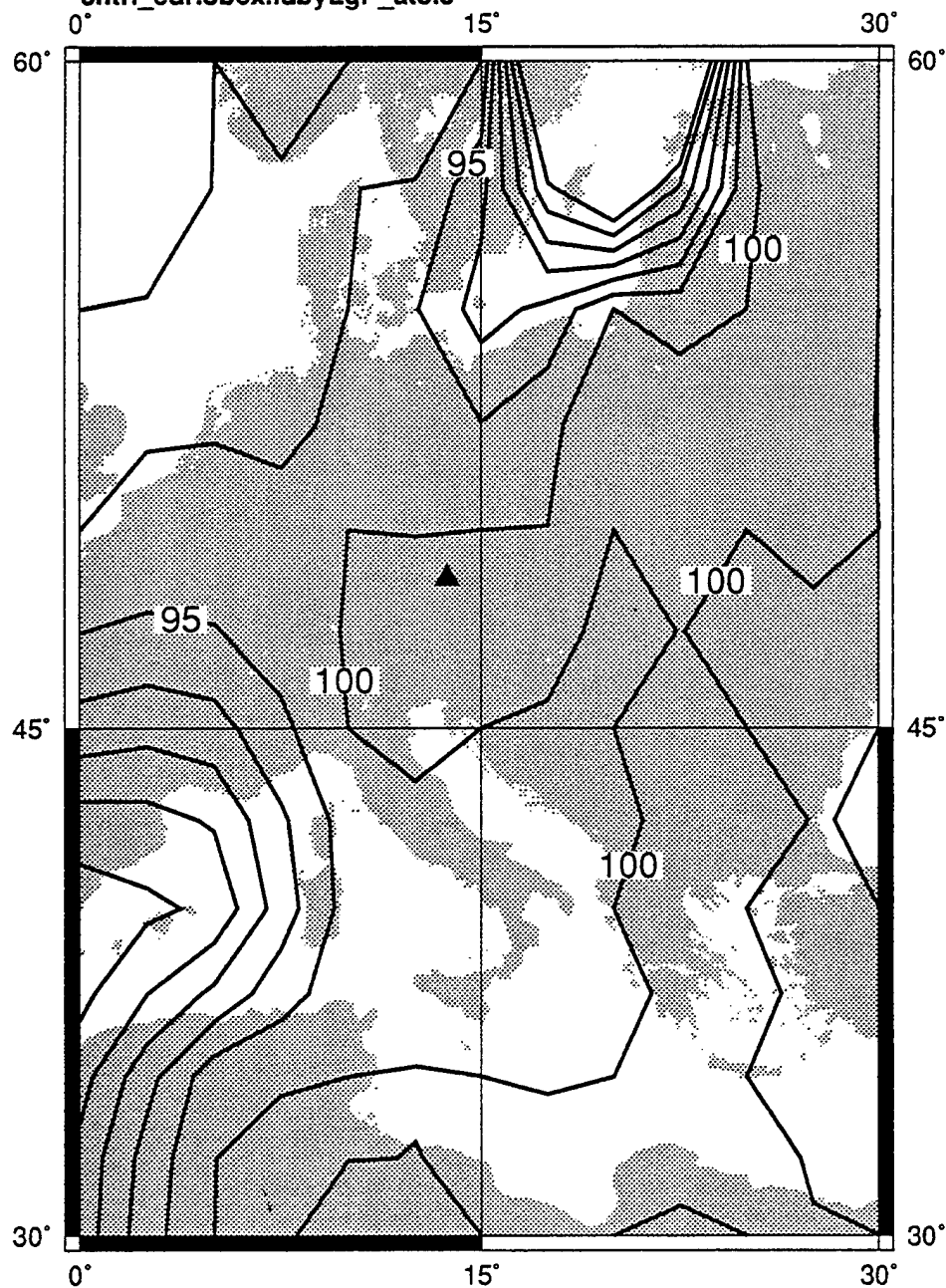
Figure 19.   Contours of the percentage of overburied explosions identified as explosion-like by the Alpha stations are shown.

Values of Lg spectral slope versus m_b(Lg) for events at 50N by 10E recorded by the Alpha stations alone are shown in Figure 20. Spectral slope is computed from the ratio of the average spectral amplitude between 1 and 2 Hz to the average spectral amplitude between 6 and 8 Hz. Except for quarry blasts, there is considerable overlap of the populations on the plot. Using Beta stations does not improve the separation of populations, as can be seen in Figure 21. These results indicate that the Lg spectral slope discriminant is effective for distinguishing earthquakes from quarry blasts in Europe, albeit with some overlap (as found by Baumgardt, *et al.*, 1991, and Pulli and Dysart, 1992), but would not be effective at identifying a localized shallow explosion.

We now consider the M_L:M_0 discriminant. At 50N by 10E, the populations of single explosions separate from earthquakes and quarry blasts in M_L space, as can be seen in Figure 22. The separation improves at larger magnitudes. The figure shows "saturation" of earthquakes magnitudes with moment, a commonly observed phenomenon, due to the effect of corner frequency. In fact, the separation of earthquakes from single explosions is due primarily to change in corner frequency, which is in turn a consequence of the low stress drop used in these simulations. Numerical experiments done with values near 10 Mpa (100 bars) show that the separation of the earthquakes does not occur. For this discriminant, the Beta stations do not improve the identification performance since the overlap of the populations is due to the earthquake corner frequencies. The performance is slightly worse for the sources at 50N by 30E, where there is considerable overlap due to increased scatter caused by longer propagation distances. There are no observations of the performance of M_L:M_0 for central Europe, but these simulations indicate that it would be an effective discriminant. Note that the values of moment that are used in these figures are those in the Events bulletin. That is, the values are not obtained by modeling the process of propagating surface waves or long period body waves and deriving the moment from them but are the true moments. This would be a simple matter using the methods for extracting M_0 in Stevens (1986), since the criteria for making a time domain M_s measurement are roughly equivalent to those for taking a spectrum and making the path and attenuation corrections. However, this is currently not implemented in Xnice. More importantly, we need good estimates of long-

A conditions:

Class c16: occurring

areas: eur.50x10.2

mb range: 0.00 to 6.21

Ms range: 0.00 to 3.90

depth range: -294.94 to 230.96

first year and number of years: 81 1
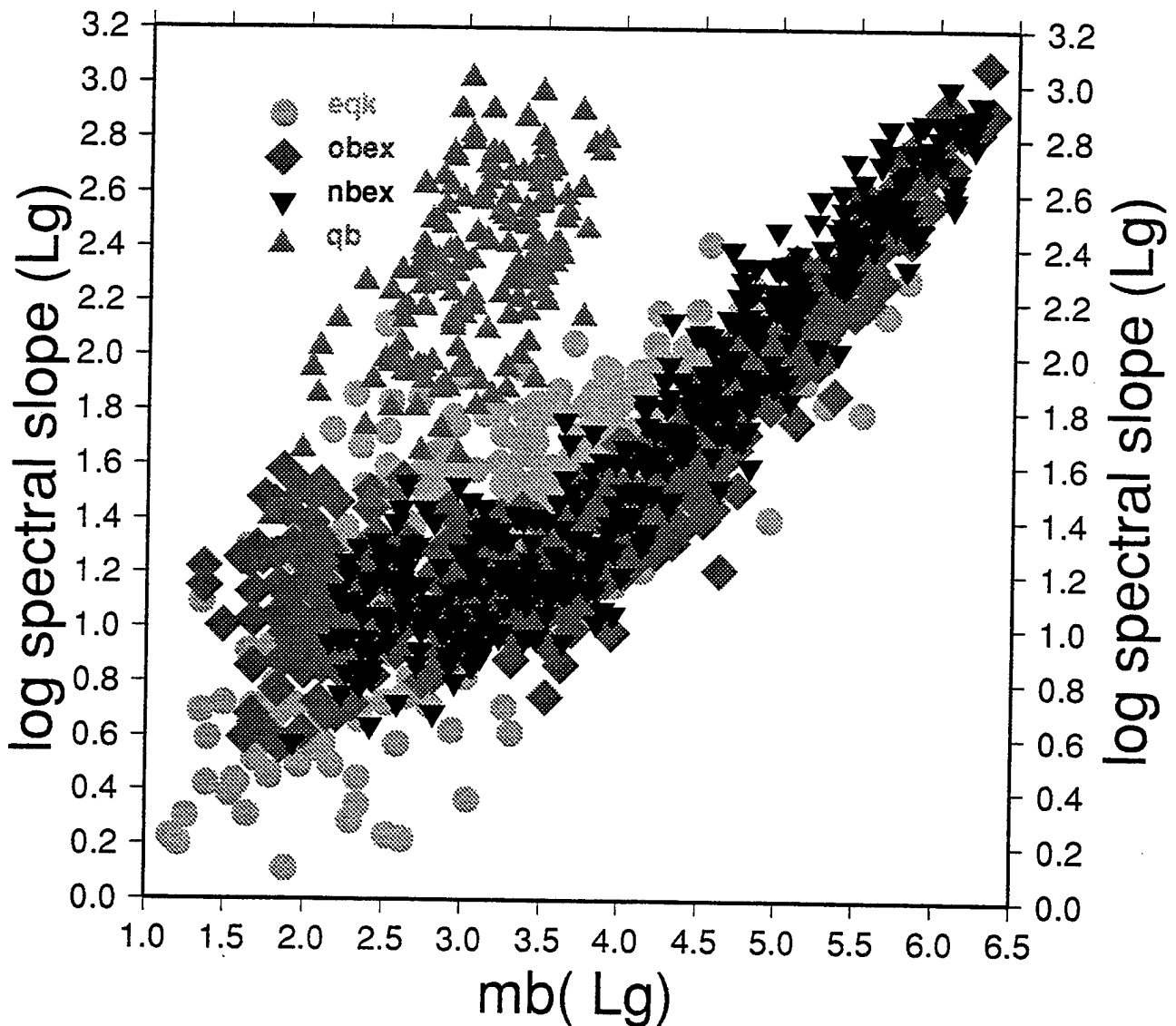
Figure 20.   Values of Lg spectral slope versus m_b for events at 50N by 10E
recorded by the Alpha stations alone.

A conditions:

Class c16: occurring

areas: eur.beta.50x10.2

mb range: 0.00 to 6.13

Ms range: 0.00 to 3.88

depth range: -213.32 to 328.38

first year and number of years: 81 1
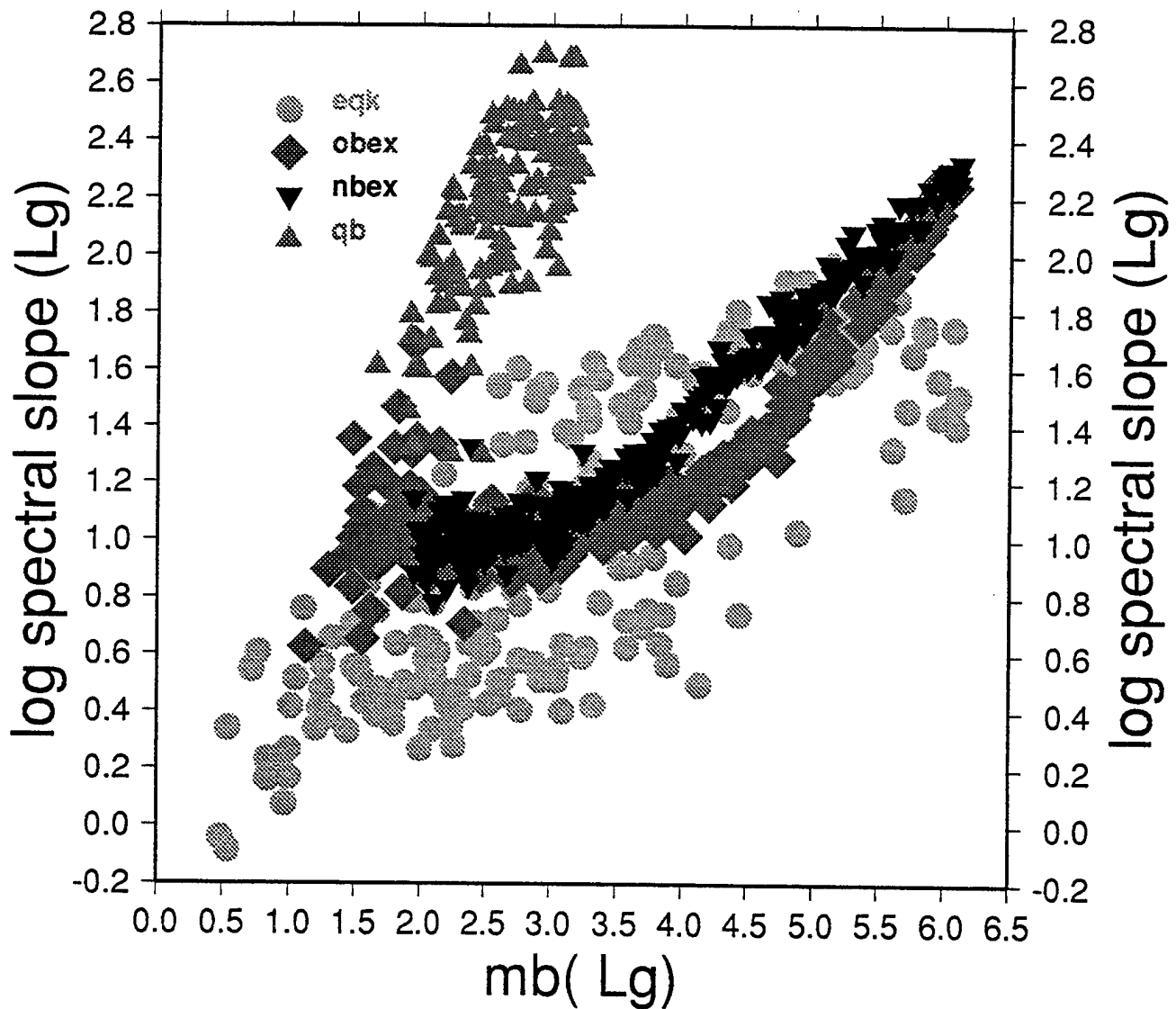
Figure 21. Values of Lg spectral slope versus m_b for events at 50N by 10E recorded by the Alpha and Beta stations.

33

Discrimination bulletin: eur.50x10.2.unf
network: wp224
A conditions:
Class c16: occurring
areas: eur.50x10.2
mb range: 0.00 to 6.21
Ms range: 0.00 to 3.90
depth range: -294.94 to 230.96
first year and number of years: 81 1
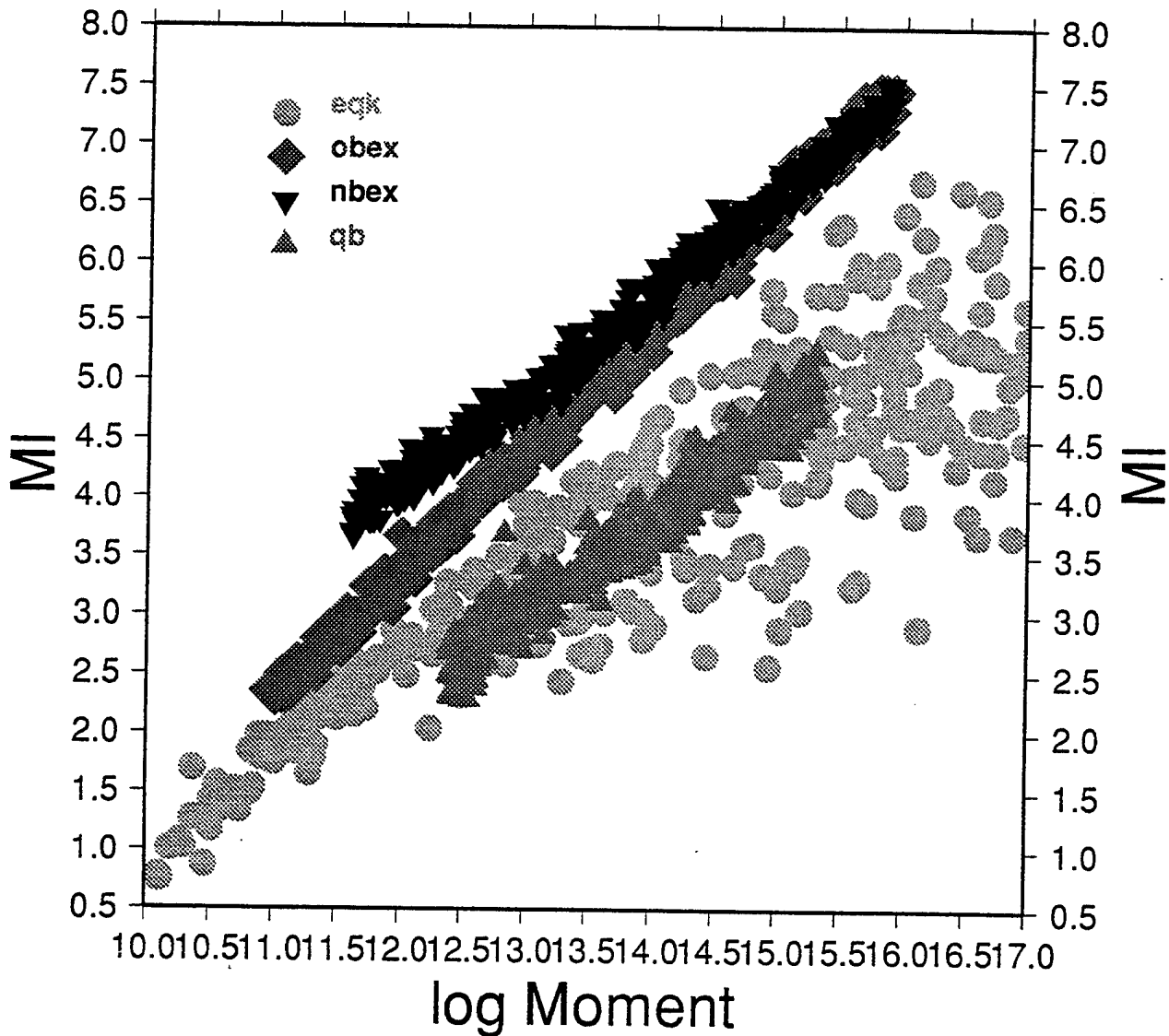
Figure 22.   Values of M_l versus log moment for events at 50N by 10E recorded by the Alpha stations alone.

period noise, which are not available at this time. For these reasons, we have not computed threshold values for the M_L:M_0 discriminant, showing only that it should be a valuable measure.

Figure 23 shows the incremental fraction of events at 50N by 10E which have a score of one using the AFTAC discriminant based on depth computed by travel times (see Appendix B). At $m_b(Lg)$ of 5.0, approximately 50% of the earthquakes are identified by this discriminant. About 15% of the normally buried explosions are determined to be earthquake-like, as are about 5% of quarry blasts and overburied explosions. These misidentifications go to zero above a magnitude of about 3.6. This is primarily due to a reduction in error estimates with larger m_b, as seen in Figure 24, which shows the vertical error ellipse axis (at 90% confidence) as a function of $m_b(Lg)$ for this population of events. Including Beta stations for events at this location raises the fraction of earthquakes identified as such to around 70% and reduces the number of explosions in this category to zero, as can be seen in Figure 25.

3.3. Simulations for the Middle East

In this section, we describe simulations for the Middle East. Since knowledge of the propagation parameters for this region is limited, and current studies in this area are in their initial stages, we have used estimates. Therefore, the results should be considered preliminary. The area is assumed to be divided into two propagation and source excitation parameter regions: the African and Arabian Shields, and the Red Sea. For the shields, the parameters were taken from those used by Barker, *et al.* (1994) for the eastern U.S. For the Red Sea, we used propagation parameters which would cause blockage of regional phases and taken source excitation parameters from Barker, *et al.* (1994) for the western U.S.

Table 3
African/Arabian Shield Parameters

Phase	Q_0	η	n	S	c_0^{exp}	c_1^{exp}	c_0^{vf}	c_1^{vf}
Lg	600.	0.39	0.833	-21.0	-0.28	-1.5	3.3	-1.6
Pg	500.	0.39	0.833	-22.0	-0.16	-0.5	3.3	-1.3
Pn	1000.	0.60	0.833	-22.0	-0.16	-0.5	3.3	-1.3

Discrimination bulletin: eur.50x10.2.unf
network: wp224

A conditions:

Class c8: 1's by spec'd discriminant

Discriminants	B conditions:
Depth from P travel times	Class c16: occurring
areas: eur.50x10.2	areas: eur.50x10.2
mb range: 0.45 to 6.24	mb range: 0.45 to 6.24
Ms range: 0.00 to 3.90	Ms range: 0.00 to 3.90
depth range: -491.62 to 252.14	depth range: -491.62 to 252.14
first year and number of years: 81 1	first year and number of years: 81 1
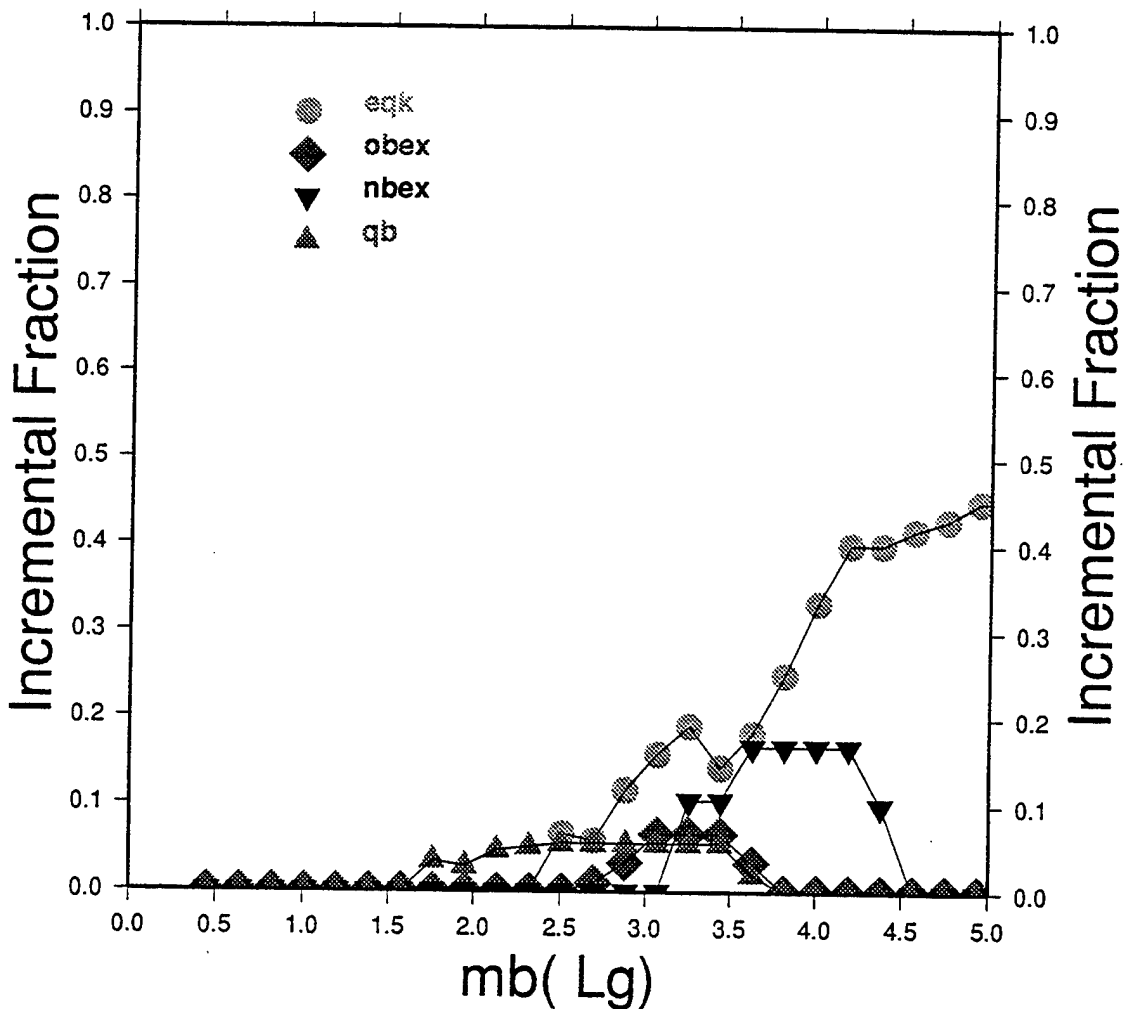
Figure 23.   The incremental fraction of events at 50N by 10E which have a score of one using the AFTAC discriminant based on depth computed by travel times (Alpha stations only).

Discrimination bulletin: eur.50x10.2.unf
network: wp224
A conditions:
Class c16: occurring
areas: eur.50x10.2
mb range: 0.45 to 6.24
Ms range: 0.00 to 3.90
depth range: -491.62 to 252.14
first year and number of years: 81 1
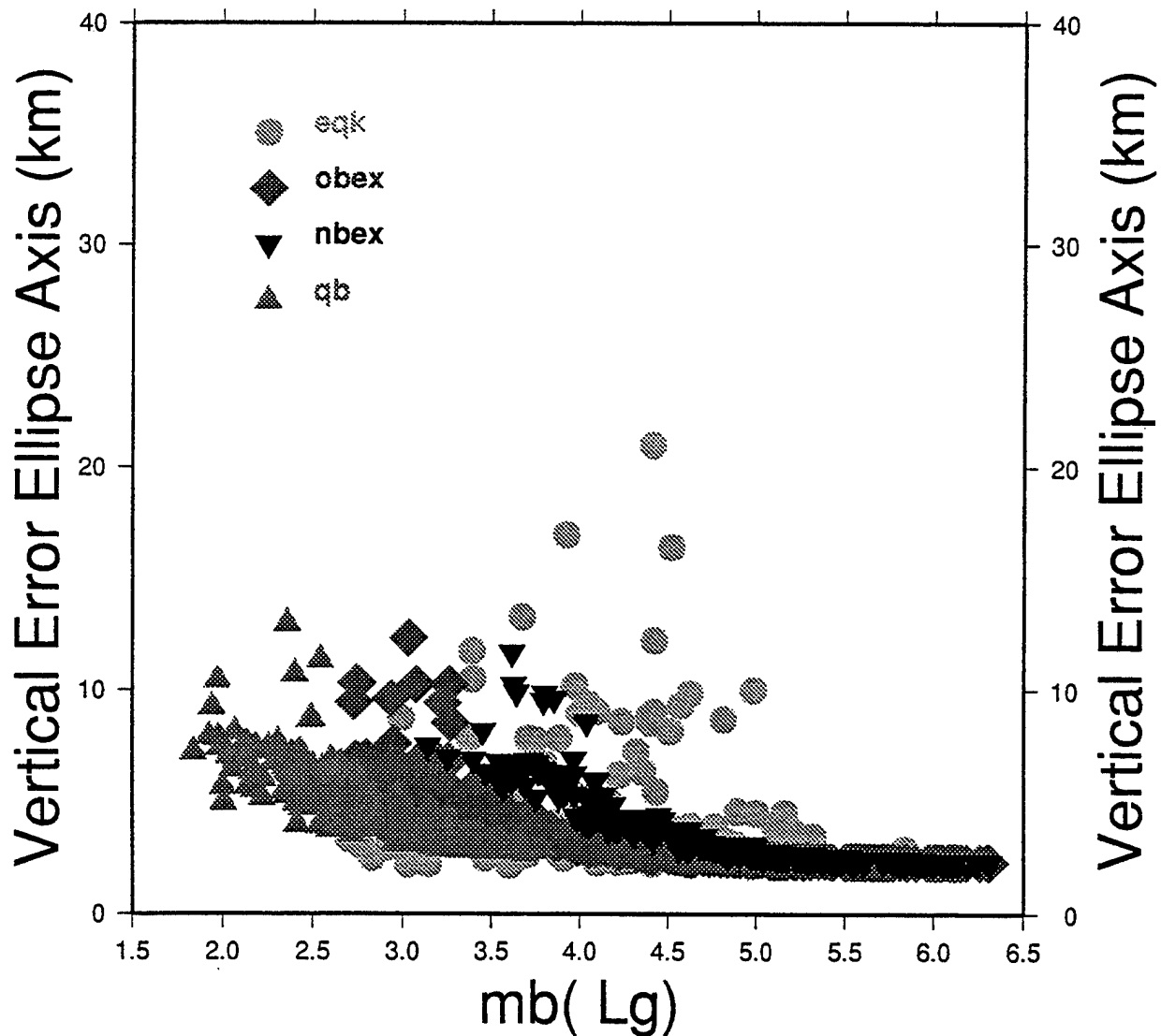
Figure 24.   Vertical error ellipse axes (at 90% confidence) for events at 50N
by 10E.
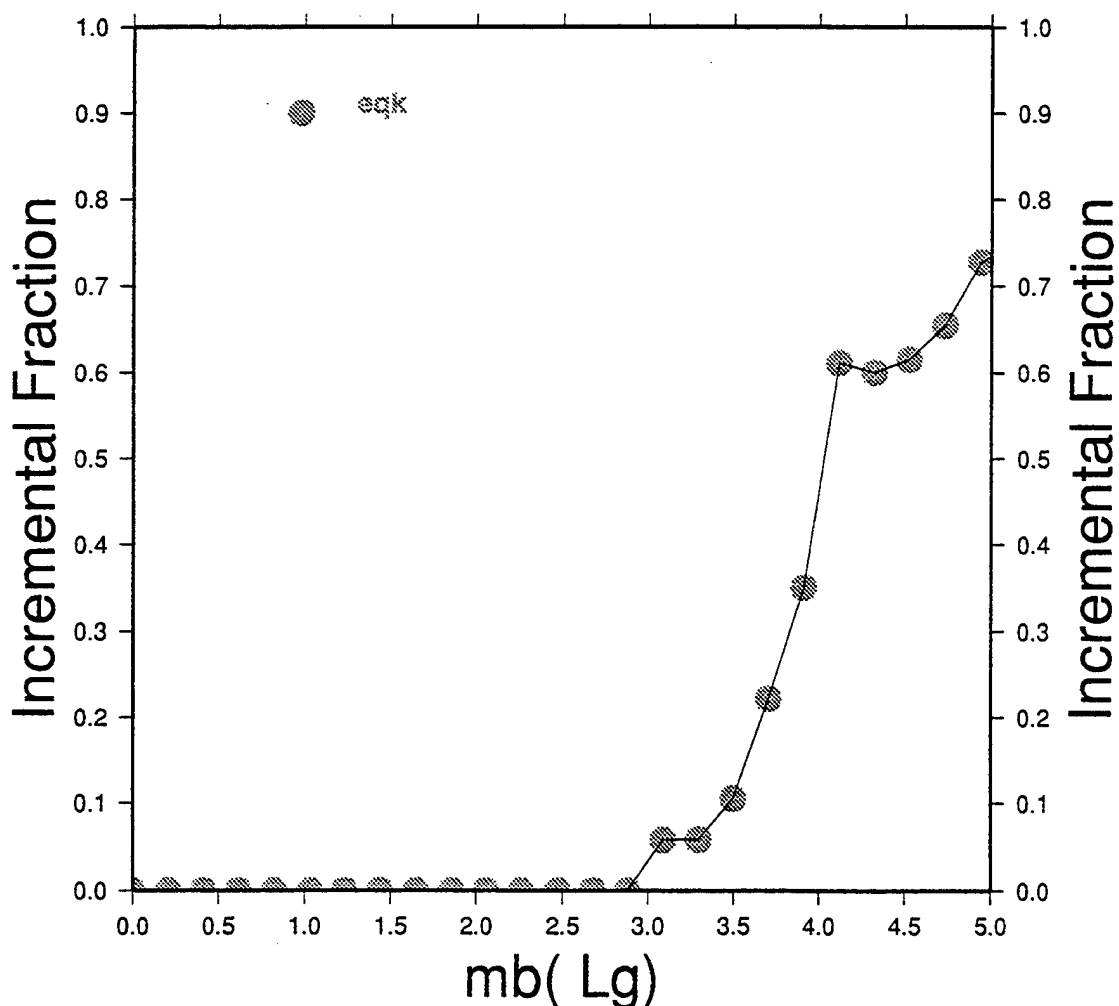
Figure 25. The incremental fraction of events at 50N by 10E which have a score of one using the AFTAC discriminant based on depth computed by travel times (Alpha plus Beta stations).

Table 4
Red Sea Parameters

Phase	Q_0	η	n	S	c_0^{exp}	c_1^{exp}	c_0^{vf}	c_1^{vf}
Lg	40.	0.45	0.833	-20.5	-0.40	-1.1	3.6	-1.2
Pg	50.	0.68	0.833	-21.2	-0.16	-0.1	4.0	-1.5
Pn	80.	0.80	0.833	-21.2	2.2	-0.1	4.0	-1.5

We have examined the Middle East by focusing on the identification performance of representative localized source regions. The stations, from the Conference on Disarmament, August, 1995, consensus, and study area are shown in Figure 26. As with the central Europe simulations (Section 3.2), station parameters (noise spectra, location, down times) were taken from the NetSim/Xnice database (McLaughlin, *et al.*, 1995), where available. When noise estimates were unavailable at a station, the parameters of the nearest available station or the station judged to be most like it were used. The average earthquake stress drop was set to 10 Mpa (100 bars). Earthquake depths were in the range 10 to 20 km.

We begin with the detection levels. Figure 27 shows contours of $m_b(Lg)$ detection threshold detected (using the GSE criteria). Values are low in the northern part of the Arabian shield and increase rapidly towards the Indian Ocean and central Africa, where station coverage becomes sparse. The incremental fraction of events as a function of $m_b(Lg)$ is shown in Figure 28 for four source types for sources at 30N by 40E. As with the central Europe simulations (Section 3.2), earthquakes have the highest detection threshold, which is approximately 2.8 at this location. This relation holds throughout the region.

The performance of the Lg/P discriminant for events at this location (30N by 40E) is shown in Figure 29. 100% of the earthquakes are identified as such above a magnitude of about 3.6. However, between 30 and 60% are the explosions are identified as earthquake-like.

In Figure 30, the incremental fraction of events determined to be explosion-like by this discriminant is shown. Between 45 and 75% of the
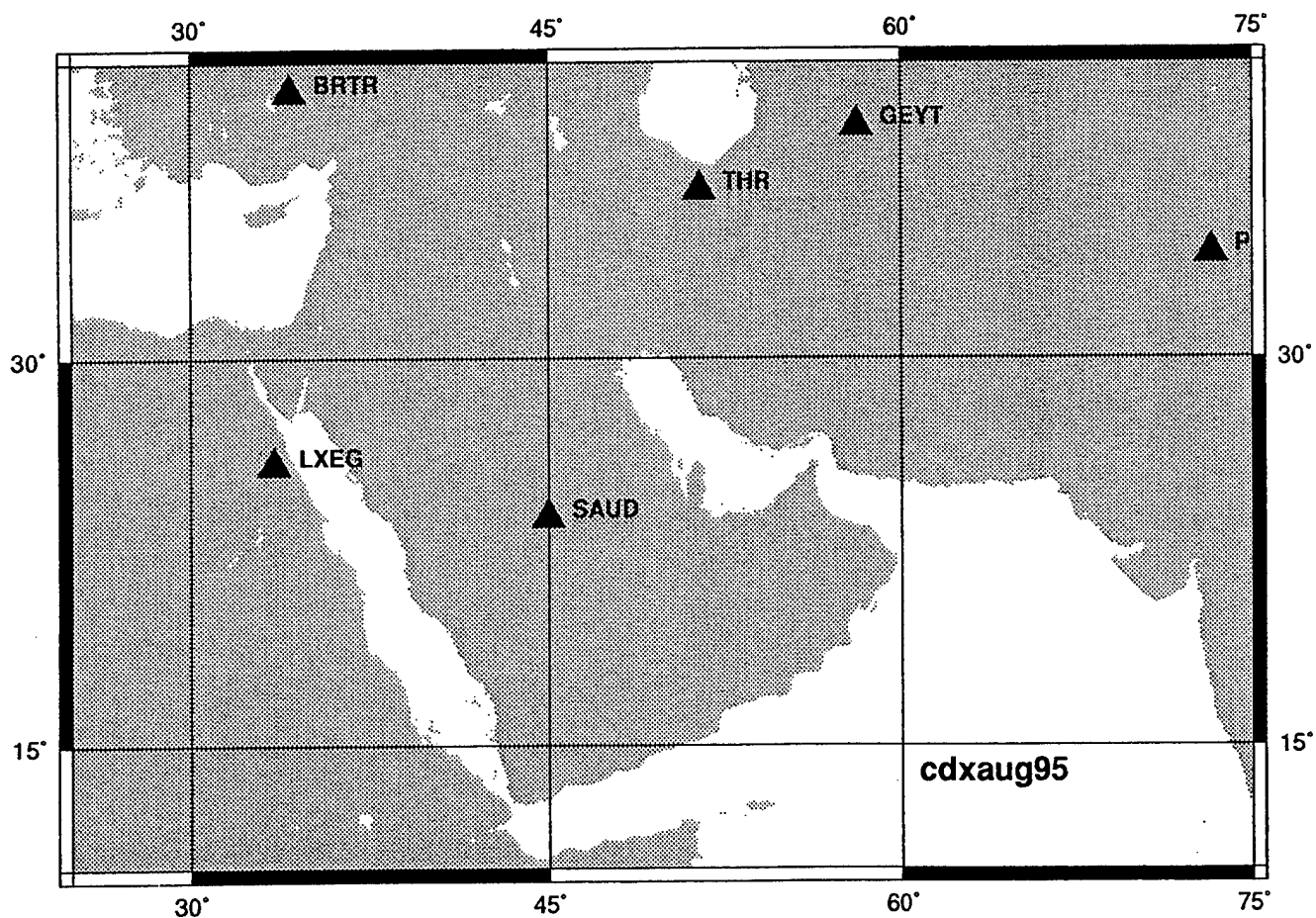
Figure 26.   Map of the Middle East showing the stations recommended by
             the Conference on Disarmament, August, 1995, consensus.

40

mb(Lg) detection thresholds (GSE criteria)

earthquakes
cdxaug95.alp.me network
mideast.eqk.4.mblg_det_thresh
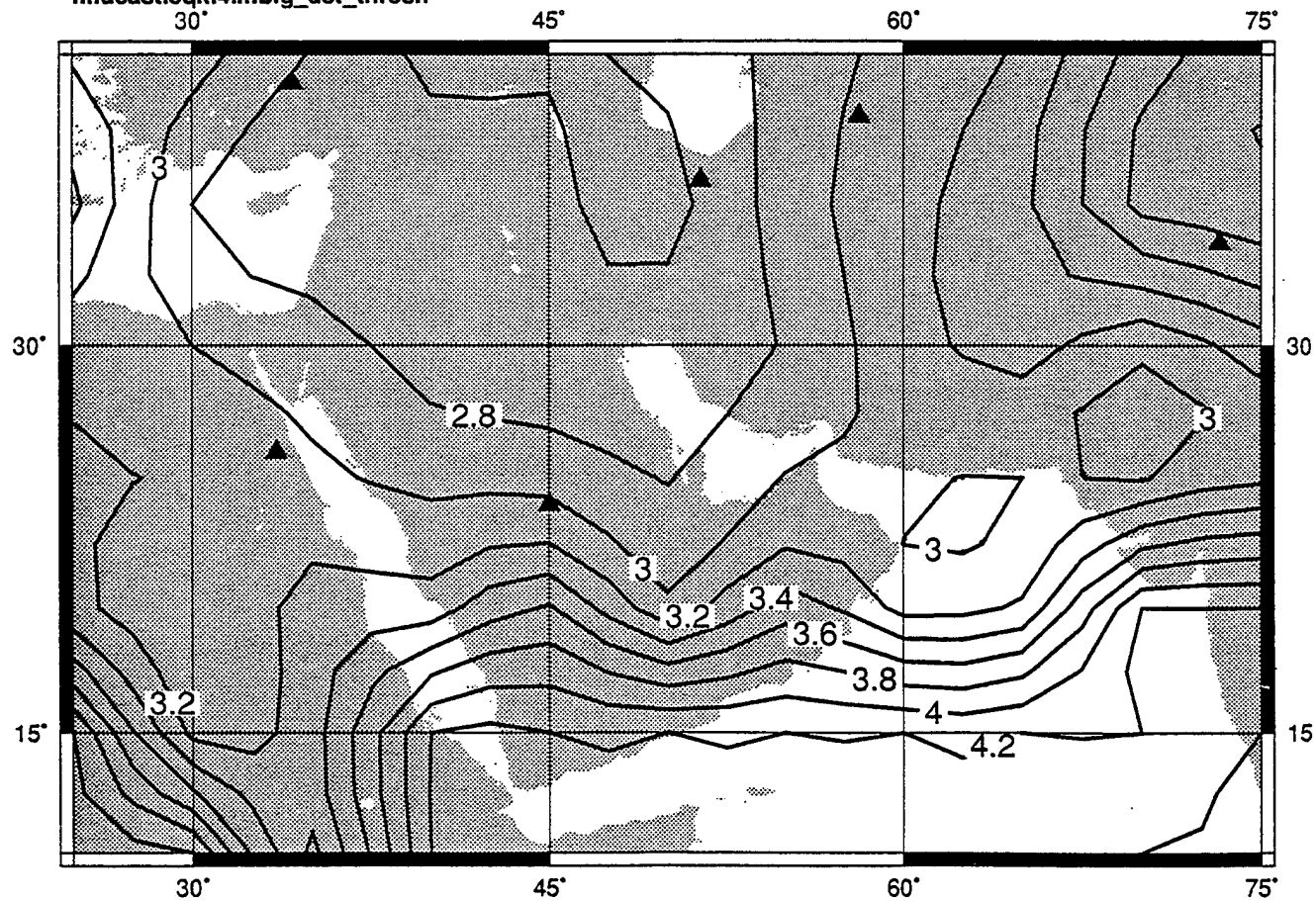
Figure 27.   Contour plot of the m_b(Lg) detection threshold for earthquakes.

41

Discrimination bulletin: mideast.30x40.unf

network: cdxaug95.alp.me

A conditions:	B conditions:
Class c14: GSE detection	Class c16: occurring
areas: mideast.30x40	areas: mideast.30x40
mb range: 0.00 to 7.01	mb range: 0.00 to 7.01
Ms range: 0.00 to 4.98	Ms range: 0.00 to 4.98
depth range: -599.53 to 145.87	depth range: -599.53 to 145.87
first year and number of years: 81 1	first year and number of years: 81 1
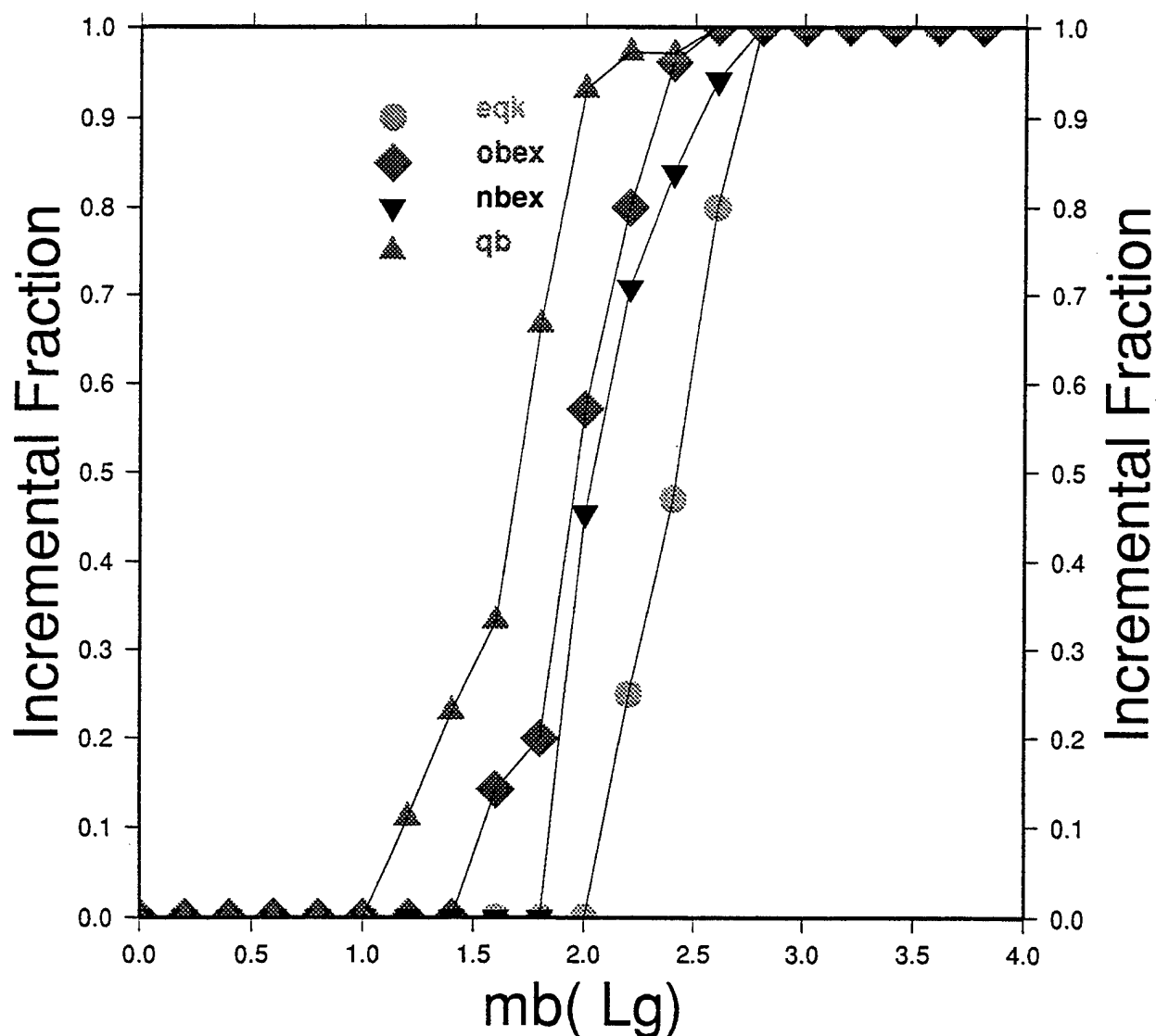
Figure 28.   The incremental fraction of events at 30N by 40E detected as a function of m_b(Lg).

A conditions:

Class c8: 1's by spec'd discriminant

Discriminants	B conditions:
Lg/Pg at one Hz	Class c16: occurring
areas: mideast.30x40	areas: mideast.30x40
mb range: 0.00 to 7.01	mb range: 0.00 to 7.01
Ms range: 0.00 to 4.98	Ms range: 0.00 to 4.98
depth range: -599.53 to 145.87	depth range: -599.53 to 145.87
first year and number of years: 81 1	first year and number of years: 81 1
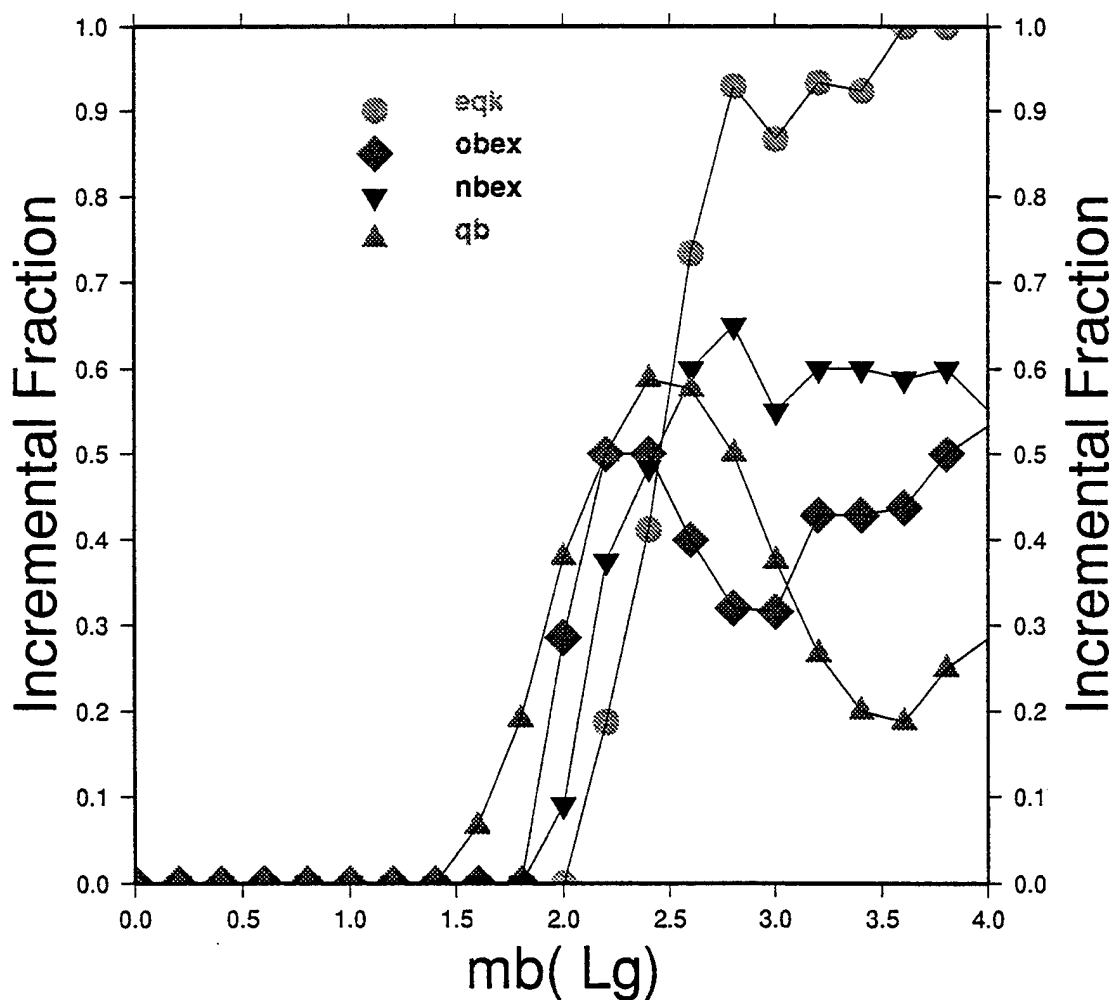
Figure 29.   The incremental fraction of events at 30N by 40E identified as earthquakes by the Lg/P discriminant a function of $m_b(Lg)$.

43

Discrimination bulletin: mideast.30x40.unf
network: cdxaug95.alp.me

A conditions:

Class c11: 2 or higher by spec'd discriminant

Discriminants   B conditions:

   Lg/Pg at one Hz   Class c16: occurring

areas: mideast.30x40   areas: mideast.30x40

mb range: 0.00 to 7.01   mb range: 0.00 to 7.01

Ms range: 0.00 to 4.98   Ms range: 0.00 to 4.98

depth range: -599.53 to 145.87   depth range: -599.53 to 145.87

first year and number of years: 81 1   first year and number of years: 81 1
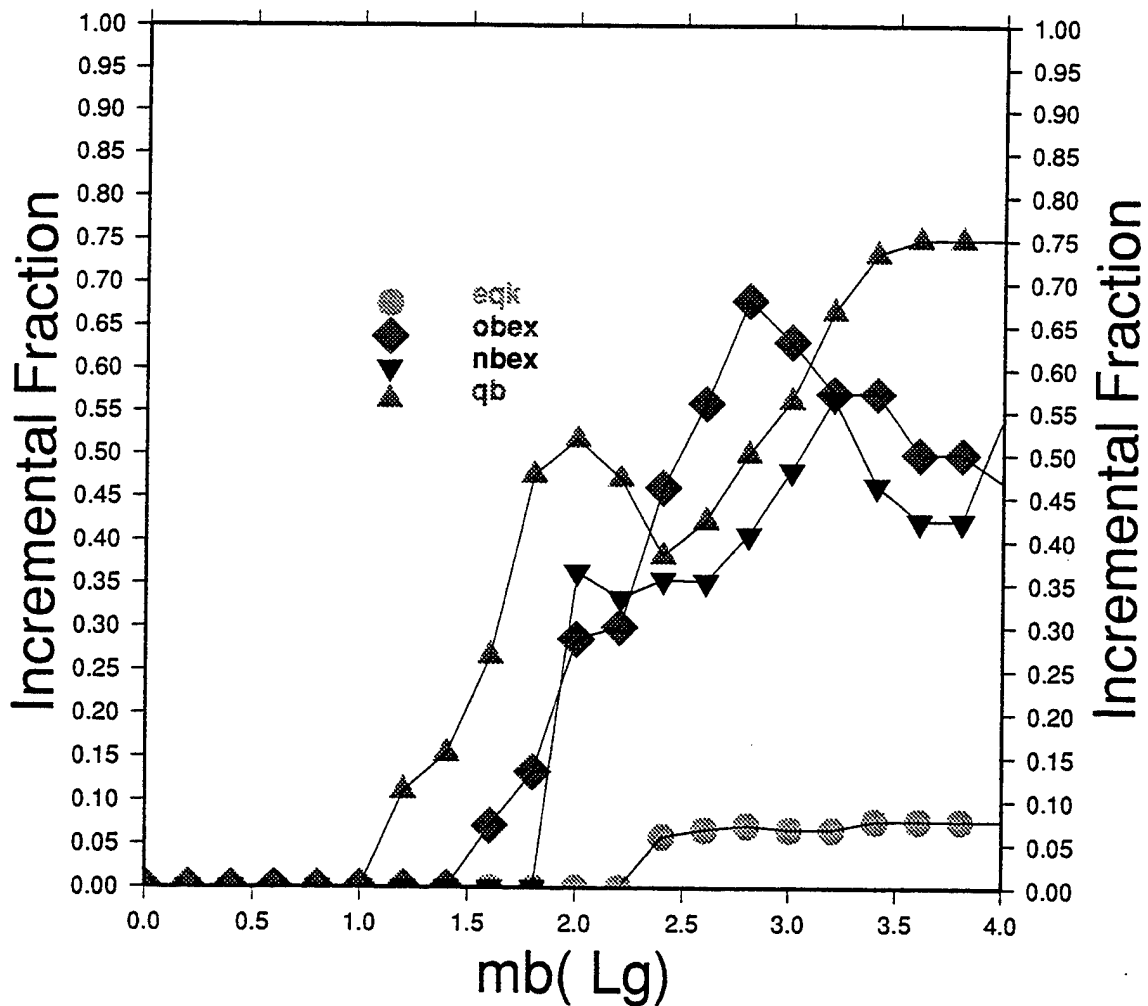
Figure 30.   The incremental fraction of events at 30N by 40E identified as explosions by the Lg/P discriminant a function of m_b(Lg).

44

explosions are identified as such and less than 10% of the earthquakes are explosion-like. This is because there is considerable overlap in the populations, as shown in Figure 31. We also find that the populations for the different sources overlap with respect to Lg spectral slope, except for quarry blasts, as shown in Figure 32. Thus, this discriminant poorly discriminates earthquakes from explosive tests.

These results are strongly dependent on the source excitation and propagation path parameters, which are, again, quite preliminary. More definitive results await calibration of the area.
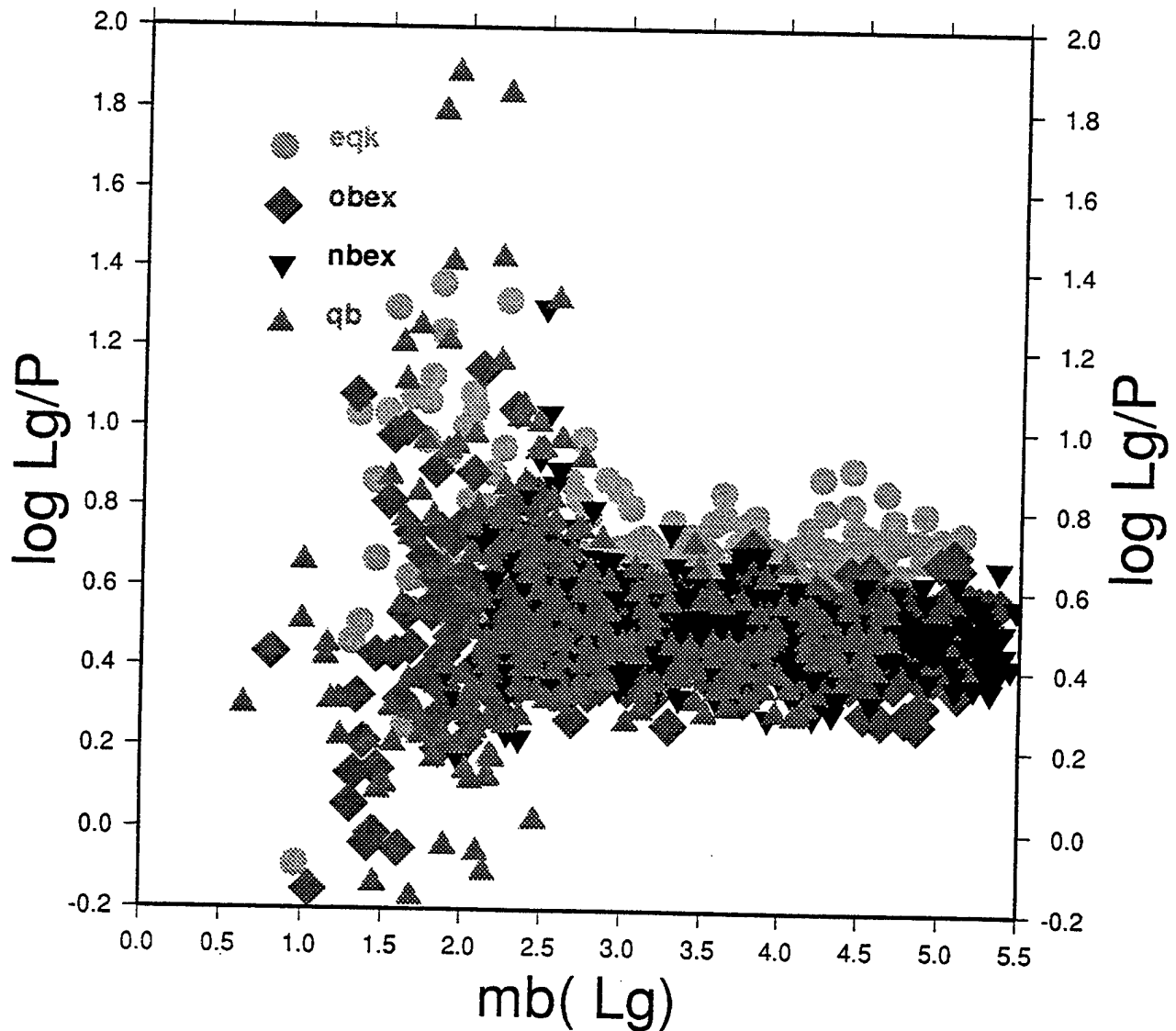
Figure 31.   Values of Lg/P versus m_b for events at 30N by 40E. P amplitudes
are the larger of Pn and Pg.

Discrimination bulletin: mideast.30x40.unf
network: cdxaug95.alp.me
A conditions:
Class c16: occurring
areas: mideast.30x40
mb range: 0.00 to 7.01
Ms range: 0.00 to 4.98
depth range: -599.53 to 145.87
first year and number of years: 81 1
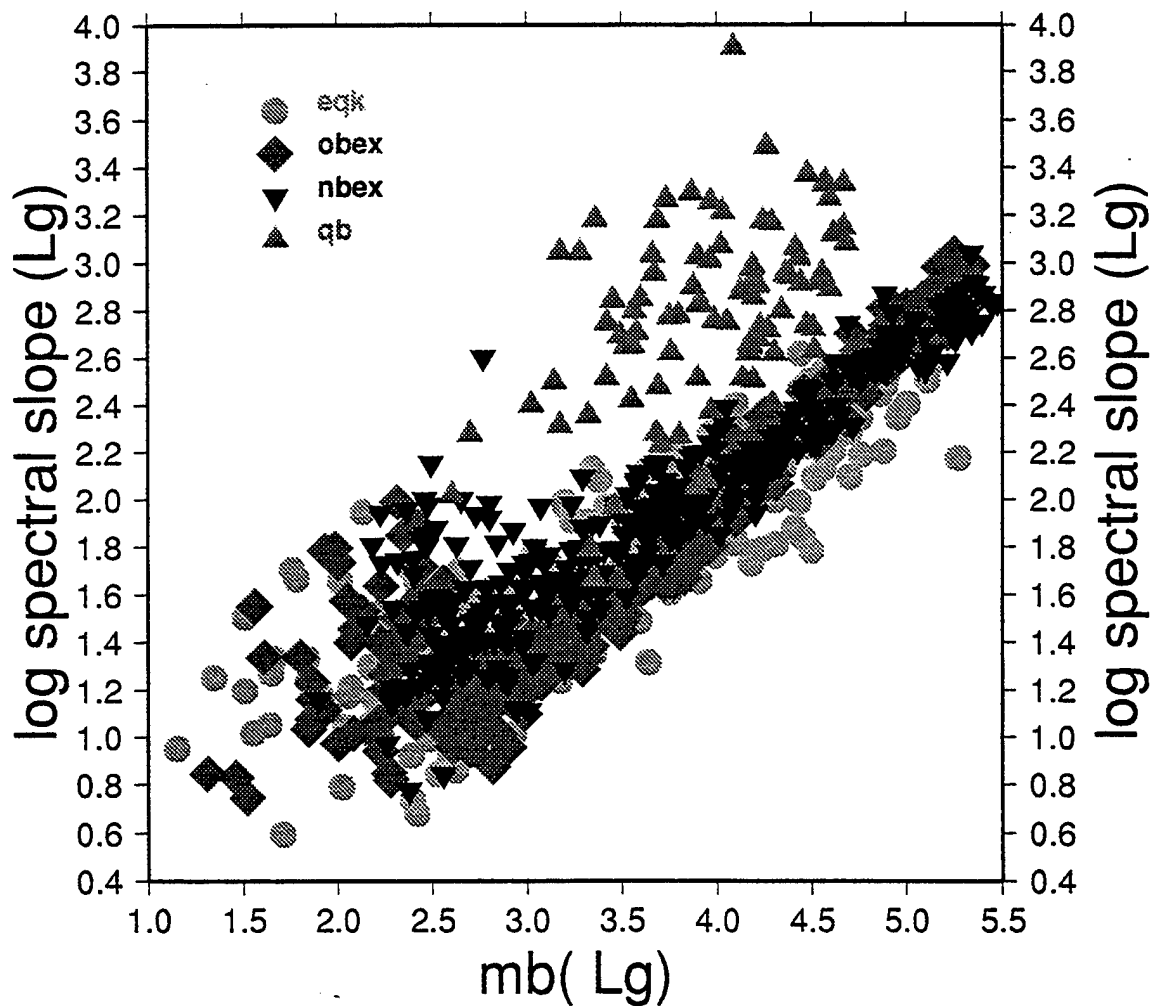
Figure 32. Values of Lg spectral slope versus m_b(Lg) for events at 30N by 40E.

4. References

Aki, K. and P.G. Richards (1980), "Quantitive Seismology," W.H. Freeman and Company, San Francisco.

Barker, T.G. and S.M. Day (1990), "A Simple Physical Model for Spall from Nuclear Explosions Based Upon Two-Dimensional Numerical Simulations," S-CUBED Technical Report GL-TR-90-0189, ADA231792.

Barker, T.G., K.L. McLaughlin and J.L. Stevens (1993), "Numerical Simulations of Quarry Blast Sources," S-CUBED Technical Report to Phillips Laboratory, PL-TR-93-13859, ADA265517.

Barker, T.G., K.L. McLaughlin and J.L. Stevens (1994), "Network Identification Capability Evaluation," S-CUBED Technical Report to Phillips Laboratory, PL-TR-94-2201, ADA292824.

Baumgardt, D.R. and G.B. Young (1990), "Regional Seismic Waveform Discriminants and Case-based Event Identification Using Regional Arrays," *Bull. Seism. Soc. Am., 80(B), 1872-1892.*

Baumgardt, D.R., G.B. Young and K.A. Ziegler (1991), "Design and Development of the Intelligent Event Identification System: Design Considerations and Processing for Regional Event Identification," S-CUBED Technical Report to Phillips Laboratory, PL-TR-91-2211, ADA246793.

Bennett, T.J., A.K. Campanella, J.F. Scheimer and J.R. Murphy (1992), "Demonstration of Regional Discrimination of Eurasian Seismic Events Using Observations at Soviet IRIS and CDSN Stations." S-CUBED Technical Report to Phillips Laboratory, PL-TR-92-2090, ADA253275.

Bouchon, M., M. Campillo, Gaffet, St., Massinon, B., Mechler, P., and F. Riviere (1991), "Propagation of Regional Seismic Phases in Western Europe," EOAD Final Report to Phillips Laboratory, PL-TR-91-2064, ADA237622.

Brune, J.N. (1970), "Tectonic Stress and the Spectra of Seismic Shear Waves from Earthquakes," *J. Geophys. Res., 75(26), 4997-5009.*

Campillo, M., Plantet, J.-L., M. Bouchon (1985), "Frequency Dependent Attenuation in the Crust Beneath Central France from Lg Waves: Data Analysis and Numerical Modeling," *Bull. Seism. Soc. Am., 75(5), 1395-1411.*

Day, S.M., N. Rimer and J.T. Cherry (1983), "Surface Waves from Underground Explosions with Spall: Analysis of Elastic and Nonlinear Source Models," *Bull. Seism. Soc. Am., 73, 247-264.*

Day, S.M. and K.L. McLaughlin (1991), "Seismic Source Representations for Spall," *Bull. Seism. Soc. Am., 81, 191-201.*

DuPont (1942), "Blaster's Handbook," E.I. duPont de NeMours & Co.

Dysart, P.S. and J.J. Pulli (1990), "Regional Seismic Event Classification at the NORESS Array: Seismological Measurements and the Use of Trained Neural Networks," *Bull. Seism. Soc. Am., 80(B), 1910-1933.*

Isrealsson,H. and J. Carter (1991), "Analysis of High Frequency Seismic Data", SAIC Scientific Report to Phillips Laboratory, PL-TR-91-2032, ADA235579.

Kvamme, L.B., R.A. Hansen and H. Bungum (1995), "Seismic-Source and Wave-Propagation Effects of Lg Waves in Scandinavia," *Geophys. J. Int, 120, 525-536.*

Langefors, U. and B. Kihlstrom (1963), "The Modern Techniques of Rock Blasting," John Wiley and Sons.

McLaughlin, K.L., T.G. Barker, S.M. Day, B. Shkoller and J.L. Stevens (1988), "Effects of Depth of Burial and Tectonic Strain Release on Regional and Teleseismic Waveforms," Technical Report to Air Force Geophysics Laboratory, AFGL-TR-88-0314, ADA207541.

McLaughlin, K.L., T.G. Barker and J.L. Stevens (1995), "Network Simulation Support," *Proceedings of ARPA CTBT Monitoring Technologies Conference, Chantilly, VA.*

Mueller, R.A. and J.R. Murphy (1971), "Seismic Characteristics of Underground Nuclear Explosions," *Bull. Seism. Soc. Am., 66, 1675-1692.*

Nuttli, O.W. (1986), "Yield Estimates of Nevada Test Site Explosions Obtained from Seismic Lg Waves," *J. Geophys. Res., 91(B2), 2137-2151.*

Ou, G.-B. and R. B. Herrmann (1990), "Estimation Theory for Peak Ground Motion," *Seism. Res. Lett., 61(2), 99-107.*

Patton, H.J. (1990), "Characterization of Spall from Observed Strong Ground Motions on Pahute Mesa," *Bull. Seism. Soc. Am., 80(5), 1326-1345.*

Patton, H. J. and S.R.Taylor (1993), "Analysis of Lg Spectral Ratios from NTS Explosions: Implications for the Source Mechanisms of Spall and the Generation of Lg Waves," *Bull. Seism. Soc. Am., XXX.*

Press, W.H., S.A Teukolsky, W.T. Vetterburg and B.P. Flannery (1986), "Numerical Recipes in FORTRAN", 2nd Edition, Cambridge University Press, New York, New York.

Pulli, J.J. and P.S. Dysart (1992), "Analysis and Testing of the High-Frequency Regional Discriminants," Technical Report to Phillips Laboratory, PL-TR-92-2125.

Schulte-Pelkum, V. (1993), "Lg Attenuation in Central Europe Inferred from GSETT-2 Data," Center for Seismic Studies Visiting Scientist Report C93-02.

Shih, X.R., Chun, K.-Y. and T. Zhu (1994), "Attenuation of 1-6 s Lg Waves in Eurasia", *J. Geophys. Res., 99(B12), 23,859-23,874.*

Richter, C.F (1958), "Elementary Seismology," W.H. Freeman and Company, Inc., San Francisco.

Stump, B.W. and R.E. Reinke (1988), "Experimental Confirmation of Superposition from Small-Scale Explosions," *Bull. Seism. Soc. Am., 78, 1059-1073.*

Stevens, J.L. (1986), "Estimation of Scalar Moments from Explosion-Generated Surface Waves," *Bull. Seism. Soc. Am., 76, 123-151.*

Taylor, S.R. and G.E. Randall (1989), "The Effects of Spall on Regional Seismograms," *Geophys, Res. Lett., 16, 211-214.*

Veith, K. F., and G. E. Claussen (1972), "Magnitude from Short-Period P-wave Data," *Bull. Seism. Soc. Am., 62, 435-452.*

Woods, B.W., S. Kedar and D.V. Helmberger (1993), "M_L:M_0 as a Regional Discriminant," *Bull. Seism. Soc. Am., 83(4), 1167-1183.*

Wuster, J. (1993), "Discrimination of Chemical Explosions and Earthquakes in Central Europe - A Case Study,"*Bull. Seism. Soc. Am., 83(4), 1184-1212.*

Zielhaus, A. and G. Nolet (1994), "Shear-Wave Velocity Variations in the Upper Mantle Beneath Central Europe," *Geophys. J. Int., 117, 685-715.*

Appendix A
File Descriptions

This appendix describes the files used by XNICE. All XNICE data files, source files, library files and executable files are assumed to be in a directory specified by the environment variable XNICE. In this directory is a file, called "Init", for initiating XNICE. The file sets additional environment variables that are used by the various programs in the XNICE system. Each man page has a "DIRECTORY" entry, which is the environment variable associated with the directory. The following is a sample Init file, with the directory tree starting at /sirius/itch/XNICE.

```
#!
# Initialize the user for XNICE

#===========================================================#
#        Variables to be set for each system this runs on        #
#===========================================================#

setenv XNICE /sirius/itch/XNICE

#===========================================================#
#       |        Environment variables   |       #
#===========================================================#

# Tell X where to find resource files
setenv XAPPLRESDIR $XNICE/Xresources

# Declare files readable, writable, executable by all
umask 0

# General use temporary
setenv XNICE_TEMP     $XNICE/temp
setenv XNICE_DATA     $XNICE/data

# Path to help screens
setenv XNICE_HELP     $XNICE/helpfiles

# The XNICE ORACLE tablespace name (not yet implemented)
setenv XNICE_ORA      XNICE/XNICE

setenv XNICE_SCRIPTS  $XNICE/scripts
```

```
# Nice environment variables
setenv SEISDIR  $XNICE_DATA/nice/seismicity
setenv EVGRIDDIR  $XNICE_DATA/nice/event_grids
setenv EVENTSDIR  $XNICE_DATA/nice/event_bulletins
setenv ARRDIR  $XNICE_DATA/nice/arrival_bulletins
setenv STNDIR  $XNICE_DATA/nice/stnfiles
setenv NTWRKDIR  $XNICE_DATA/nice/networks
# setenv DISCDIR $XNICE_DATA/nice/discrim_bulletins
setenv DISCDIR /sirius/itch2/barker/nice/discrim_bulletins
setenv BWTABLS $XNICE_DATA/nice/bwtables
setenv RGNLTABLS $XNICE_DATA/nice/regional_tables/regional_parms
setenv BWREFS  $XNICE_DATA/nice/reftab
setenv EIGDIR  $XNICE_DATA/nice/eigfiles
setenv INSTDIR $XNICE_DATA/nice/inst
setenv STRDIR  $XNICE_DATA/nice/str
setenv SYNDFL  $XNICE_DATA/nice/synwav_defaults
setenv ANALDFL  $XNICE_DATA/nice/anlyst_defaults
setenv RUNPARDIR  $XNICE_DATA/nice/run_parameters
setenv CONTOURDIR  $XNICE_DATA/nice/contour_data
setenv XYDATADIR  $XNICE_DATA/nice/xy_data
setenv NOISEDIR  $XNICE_DATA/nice/noise_spectra
setenv SRSDIR  $XNICE_DATA/nice/srs_spectra
setenv LATLONDIR  $XNICE_DATA/nice/latlon_parms
setenv MAGDIR  $XNICE_DATA/nice/magnitude_relations
setenv PMDDIR  $XNICE_DATA/nice/path_files
setenv PGRDIR  $XNICE_DATA/nice/path_files
setenv THRLOGDIR  $XNICE_DATA/nice/thresh_logs


#=============================================================#
#      |      set path and PATH |      #
#=============================================================#
setenv PATH ".:$XNICE/scripts:$XNICE/bin:$PATH"
setenv path ". $XNICE/scripts $XNICE/bin $path"
```

File Descriptions

FILE TYPE

    body wave reference amplitude file

USED BY

    synwav, evswan

CREATED BY

    user

DIRECTORY

    BWREFS

DESCRIPTION

This an ASCII file containing three reference values for which the body wave amplitude tables were computed. The files are read with FORTRAN free format statements (* format). There is a file for each teleseismic phase and are named to correspond to the phase name (e.g., P, pP). The three numbers are

1   The reference moment (N-m).
2   The reference value on the radiation pattern.
3   The reference receiver amplification function.

Here is an example file:

    4.e5 1. 1.

Values of the amplitude in the corresponding amplitude tables are scaled by the product of these three num bers.

FILE TYPE

body wave travel time and amplitude tables

USED BY

synwav, evswan

CREATED BY

user

DIRECTORY

BWTABLS

DESCRIPTION

This an ASCII file containing tables of travel time and amplitude versus distance for a sequence of focal depths. The files are read with FORTRAN free format statements (* format). There is a file for each teleseismic phase and are named to correspond to the phase name (e.g., P, pP). The data are stored in the following order:

record number	contents	description
1	n	number of depth samples
2	$z_1 z_2 \dots z_n$	focal depths
3	m	number of distance samples
4	$\Delta_1 \Delta_2 \dots \Delta_m$	distances
5	$T_{11} A_{11} \dots T_{n1} A_{n1}$	travel times and amplitudes for first depth
6	$T_{12} A_{12} \dots T_{n2} A_{n2}$	travel times and amplitudes for second depth
4+m	$T_{1m} A_{1m} \dots T_{nm} A_{nm}$	travel times and amplitudes for mth depth

Depths z are in km, distances Δ are in degrees, travel times in seconds and amplitudes have units m^{-1}. The amplitude curves are scaled by the reference amplitudes in the body wave reference files to match observed source strength-magnitude relations.

FILE TYPE

path: surface wave source and propagation functions

USED BY

CREATED BY

S-subed utility program

DIRECTORY

EIGDIR

DESCRIPTION

This file is a binary filke containing surface wave dispersion curves and eigenfunctions for a sequence of depths. The file is formed by using the S-subed utility program **eigcom** to combine files at individual source depths. These files are created by another S-subed utility program **synsrf** which computes surface waves according to the formalism in Appendix A. The binary files are written with the following FORTRAN statements:

```
write (luout) pathid
write (luout) nf
write (luout) (fr(i), i=1,nf), (pv(i), i=1,nf), (gv(i), i=1,nf),
(ar(i), i=1,nf), (el(i), i=1,nf), (gm(i), i=1,nf)
do over depths:
write (luout) zsrc, alpha, beta, rho, mu, lambda, sigma write (luout)
    ((eig(i,j), i=1,nf), j=1,4)
```

The variables have the following meaning (symbols in parentheses correspond to those in Appendix B):

name	description
pathid	80-character identifier
nf	the number of frequencies
fr	frequency array
pv	phase velocity array (c)
gv	group velocity array
ar	structure excitation function array (A_R)
el	ellipiticity array (e)
gm	the distance attenuation parameter γ array (γ)
zsrc	source depth (η_s)

alpha	P wave velocity at the source (α)
beta	S wave velocity at the source (β)
rho	density at the source (ρ)
m u	rigidity at the source (μ)
lambda	Lame' paramaeter λ at the source (λ)
σ	Poisson's ratio at the source (σ)
eig	source excitation function arrays array ($E_j, j=1,4$)

FILE TYPE

Event grid parameters

USED BY

events, evswan

CREATED BY

user

DIRECTORY

EVGRIDDIR

DESCRIPTION

As described in the **events** module manual page, the seismic event generator operates in one of two modes (specified by the grid flag in the run parameters file). Events can be located on a grid for making map views of identification properties or can be located in an area. The properties of the seismicity in the area described in the seismicity parameter file, described below. See the file description page for the seismicity parameter files for a description of events located in an area.

The event grid parameter file is an ASCII file that is used to describe attributes of the different source types. The keyword "type", followed by a source type string indicates that records to follow apply to that source type. The end of data for that source type is signaled by the keyword "end" (or the end-of-file). The entries are as follows:

type eqk (earthquakes)

keyword	fields	description
moment	minMo maxMo incMo	moment distribution (N-m)
depth	depth	source depth
latitude	minlat maxlat inclat	latitude bounds and increment (degrees)
longitude	minlon maxlon inclon	longitude bounds and increment (degrees)
fault	strike dip rake	fault orientation (degrees)
sdrop	stress_drop	stress drop (Pa)
nrealize	nrealize	number of realizations

Moments are distributed between minMo and maxMo at uniform intervals incMo. The grid spans "minlat" to "maxlat" latitudes at "inclat" intervals, and similarly for longitude. For each location, fault orientation and stress drop, "nrealize" realizations of the event are generated. This is done to compute thresholds in the examine module.

type nbex (normally buried explosions)

keyword	fields	description
yield	minY maxY incY	log yield bounds and increment
material	material_string	emplacement material
latitude	minlat maxlat inclat	latitude bounds and increment (degrees)
longitude	minlon maxlon inclon	longitude bounds and increment (degrees)
nrealize	nrealize	number of realizations

The material types are those programmed for the Mueller-Murphy source. Permissible values are tuff, granite, shale and salt. Epicenters are specified as with earthquakes (above). Depths of burial are assumed to occur at depths

$$d = 125\, Y^{1/3}.$$

type obex (overburied explosions)

keyword	fields	description
yield	minY maxY incY	log yield bounds and increment
material	material_string	emplacement material
latitude	minlat maxlat inclat	latitude bounds and increment (degrees)
longitude	minlon maxlon inclon	longitude bounds and increment (degrees)
dob	dob	depth of burial

The material types are those programmed for the Mueller-Murphy source. Permissible values are tuff, granite, shale and salt. Epicenters are specified as with earthquakes (above).

type qb (quarry blasts)

keyword	fields	description
yield	minY maxY incY	log yield bounds and increment
material	material_string	emplacement material
latitude	minlat maxlat inclat	latitude bounds and increment (degrees)
longitude	minlon maxlon inclon	longitude bounds and increment (degrees)

Yield here refers to the total yield (as opposed to individual charges). The material types are those programmed for the Mueller-Murphy source. Permissible values are tuff, granite, shale and salt. Epicenters are specified as with earthquakes (above). Depths of burial are computed according to standard blasting practices (see section of text describing source models).

A sample file follows:

```
type obex
latitude 10.0 40.0 15.0
longitude 25.0 70.0 15.0
yield .05 5. 20
dob 0.5
material granite
nrealize 10
end
type eqk
latitude 10.0 40.0 15.0
longitude 25.0 70.0 15.0
depth 10.0
moment 13.5 15.5 0.1
fault 90.00 60.00 -90.0
sdrop 1.00e+07
nrealize 10
end
```

FILE TYPE

instrument response

USED BY

CREATED BY

user

DIRECTORY

INSTDIR

DESCRIPTION

This file contains a long period or short period instrument response in the form of poles and zeros:

$$I(s) = \frac{A \prod_{j=1}^{n} (s - z_j)}{\prod_{j=1}^{m} (s - p_j)} ,$$

where I(s) is the Laplace transform of the instrument response (s = iω), A is a scale factor, z_1, ..., z_n are the zeros and p_1, ..., p_m are the poles. The contents of the ASCII instrument file are as follows:

record number	entry(s)
1	identifier/comment line (<= 80 characters)
2	A (the scale factor)
3	n (the number of poles)
4 through 4+m	real and imaginary parts of poles
5+m through 4+m+n	real and imaginary parts of zeros

Here is an example file:

+.461E-02
14

60

```
-.209E+00 +.341E-02
-.209E+00 -.341E-02
-.129E+00 +.270E+00
-.129E+00 -.270E+00
-.595E-01 +.236E-01
-.595E-01 -.236E-01
-.159E+00 +.594E+00
-.159E+00 -.594E+00
-.630E+00 0.
-.885E-01 0.
-.856E+00 +.255E+00
-.856E+00 -.255E+00
-.541E+00 +.683E+00
-.541E+00 -.683E+00
4
0. 0.
0. 0.
0. 0.
0. 0.
```

FILE TYPE

magnitude vs yield or moment relations

USED BY

synwav, anlyst, evswan, xnice

CREATED BY

user

DIRECTORY

MAGDIR

DESCRIPTION

This file contains coefficients for linear relationships between magnitude (mb) and yield or moment. Each record contains information for a particular phase, and records are read until an end-of-file is sensed. The data for each record in the order

phase_name yield_or_moment c1 c2

where phase_name is a string giving the name of the phase (P, Lg), yield_or_moment is a string which is either "moment" or "yield", and c1 and c2 are the coefficients.

$$m_b = c1 + c2 \log (\text{moment})$$

if yield_or_moment is "moment", or

$$m_b = c1 + c2 \log (\text{yield})$$

if yield_or_moment is "yield."

Here is an example file:

P yield 3.5 0.75
P moment -12.2 1.0
pP yield 3.5 0.75
pP moment -12.2 1.0
S yield 3.5 0.75
S moment -12.2 1.0
Lg yield 3.5 0.75

Lg moment -12.2 1.0
Pg yield 3.5 0.75
Pg moment -12.2 1.0
Pn yield 3.5 0.75
Pn moment -12.2 1.0
Sn yield 3.5 0.75
Sn moment -12.2 1.0
R yield 2.0 1.0
R moment -12.1 1.0

FILE TYPE

network station list

USED BY

events, synwav, anlyst, evswan, xnice

CREATED BY

user

DIRECTORY

NTWRKDIR

DESCRIPTION

This file conains a list of the stations that comprise the network to be modeled. The names correspond to those in the STNFILES station description files. The file is ASCII with one station name per record.

FILE TYPE

noise spctrum

USED BY

synwav, evswan

CREATED BY

user

DIRECTORY

NOISEDIR

DESCRIPTION

This is an ASCII file containing a ground noise spectrum. The file contains an 80 character header in the first record followed by the number of spectral values in the second record. The remainder of the file is a sequence of records each having three values: frequency, log of mean noise (in microns), log of standard deviation of noise.

FILE TYPE

Regional propagation parameters

USED BY

synwav, anlyst, evswan, xnice

CREATED BY

user

DIRECTORY

RGNLTABLS

DESCRIPTION

This is an ASCII file containing propagation and source excitation relations for regional phases. The file names associate the files with phases (e.g., Lg, Pg). The first entry of each record is a keyword, with one or more entries on the record. Earthquake amplitudes are assumed to follow a Nuttli-type law:

$$A(f) = S(\Delta/\Delta_0)^{-n} e^{-\gamma(\Delta-\Delta_0)} \tag{1}$$

where γ is related to Q through the relation

$$\gamma(f) = \frac{\pi f}{U_g Q(f)} \tag{2}$$

and

$$Q(f) = Q_0 f^\eta$$

In addition, the excitation of an explosion and vertical force relative to an earthquake is specified as polynomials in log(f). That is,

$$\log \frac{A_{src}(f)}{A_{eqk}(f)} = \sum_{i=0}^{m} a_i^{src} \log^i(f)$$

where src is either explosion or vertical force.

66

The fields following the keywords are as follows (referring to the equations above):

keyword	description	units
Ug	U_g	m/sec
delta0	Δ_0	m
n	n	dimensionless
Q0	Q_0	dimensionless
S	S	m/N-m (amplitude per moment)
exs	$m\ c_1^{exp} \ldots c_m^{exp}$	dimensionless
sps	$m\ c_1^{vt} \ldots c_m^{exp}$	m (moment per force)

Here is an example file:

```
Ug 3500.
delta0 1.264e5
n 0.83333
Q0 4.e2 0.45
S -20.5
exs 2 0.4 -1.1
sps 2 3.6 -1.2
```

FILE TYPE

propagation parameters

USED BY

events, synwav, anlyst, evswan, xnice

CREATED BY

user

DIRECTORY

RUNPARDIR

DESCRIPTION

The propagation parameter files contain file and directory names that are used by the **xnice** system. Most of the files are used by several of the modules. The files can be created using the **xnice** users interface or by entering the values with an editor. The files are ASCII, with each record containing a keyword followed by a file name or parameter values. The entries are as follows. Descriptions of the files can be found in this appendix. The last word in parentheses in the following descriptions indicates which modules use the file (and where more details can be found). The records may be in any order.

keyword	description
network	network station list file name (events, synwav, anlyst)
events	events catalog file name (events, synwav)
arrivals	arrivals catalog file name (synwav, anlyst)
discrim	discrimination catalog file name (anlyst, xnice)
grid	This entry indicates whether the event locations are specified by a seismicity or grid file (events).
year	years in which events occur (used only if natural seismicity is specified). (events)
area	area (seismicity file) name (events)
lpinst	long period instrument response file name (synwav)
spinst	short period instrument response file name (synwav)

path	surface wave eigenfunction and dispersion file name (synwav)
str	structure file name (synwav)
bwdir	body wave travel time and amplitude directory (synwav)
refdir	body wave reference amplitude directory (synwav)
rgnldir	regional wave propagation parameter directory (synwav, anlyst)
properr	propagation errors list (synwav, anlyst)
freq	frequencies at which regional amplitude spectra are computed (synwav, anlyst).
magrels	magnitude relations file name (synwav, anlyst)
bwmeth	body wave calculation method (convolution or magnitude) (synwav)
swmeth	surface wave calculation method (synsrf or magnitude). If magnitude is specified, the magnituude relation and tectonic type must follow (synwav).
pmdfil	path medium description file name (synwav)
pgrfil	path grid file name (synwav)

FILE TYPE

Seismicity parameters

USED BY

events, evswan

CREATED BY

xnice, user

DIRECTORY

SEISDIR

DESCRIPTION

As described in the **events** module manual page, the seismic event generator operates in one of two modes (specified by the grid flag in the run parameters file). Events can be located on a grid for making map views of identification properties or can be located in an area. The properties of the seismicity in the area described in the seismicity parameter file, described below. See the file description page for the event grid parameter files for a description of events located on a grid.

The seismicity parameter file is an ASCII file that is used to describe attributes of the different source types. The keyword "type", followed by a source type string indicates that records to follow apply to that source type. The end of data for that source type is signaled by the keyword "end" (or end-of-file). The entries are as follows:

type eqk (earthquakes)

keyword	fields	description
moment	a b minMo natural	b-value recurrence rate (N-m)
moment	minMo maxMo numMo uniform	uniform moment distribution (N-m)
years	year1 nyrs	interval for natural recurrence
depth	ndep	number of segments in depth distribution

z_1 f_1 depth and cumulative fractions

.   .
.   .
.   .

$z_{ndep}f_{mdep}$
epicenters   lat1 lon1 lat2 lon2 l12   epicenter box (degrees)
strike   strike σ strike and standard deviation (degrees)
dip   dip σ dip and standard deviation (degrees)
rake   rake σ rake and standard deviation (degrees)
sdrop   stress_drop σ stress drop and standard deviation (Pa)

The moment distribution is specified in two ways, depending on the fourth field in the "moment" record. If the fourth field is "uniform", moments are distributed between minMo and maxMo at uniform intervals numMo. If the fourth field is "natural", the cumulative number of events having a moment greater than M_0 follow the relation

$$\log N(M_0) = a - b\,\log(M_0), M_0 > \min M_0 .$$

where a is the average number of events per year. The interval in seconds between events at a particular moment is

$$t = -\log(1.-RV)/n_s$$
$$n_s = N(M_0)/N_{sec}$$

where N_{sec} is the number of seconds per year. Origin times begin at the beginning of the first year "year1" and continue to the end of year "year1" + "nyrs" - 1.

The cumulative number of events occuring at or below a particular depth is piecewise linear. The number of linear segments is the field after the keyword "zdist". The values of depth z_j and the cumulative fraction f_j of events occuring at or below that depth are entered in ndep records following the "zdist" record. A realization of the depth distribution will have a source depth z_s at

$$z_s = z_j + \left(f_R - f_j\right)\frac{z_{j+1} - z_j}{f_{j+1} - f_j}$$

where f_R is a random variable distributed on [0,1] and j satisfies $f_j \le f_R < f_{j+1}$.

Epicenters are distributed over boxes in the surface of the globe. Denote by $P_j = (\theta_\varphi, \varphi_j), j = 1,2,3,4$ the colatitude-longitude pairs at the corners of the box, as shown in Figure A.1. The lines connecting the corners are great circles and

71

intersect at right angles. The indeces increase counter-clockwise from P_1. The arcs connecting P_i to P_j have lengths l_{ij} and the bearing (clockwise from north) of P_j to P_i is α_{ij} The positions P_1, P_2 and the arc l_{12} are specified as the lat1, lon1, lat2, lon2, l12 fields following the "epicenter" keyword. The coordinates of a realization of the epicenter distribution are given by

$$\theta_R = \cos^{-1}\left[\cos(\theta_1)\cos(\Delta_{1R}) - \sin(\theta_1)\sin(\Delta_{1R})\cos(\alpha_{12} - \alpha_{1R})\right]$$

$$\phi_R = \phi_1 + \sin^{-1}\left[\sin(\Delta_{1R})\sin(\alpha_{12} - \alpha_{1R})/\sin(\theta_R)\right]$$

where
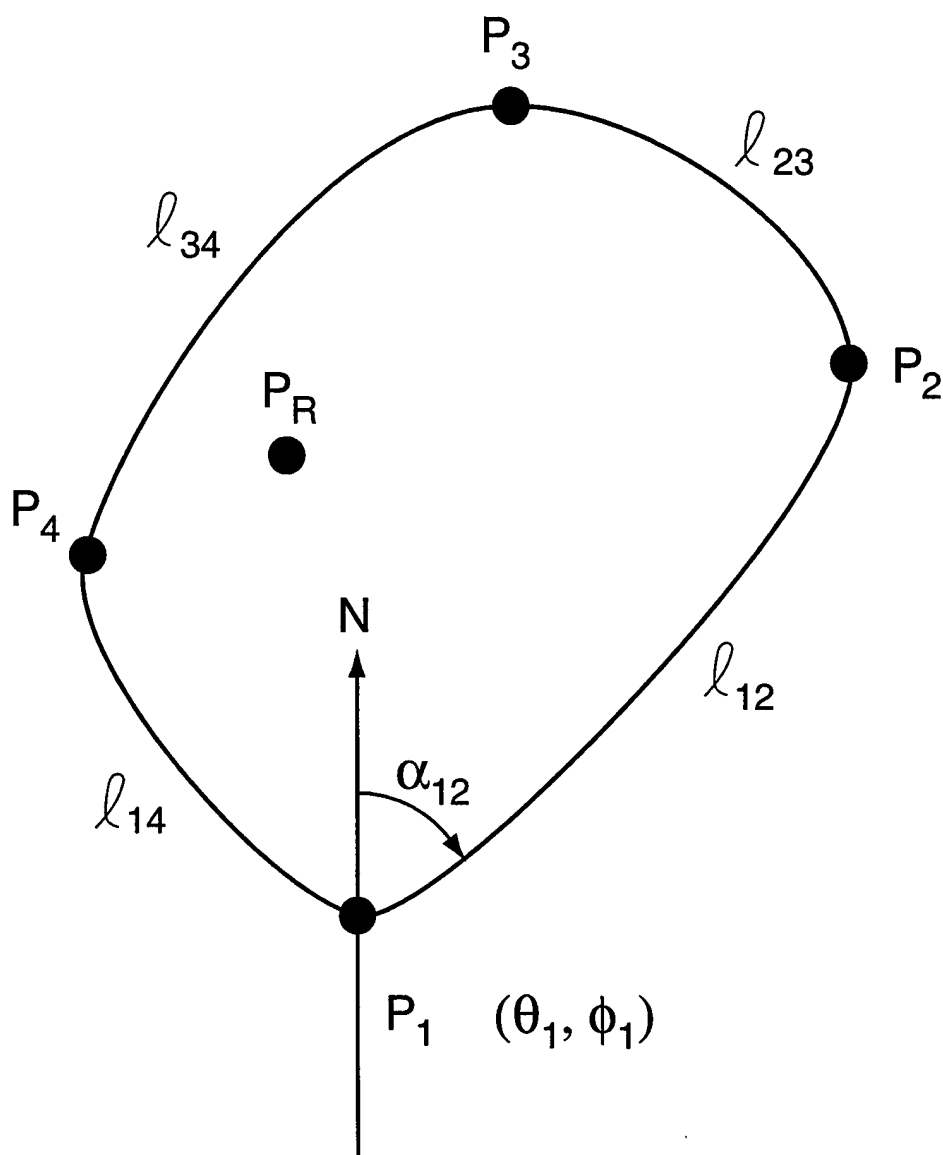
Figure A.1   The box containing epicenters is shown. Arcs are great circles of length ℓ_{ij} intersecting at right angles at points P_j with colatitude-longitude pairs (θ_j, ϕ_j). The meridian through P_1 is shown to illustrate the angle α_{12}.

$$\Delta_{1R} = \cos^{-1}\left[\cos(\rho_{12})/\cos(\rho_{14})\right]$$

$$\alpha_{1R} = \sin^{-1}\left[\sin(\rho_{14})/\sin(\Delta_{1R})\right]$$

The arcs ρ_{12} and ρ_{12} are random variables uniformly distributed on $[0, l_{12}]$ and $[0, l_{14}]$, respectively.

type nbex (normally buried explosions)

keyword	fields	description
yield	minY maxY numY	yield bounds and number of yields
material	material_string	emplacement material
epicenters	lat1 lon1 lat2 lon2 l12	epicenter box (degrees)
date	day/month/year	date of occurence of explosions
time	hr/min/sec	time of day of occurence of explosions

The material types are those programmed for the Mueller-Murphy source. Permissible values are tuff, granite, shale and salt. Epicenters are specified as with earthquakes (above). In addition, if a single pair of numbers follows the "epicenter" keyword, the pair is interpreted as a latitude and longitude at which all events are placed. Depths of burial are assumed to occur at

$$d = 125\,Y^{1/3}$$

type obex (over buried explosions)

keyword	fields	description
yield	minY maxY numY	yield bounds and number of yields
material	material_string	emplacement material
epicenters	lat1 lon1 lat2 lon2 l12	epicenter box (degrees)
depth	ndep	number of segments in depth distribution
z_1 $\quad f_1$		depth and cumulative fraction
. .		
. .		
. .		
z_{ndep} f_{ndep}		
date	day/month/year	date of occurrence of explosions
time	hr/min/sec	time of day of occurence of explosions

The material types are those programmed for the Mueller-Murphy source. Permissible values are tuff, granite, shale and salt. Epicenters are specified as with earthquakes (above). In addition, if a single pair of numbers follows the "epicenter" keyword, the pair is interpreted as a latitude and longitude at which all events are placed. Depths of burial are specified as with earthquakes, as well. A velue of ndep=1, followed by a record with a single depth value will cause all the explosions to occur at that depth.

type qb (quarry blasts)

keyword	fields	description
yield	minY maxY numY	log yield bounds and number of yields
material	material_string	emplacement
material epicenters	lat1 lon1 lat2 lon2 l12	epicenter box (degrees)
date	day/month/year	date of occurence of explosions
time	hr/min/sec	time of day of occurence of explosions

Yield here refers to the total yield (as opposed to individual charges). The material types are those programmed for the Mueller-Murphy source. Permissibale values are tuff, granite, shale and salt. Epicenters are specified as with earthquakes (above). In addition, if a single pair of numbers follows the "epicenter" keyword, the pair is interpreted as a latitude and longitude at which all events are placed. Depths of burial are computed according to standard blasting practices (see section of text describing source models).

A sample file follows:

```
type obex
yield 0.01 20. 100
depth 1
0.5
material granite
date 22/3/72
time 01:02:22.4
epicenters 30. 15.0
end
# ----------
type nbex
yield 0.01 20. 100
material granite
date 02/5/72
time 01:02:22.4
epicenters 30. 15.0
```

```
end
# ----------
# ----------
type qb
yield .1 20. 100
material  shale
date 22/3/74
time 01:02:22.4
epicenters 30. 15.0
end
# ----------
type eqk
moment        13.5 15.5 100 uniform
depth 2
0.000  1.000
50.000 0.000
epicenters    30.00   14.50   30.00 14.50    1.00
strike 28.00  30.00
dip     34.00  30.00
rake   -80.00 30.00
sdrop 1.e7 2.e6
end
```

FILE TYPE

site response spctrum

USED BY

synwav, evswan

CREATED BY

user

DIRECTORY

SRSDIR

DESCRIPTION

This is an ASCII file containing a site response spectrum. The file contains an 80 character header in the first record followed by the number of spectral values in the second record. The remainder of the file is a sequence of records each having two values:

frequency, log of gain

FILE TYPE

station file

USED BY

events, synwav, anlyst, evswan, xnice

CREATED BY

user

DIRECTORY

STNDDIR

DESCRIPTION

The station files contain locations, noise values, downtime values and names of noise and array gain files. These are ASCII files which are read in FORTRAN free format. After the first record, which contains the station name and type, keywords are used to indicate what data follow the keywords. The contents of the files are as follows:

Record 1:

station_name station_type

The character string station_name is usually the same as the file name, and the string station_type has the permissible values
    1C (one component single station)
    3C (three component single station)
    array (three component array)

For a record starting with the keyword **loc**

loc latitude longitude elevation

For a record starting with the keyword **down**

down f

where f is the fraction of time the station is expected to be down.

Records starting with and including the keyword **bwnoise** contain telesesmic and regional noise statistics.

Record number	contents	description
1	bwnoise nph	nph is the number of phase noise data to follow
2 to 2+nph	name mb A σ tt time σ sl σ az σ	amplitude, travel time, slowness and azimuth noise levels

The string "name" is the phase name (e.g., P, Lg). The two values that follow the keyword mb are the mean and standard deviation of the log of ground noise at the frequency at which the amplitude measurement is made. Note that these values are not used if a noise spectrum file is specified (see below). The two values that follow the keyword tt are the mean and standard deviation of the travel time at the frequency at which the measurement is made. The value that follows the keyword sl is the standard deviation of slowness and the value that follows the keyword az is the standard deviation of azimuth (applicable only to 3 component stations and arrays). Negative values for the azimuth and slowness standard deviations are used to indicate they are not applicable (e.g., for 1C stations or they are unknown).

Records starting with and including the keyword **swnoise** contain telesesmic surface wave noise statistics.

Record number	contents	description
1	swnoise nph	nph is the number of phase noise data to follow
2 to 2+nph	name ms A σ	amplitude noise levels

The string name is the phase name (e.g., R, L). The two values that follow the keyword ms are the mean and standard deviation of the log of ground noise at the frequency at which the amplitude measurement is made. Note that these values are not used if a noise spectrum file is specified and there is an entry in the spectrum for a period of 20 seconds (see below).

For record starting with the keyword **noise_spectrum**

noise_spectrum file_name

where file_name is the name of the noise spectrum file.

For record starting with the keyword **srs_spectrum**

srs_spectrum file_name

where file_name is the name of the site response spectrum (array gain) spectrum file.

Here is an example file:

```
ALQ 1C
loc 34.9425 -106.4575
down 0.05
bwnoise 7
P mb -3.62212 0.200000 tt 0.0 1.0 sl -1az -1.
pP mb -3.62212 0.200000 tt 0.0 1.0 sl -1. az -1.
S mb -3.62212 0.200000 tt 0.0 3.0 sl -1. az -1.
Lg mb -3.62212 0.200000 tt 0.0 2.0 sl -1. az -1.
Pn mb -3.62212 0.200000 tt 0.0 2.0 sl -1. az -1.
Pg mb -3.62212 0.200000 tt 0.0 2.0 sl -1.
Sn mb -3.62212 0.200000 tt 0.0 2.0 sl -1. az -1. swnoise 1
R ms 0.0 0.2
noise_spectrum ALQX_day
```

FILE TYPE

Earth structure file

USED BY

synwav, anlyst, evswan

CREATED BY

user

DIRECTORY

STRDIR

DESCRIPTION

This file contains the plane layered earth model. The contents of the ASCII file are as follows:

Record 1 contains an 80 characters comment/identifier. Record 2 contains two integers, the number of layers and a units flag (0 indicates mks units, 1 indicates "seismologist" units, viz. velocities in km/sec and densities in gm/cc). The remainder of the file has the elastic properties with one record per layer.

Records 3 through 3+nlayrs:

$$h \; \alpha \; \beta \; \rho \; Q_\beta \; Q_\alpha$$

where h is the layer thicknes, α, β , ρ are the layer P velocity, S velocity and density, respectively, and Q_β and Q_α are the shear and compressional quality factors.

Here is an example file:

```
Eastern U.S. structure from Herrmann and Kijko (1983)
5 1
1.     5.0     2.89    2.5     1200.   600.
9.     6.1     3.52    2.7     1200.   600.
10.    6.4     3.70    2.9     1200.   600.
20.    6.7     3.87    3.0     8000.   4000.
20.    8.15    4.7     3.4     8000.   4000.
```

Appendix B
Synthetic Surface Wave Seismograms

Because surface waves are dispersed, it is necessary to compute a complete time series at each value of range. At a given range, source depth and orientation, the surface wave displacement spectrum is computed using the formulation in Harkrider (1970) and Aki and Richards (1980):

$$u(\omega,r,h,\phi) = (2\pi kr)^{-1/2} A_R(\omega) \sum_{j=1}^{3} \chi_j(\omega,r,h_s,\phi) \exp\left[i\frac{\pi}{4} - ik(\omega)r - \gamma r\right]\varepsilon(\omega)I(\omega)$$

where

ω = is angular frequency,

r = range,

ϕ = azimuth, measured clockwise from North,

h_s = source depth,

$A_R(\omega)$ = structure excitation function,

$X_j(\omega,h_s,\phi)$ = source excitation function,

$S(\omega)$ = source spectrum,

$\varepsilon(\omega)$ = a function depending on the desired component of motion,

$c(\omega)$ = phase velocity,

$k(\omega) = \omega/c(\omega)$ is the horizontal wave number,

$\gamma(\omega)$ = radial attenuation operator,

$I(\omega)$ = the instrument response.

The excitation functions X_j are given in terms of the four stress-displacement eigenfunctions $E_i(h_s)$, i=1,2,3,4 and components of the moment tensor

$$\chi_1 = E_1\left[M_{xx}\cos^2\phi + 2M_{yy}\sin^2\phi\right]$$

$$\chi_2 = \frac{i}{\mu}E_4\left[M_{xz}\cos\phi + M_{yz}\sin\phi\right]$$

$$\chi_3 = -\frac{1}{\rho\alpha^2}(E_3 + \lambda E_1)M_{zz}$$

The functions A_R and E are related to the functions r_i, i=1,2,3,4 in Aki and Richards (1980) in the following way:

83

$$E_1 = k r_1$$

$$E_3 = -k\lambda r_1 - (\lambda + 2\mu)\frac{\partial r_2}{\partial z}$$

$$E_4 = \mu\left(\frac{\partial r_1}{\partial z} - k r_2\right)$$

$$A_R = \frac{r_2}{4c U I_1}$$

where U is group velocity and

$$I_1 = \frac{1}{2}\int_0^\infty \rho\left(r_1^2 + r_2^2\right)dz$$

The function $\varepsilon(\omega)$ is given by

$\varepsilon = -1$ for the vertical component (positive up), and

$\varepsilon = ie(\omega)$ for the radial component, where e is the ellipticity.

The elastic parameters ρ, α, β and λ are the density, compressional velocity, shear velocity and Lame' parameter, respectively, at the source.

The functional form of the moment tensor depends on the source type. For earthquakes, the moment tensor is given of the fault strike ϕ_s, dip δ, rake Λ, scalar moment M_0 and source spectrum $\Omega(\omega)$ by (Aki and Richards, 1980):

$$M_{xx} = -\Omega(\omega)M_0\left(\sin\delta\cos\Lambda\sin2\phi + \sin2\delta\sin\Lambda\sin^2\phi_s\right)$$

$$M_{xy} = -\Omega(\omega)M_0\left(\sin\delta\cos\Lambda\sin2\phi + \frac{1}{2}\sin2\delta\sin\Lambda\sin2\phi_s\right)$$

$$M_{xy} = -\Omega(\omega)M_0\left(\cos\delta\cos\Lambda\cos2\phi + \sin2\delta\sin\Lambda\sin2\phi_s\right)$$

$$M_{yy} = -\Omega(\omega)M_0\left(\sin\delta\cos\Lambda\sin2\phi - \sin2\delta\sin\Lambda\cos^2\phi_s\right)$$

$$M_{yz} = -\Omega(\omega)M_0\left(\cos\delta\cos\Lambda\sin2\phi - \cos2\delta\sin\Lambda\cos\phi_s\right)$$

$$M_{zz} = \Omega(\omega)M_0\sin2\delta\sin\Lambda$$

We use the source spectrum moment from Brune (1970):

84

$$L = \left(0.39 \frac{M_0}{\sigma} \right)^{1/3}$$

$$f_c = 2.22 \frac{\beta}{L}$$

$$\Omega(\omega) = \frac{f_c^2}{f_c^2 + \omega^2}$$

where σ is the stress drop.

For overburied explosions,

$$M_{xx} = M_{yy} = M_{zz} = 4\pi\rho\alpha^2\Psi(\omega)$$

$$M_{xy} = M_{xz} = M_{yz} = 0$$

where $\Psi(\omega)$ is the reduced displacement potential, for which we use the expressions derived by Mueller and Murphy (1971). Normally buried explosions induce a spall phase, but, as shown by Day, *et al.* (1983), the contribution from spall to surface waves at long periods is negligible. Thus normally buried and overburied explosions are modeled the same. For the same reason, surface waves from quarry blasts include only the explosive component.

Body Wave Synthetic Seismograms

The vertical displacement at a position $\underline{r}$ can be expressed as the product of a source excitation term times the product of transfer functions that quantify the effects of propagation and the recording instrumentation:

$$u(\omega,\underline{r}) = S(\omega,\theta,\phi)T^{(S)}(\omega,\theta)T^{(M)}(\omega)T^{(R)}(\omega,r)A(\omega)I(\omega)$$

where

$\underline{u}(\omega,\underline{r})$ is the displacement vector at the position $\underline{r} = (r,\omega,\phi)$ measured in a spherical coordinate system whose origin is the source.

$S(\omega,\theta,\phi)$ is the displacement spectrum as a function of the azimuth ϕ and takeoff angle θ.

$T^{(S)}(\omega,\theta)$ is the source region transfer function which quantifies the change in the wavefield leaving the source due to the source region structure.

$T^{(M)}(\omega)$ is the mantle transfer function which accounts for geometric spreading in the mantle.

$T^{(R)}(\omega, r)$ is the receiver function which propagates a wave impinging on the receiver region from below to the earth's surface as either vertical, radial of transverse components.

$A(\omega)$ is the anelastic attenuation operator.

$I(\omega)$ is the recording instrument response.

In XNICE, we have assumed that the mantle transfer function obeys geometric ray theory, that is

$$T^{(M)}(\omega) = \frac{1}{R}\delta(t - t_0)$$

where R^{-1} is a geometric spreading factor and t_0 is the travel time. The **synwav** module finds the values of R^{-1} and t_0 from bilinear interpolation of tables of $R^{-1}(r,z)$ and $t_0(r,z)$ (r is angular distance and z is focal depth).

The source excitation is given by (following Aki and Richards, 1980)

$$S^P = \frac{1}{4\pi\rho\alpha^3} \gamma \dot{\underline{M}} \cdot \underline{\gamma}$$

$$S^{SV} = \frac{1}{4\pi\rho\beta^3} \hat{\underline{p}} \dot{\underline{M}} \cdot \underline{\gamma}$$

$$S^{SH} = \frac{1}{4\pi\rho\beta^3} \hat{\phi} \dot{\underline{M}} \cdot \underline{\gamma}$$

where the vectors $(\gamma, \hat{p}, \hat{\phi})$ form a coordinate system moving with the ray with γ pointing along the ray, $\hat{p}$ transverse and in a vertical plane and $\hat{\phi}$ transverse and in a horizontal plane. The tensor $\underline{M}$ is the time rate of change of the moment tensor. In a coordinate system (x,y,z) whose unit vectors point north, east and down, the ray vectors are

$$\gamma = \chi \sin\theta\cos\phi + y \sin\theta\sin\phi + z \cos\theta$$
$$p = \chi \cos\theta\cos\phi + y \cos\theta\sin\phi - z \sin\theta$$
$$\phi = \chi \sin\phi + y \cos\phi.$$

The values of θ are found by first finding the phase velocity from the travel time tables

$$c = \frac{dt_0}{dr}$$

and computing

$$\theta = \sin^{-1}(\alpha/c)$$

where α_s is evaluated at the source (with a similar expression for S waves).

The functional form of the moment tensor depends on the source type. For earthquakes, the moment tensor withfault strike ϕ_s, dip δ, rake Λ, scalar moment M_0 and source spectrum $\Omega(\omega)$ is given by (Aki and Richards, 1980):

$$M_{xx} = -\Omega(\omega)M_0\left(\sin\delta\cos\Lambda\sin2\phi + \sin2\delta\sin\Lambda\sin^2\phi_s\right)$$

$$M_{xy} = \Omega(\omega)M_0\left(\sin\delta\cos\Lambda\sin2\phi + \frac{1}{2}\sin2\delta\sin\Lambda\sin2\phi_s\right)$$

$$M_{xy} = -\Omega(\omega)M_0\left(\cos\delta\cos\Lambda\cos2\phi + \sin2\delta\sin\Lambda\sin2\phi_s\right)$$

$$M_{yy} = \Omega(\omega)M_0\left(\sin\delta\cos\Lambda\sin2\phi - \sin2\delta\sin\Lambda\cos^2\phi_s\right)$$

$$M_{yz} = -\Omega(\omega)M_0\left(\cos\delta\cos\Lambda\sin2\phi - \cos2\delta\sin\Lambda\cos\phi_s\right)$$

$$M_{zz} = \Omega(\omega)M_0\sin2\delta\sin\Lambda\ .$$

We use the source spectrum moment from Brune (1970):

$$L = \left(0.39\frac{M_0}{\sigma}\right)^{1/3}$$

$$f_c = 2.22\frac{\beta}{L}$$

$$\Omega(\omega) = \frac{f_c^2}{f_c^2 + \omega^2}$$

where σ is the stress drop.

For overburied explosions,

$$M_{xx} = M_{yy} = M_{zz} = 4\pi\rho\alpha^2\Psi(\omega)$$

$$M_{xy} = M_{xz} = M_{yz} = 0$$

where $\Psi(\omega)$ is the reduced displacement potential, for which we use the expressions derived by Mueller and Murphy (1971). A free surface reflection is modeled as an elastic reflection and is added to the direct solution above with the appropriate lag.

Normally buried explosions induce a spall phase, which is modeled as a tension crack. The tension crack solution is added to the direct explosion signal above (Barker, *et al.*, 1990). The tension crack is also used to model the spall associated with quarry blasts (Barker, *et al.*, 1993). For a horizontal tension crack

$$M_{yy} = M_{xx} = \lambda s(t)$$

$$M_{zz} = (\lambda + 2\mu)s(t)$$

where s(t) describes the tension crack opening. Following Barker and Day (1990), we write the results for a tension crack which moves a mass m_{sp} upwards at a velocity v_{sp} for a duration T and approximate the free surface reflection at steep takeoff angles. Then

$$s(t) = \frac{m_{sp}}{2(\lambda + 2\pi)} \left[v_{sp} \delta(t) - g\Delta H(0,T) + \frac{g}{v_{sp}}\left(-v_{sp} + \frac{3}{4}gt\right)\Delta H(0,T) \right]$$

where

$$\Delta H(t_1, t_2) = H(t - t_1) - H(t - t_2).$$

(H(t) is the Heaviside function). For spall which changes the center of mass of m_{sp} by an amount z_m from an initial position z_{sp0}, the duration T is found from

$$z_m = z_{sp0} + \frac{v_{sp}^2}{2g}$$

$$T = \frac{v_{sp}}{g} + \left(\frac{2z_m}{g}\right)^{1/2}.$$

For normally buried explosions, $z_{sp\,0}=0$. In addition, for quarry blasts, we model the effects of source duration (ripple firing of multiple charges) by convolving the signal from an individual charge (an explosion plus a tension crack) with $\Delta H(0, T_{rf})$, where T_{rf} is the duration of the ripple fire.

A "standard" model is used for most Xnice calculations. For normally buried explosions, the depth of burial is related to yield through $z = 125Y^{1/3}$, and following Patton (1989), the detachment velocity $v_o = 5 \times 10^{10}\ z_b^{1.6}$, and spall mass $m_{spall} = 10^{10}Y$. The "standard" quarry blast model is discussed in the next subsection in this Appendix on regional synthetic seismograms.

Synthetic Regional Seismograms

A number of authors have derived empirical or heuristic expressions of regional phase propagation (see, for example, Goncz, *et al.*, 1986 or Nuttli, 1975). We use a form, modified from Campillo, *et al.* (1985), which includes the effects of propagation and source excitation explicitly. The observed signal amplitude (peak narrow-bandpass or spectrally averaged amplitude) at range Δ and frequency f has the form:

$$A(f,\Delta) = \Omega(f)\hat{G}(\Delta,f),$$
$$\hat{G}(f,\Delta) = E(f)P(\Delta,f), \tag{1}$$

where $\Omega(f)$ is the source spectrum. The function $\hat{G}(f,\Delta)$ is an effective Green's function comprised of $E(f)$, the source excitation spectrum and a propagation term, specified by

$$\log(P(\Delta,f)) = -n \log(\Delta/\Delta_0) + \log(e)\,\gamma(f)(\Delta - \Delta_0) + \varepsilon,$$

where Δ_0 is a reference distance, $\gamma(f)$ is the anelastic attenuation parameter, n is a factor for geometric spreading (typically=5/6), and ε incorporates random effects of local station response and noise. The source excitation spectrum $E(f)$ depends on source type (earthquake, explosion, etc.) and source depth. The source excitation spectra are calibrated from calculations of synthetic seismograms or from observations of signals from different sources along common paths. The basic assumption underlying this approach in XNICE is that differences in spectral slopes for different types of sources and waves (Lg, Pg) are caused by differences in source $\Omega(f)$ and excitation $E(f)$. In the following, we describe these source and excitation functions in detail.

Source Spectra

XNICE computes signals from four source types: earthquakes, quarry blasts, and both overburied and normally buried explosions. Earthquake source spectra have been thoroughly studied. For large events ($m_b > 5$), spectra are quite complicated at frequencies above 1 Hz. For smaller events, however, there is general agreement that a good model for the source spectrum is flat at low frequencies, and rolls off at f^{-2} at frequencies above a corner which is proportional to the cube root of the moment divided by the stress drop. For events in the range $2.5 < m_b < 4$, the effects of changing the corner frequency with magnitude or moment changes the ratio of low (near 1 Hz) to high frequency amplitudes (> 1 Hz). The formulation by Brune (1970) (for complete stress drop) is implemented in XNICE:

$$L = \left(0.39 \frac{M_0}{\sigma} \right)^{1/3}$$

$$f_c = 2.22 \frac{\beta}{L}$$

$$\Omega(\omega) = \frac{f_c^2}{f_c^2 + \omega^2}$$

where σ is the stress drop and M_0 is the static moment. Distributions of source parameters (recurrence intervals, epicenter, depth, fault plane orientation, and moment) are specified on files as described in Appendix A. The amplitude of the signals from an earthquake is simply

$$A_{eqk}(f, \Delta) = \Omega_{eqk}(f) E_{eqk}(M_0, f) P(\Delta, f) . \tag{2}$$

We discuss the calculation of E_{eqk} in the next subsection.

Nuclear explosion source spectra have also been studied extensively. XNICE uses the equations given by Mueller and Murphy (1971). Like earthquakes, the spectra are flat at low frequencies and decrease as f^{-2} at high frequencies. The parameters of the Mueller-Murphy source are explosive yield, material type and depth of burial. Normally buried explosions are observed to interact non-linearly with the free surface, producing spall and appreciable secondary regional signals (e.g., Taylor and Randall, 1989). McLaughlin, et al. (1988) show that two-dimensional effects such as spall must be added to a simple point source to match Lg excitation. Day, et al (1983) proposed that the spall phase be modeled as a horizontal tension crack, and Barker and Day (1990) showed that the model fit two-dimensional simulations of explosions in the frequency band of 1 to 10 Hz. Recently, Patton and Taylor (1993) found that the tension crack model could be used to fit Lg spectral ratios from NTS explosions. The tension crack model is parameterized by the depth and radius of the crack and the distribution of velocities at which material moves upward from the crack (or equivalently, the spall mass and momentum). The parameters found by Barker and Day (1990) were consistent with near-field observations of spall summarized by Patton (1989). There is considerable scatter in those parameters and we use averages found from regressions in Patton (1989). In XNICE, we model the spall time history as

$$\Omega_{spall}(t) = m_{spall} \left[v_0 \delta(t) + (g t_d - v_0) \delta(t - t_d) - g(H(t) - H(t - t_d)) \right] , \tag{3}$$

where v_0 is the detachment velocity (assumed constant over the tension crack surface), g is the acceleration due to gravity, t_d is the dwell time

$$t_d = 2v_0/g,$$

and δ and H are the Dirac delta and Heaviside functions. For an overburied explosion, the user specifies the source material and depth of burial and a range of yields. For a normally buried explosion, a depth of burial of

$$z_b = 125W^{1/3}$$

where the W is the yield in kilotons, is assumed (in these and subsequent formulas, all units are SI, unless otherwise specified). Following Patton (1989), the detachment velocity is found from

$$v_0 = 5 \times 10^3 z_b^{1.6}$$

and the spall mass is

$$m_{spall} = 10^{10} W.$$

Barker and Day (1990) show that the spall signal for normally buried explosions is strongly peaked near a frequency equal to $1/t_d$, which is typically near 1 Hz. For the overburied explosion, the amplitudes are computed from

$$A_{obex}(f,\Delta) = \hat{G}_{exp}(h,f)\Omega_{exp}(W,f)P(\Delta,f), \tag{4}$$

where $\hat{G}_{exp}$ is the amplitude of the Green's function for an isotropic source, and S_{exp} is the Mueller-Murphy source spectrum. The amplitude for a normally buried explosion is

$$A_{nbex}(f,\Delta) = \left[\hat{G}_{exp}(f)\Omega_{exp}(W,f) + \hat{G}_{vf}(f)\Omega_{spall}(W,f)\right]T(\Delta,f)$$

$$\hat{G}_{vf}(f) = E_{vf}(f)P(\Delta,f). \tag{5}$$

Here, $\hat{G}_{vf}(f)$ is the Green's function for a vertical force on the free surface. Day and McLaughlin (1991) show that for wavelengths long compared to the source depth, the vertical force and horizontal tension crack Green's functions are approximately equal. We use the vertical force formulation because it is simpler (Barker, et al., 1993). The Green's functions are discussed in the next subsection.

We model quarry blasts as the superposition of rows of charges fired in sequence, a well established paradigm (e.g., Stump and Reinke, 1988). Following the modeling studies by Barker, et al, (1993), each charge consists of an explosion with an accompanying spall, which moves material from its original location. For the explosive part, we again use the Mueller-Murphy

source, and for the spall part we use a form similar to the relation for spall from a nuclear blast (above). A difference is that, for the quarry charge, the center-of-mass of the spalled material has a net displacement. Barker, *et al.* (1993) show that this has a significant effect on synthetic regional signals from quarry blasts. In this case, the dwell time is

$$t_d = \left[v_0 + \left(v_0^2 + 2z_0g \right)^{1/2} \right] \Big/ g \, ,$$

where z_0 is the vertical change in the center-of-mass of the spalled material. The histories from the individual charges are convolved with a firing pattern for a rectangular array of charges:

$$F(\omega) = N_{cols} \sum_1^{N_{rows}} B_j e^{-i\omega}$$

where N_{rows} is the number of rows of charges (rows are parallel to the quarry face), N_{cols} is the number of columns or charges per row, B_j is the source strength for each row and t_j is the firing time for the row. Here, we have assumed that the Green's functions do not vary over the quarry dimension, and that charges within a row are fired simultaneously. These assumptions are discussed in detail in Barker, *et al.* (1993). We have constructed a "standard" quarry blast for XNICE based on typical blasting practices. The user specifies a total yield for the blast. A burden Q of 15 m is assumed (blasts of interest will have yields of 100 tons or more, very large blasts with large benches and burdens). We then use relations from blasting handbooks (Dupont, 1942, Langefors and Kihlstrom, 1963) for the remaining parameters:

$$dx = 1.25Q$$
$$Y_H = 0.6Q^3 \, ,$$
$$dt_f = 4 \times 10^{-3} Q \, ,$$

where dx is the hole spacing, Y_H is the charge per hole (kilograms), and dt_f is the firing interval between rows. The number of holes is the total yield divided by Y_H. The blasts typically are rectangular, with the dimension parallel to the bench longer than the dimension normal to the bench. We assume that the aspect ratio is 2:1. To specify the spall parameters at each charge, we rely on observations by Langefors and Kihlstrom (1963) and set the change in center-of-mass z_0 at Q/2, material take-off velocity v_0 at 3.5 m/sec and the spall mass at $1.4 \times 10^4 Y_H$. We assume that the mean firing interval dt_f between rows is constant, as well as the mean source strength B but each has a random variation of 20%. The source spectrum for each individual charge has an explosive part whose corner frequency is much higher than the frequencies of interest here, while the spall component peaks in the

bandwidth of interest. The firing pattern spectrum F(ω) is flat at low frequencies and rolls off as f^{-1} above a corner frequency equal to the inverse of the total duration of the blast, or $(N_{rows}\, dt_f)^{-1}$, which for larger blasts will be around 1 Hz or less. Barker, *et al.* (1993) show that synthetic regional signals from the explosive and spall components are comparable. The amplitudes from the quarry blast are found from

$$A_{nbex}(f,\Delta) = \left[\hat{G}_{exp}(f)\Omega_{exp}(Y_H,f) + \hat{G}_{vf}(f)\Omega_{spall}(Y_H,f)\right]F(\omega). \qquad (6)$$

The effects of the firing pattern have been observed in several regional studies (e.g., Bennett, *et al.*, 1989; Hedlin, *et al.*, 1990; Smith, 1988).

Source Excitation Spectra

Ideally, one would find the source excitation spectra for each source type by recording signals from the different types along common propagation paths. This is possible in many areas for quarry blasts and earthquakes, although in many areas it is not. Of course, the number of nuclear test sites is small. When these recordings are available, $E(f)$, or $\Omega(f)E(f)$, can be inferred using analyses such as in Campillo (1985). Otherwise, we must rely on synthetic seismogram calculations.

For the test cases described in Section 3, we used synthetic seismograms to compute $E(f)$ for explosion, double-couple and point-force at the required depths. We recognize that the current technology for computing synthetic seismograms is limited to plane-layered models which do not completely represent the observed wavefields. We assume, however, that spectral differences in regional wavefields due to different sources can be predicted by the 1D synthetic calculations. The approach is to use relations derived from earthquake observations as a basis for calculating ground motions and rely on comparisons with synthetics to calculate motions from other sources with respect to earthquakes. For most regions of interest there are derived amplitude-distance formulas of the form

$$A(f_0,\Delta) = s(m_b,f_0)P_{obs}(\Delta,f_0), \qquad (7)$$

where $P_{obs}(\Delta,f)$ is as used in Equation (1). We emphasize that P is found from observations with the subscript obs. The propagation parameters γ and n and the source term $P_{obs}(\Delta,f)$ are found from measurements of a suite of events (Goncz, *et al.* 1986; Herrmann, 1983). The measurements in this type of study are typically made at or near $f_0 = 1\,Hz$, with the determination of $\gamma(f)$ requiring additional spectral information. There is clearly a trade-off between both source terms and the propagation term. For most regions, the majority of these events will be earthquakes, and we make the correspondence

94

$$s(m_b, f_0) = E_{eqk}(f_0)\Omega_{eqk}(M_0(m_b), f_0).$$ (8a)

Now, the synthetic Green's functions for a source type src can be represented in a similar way:

$$G_{src}(f, \Delta, z) = E_{src}(f, z)P_{syn}(\Delta, f).$$ (8b)

where z is source depth, and P_{syn} is the synthetic propagation operator. Our assumption stated above that although synthetic seismograms are not absolutely correct, but relative values are correct, is roughly equivalent to assuming that the ratio

$$\frac{G_{src1}(f, \Delta, z_1)}{G_{src2}(f, \Delta, z_2)} = \frac{E_{src1}(f, z_1)}{E_{src2}(f, z_2)}$$

is accurate. Although not essential, we make a further simplifying assumption that the earthquake excitation spectrum E_{eqk} is nearly flat (Campillo, 1985 and Herrmann and Kijko, 1983). Thus, the amplitude formula for source src is given by

$$A_{src}(f, \Delta, z) = \frac{E_{src}(f, z)}{E_{eqk}(f, z)}E_{eqk}(f_0)\Omega_{src}P_{obs}(\Delta, f).$$ (9)

Studies by Campillo, *et al.* (1984) and by the authors of this report show that excitation of regional signals is nearly constant for sources within three depth regions: the very shallow crust, the mid-crust, and the lower crust. The locations of the zones vary with earth structure, but the shallow zone is where the velocities are changing rapidly with P-wave velocities less than 6 km/sec. Most earthquakes have their hypocenters in the mid-crust while man-made sources will be in the upper crust. With this in mind, we write for the excitation functions for bombs and quarry blasts:

$$A_{src}(f, \Delta, z_{sc}) = \frac{E_{src}(f, z_{sc})}{E_{eqk}(f, z_{mc})}E_{eqk}(f_0)\Omega_{src}P_{obs}(\Delta, f).$$ (10)

Where the subscripts sc and mc indicate that the source is in shallow crust and mid-crust, respectively.

In practice, the spectral ratio is found from quotients of smoothed spectra computed by a wavenumber integration program.

Local Magnitudes

The M_L:M_0 discriminant has been proposed for regional signals (e.g. Woods, *et al.*, 1994). Since M_L is a time domain measurement, we need to

relate peak time domain amplitudes to the corresponding spectral amplitudes described above. To do this, we have relied on the work by Ou and Herrmann (1990). The expected peak amplitude $\hat{a}$ is found from moments of the spectrum

$$m_j = \int\limits_{f_{min}}^{f_{max}} A(f)f^j\,df$$

and from the equations:

$$\hat{f} = \frac{1}{2\pi}\frac{m_3}{m_1}$$

$$z = 2\ln\left(2\tilde{f}T\right)$$

$$\hat{a} = m_1^{1/2}\left(z + \gamma/z\right)$$

where $\gamma = 0.57222$ (Euler's constant) and T is the duration of the phase. Lee and Wetmiller (1976) present a compilation of observations of duration and M_L, and a rough average of their results is

$$\log(T) = \frac{1}{2}(M_L - 2)$$

since we are trying to find M_L, and we know the source moment, we use

$$M_L = \frac{2}{3}M_0 - 6$$

for earthquakes, and

$$M_L = \frac{2}{3}M_0 - 5.2$$

for other sources, to get a value of M_L find duration. In XNICE, a value if $\hat{a}$ is found for each regional phase, and the maximum is then used in a standard relation for local magnitude (p. 342, Richter, 1954).

Methods for Calculating Discrimination Results

The **analyst** module reads an arrivals bulletin and applies detection, location and discrimination algorithms. The results are reported in a discrimination bulletin which contain estimates of event origin time, location, magnitudes for teleseismic and regional phases and discrimination scores which summarize the results. In the following, we discuss the methods used to compute the quantities in the discrimination bulletin.

Detection criteria

An event is classified as detected by Xnice if the criteria for detection used by GSETT-3 are met. Those criteria are based on the wave type and number of measurements and type of measurement that are made. The rules are based on a weighted sum of measurements (J. Carter, Center for Monitoring Research, personal communication). The weights are:

Primary time	1.0
Secondary time	0.7
Array azimuth	0.4
Array slowness	0.4
Single station azimuth	0.2
Single station slowness	0.2

Here, "primary" refers to teleseismic P or regional Pg or Pn and "secondary" refers to teleseismic pP or S or regional Lg. All azimuths are determined from P, Pg or Pn. A sum is formed from the number of measurements which exceed the specified the signal-to-noise ratio times their respective weights for the stations in the network . An event is considered detected when the sum exceed 3.55. For example, three P wave travel time measurements and two array azimuth measurements would have a score of 3.8 and would flagged as a detection, while only three P wave travel times (sum=3.0) would not be a detection.

Scoring

In XNICE, we follow the AFTAC convention of scoring events on a one to five scale. A score of one for a particular discriminant indicates that the event has earthquake-like properties with respect to that discriminant AND that the data are of good quality. Here, "good quality" means that there were enough stations reporting to locate the event (3 or more), along with criteria particular to the discriminant. A score of 5 generally means that the event was located but a determination of discrimination properties could not be made.

Location

Locations are done with a non-linear least-squares procedure based on the Levenberg-Marquardt algorithm (Press, *et al.*, 1992). This algorithm seeks to minimize the X^2 merit function

$$\chi^2 = \sum_{i=1}^{N}\left(\frac{y_i - d_i}{\sigma_i}\right)^2$$

where y_i are model quantities, d_i are data. and σ_i are standard deviations of error in the data. Of course, here the "data" are the values in the arrivals bulletin computed by **synwav**. The Levenberg-Marquardt procedure uses a gradient method to guide successive iterations and a damping algorithm to prevent excessive steps. The data are observed travel times and, for arrays and three component stations, azimuths and slownesses. Values of σ_i are entered in the station files (see Appendix A).

The error ellipses from the location calculation are used as parameters for a location and depth score. We find the error ellipse axes from (Press, *et al.*, 1992)

$$\zeta_i = \left(\frac{\Delta\chi^2}{\lambda_i}\right)^{1/2}$$

where λ_i are the eigenvalues of C^{-1} (C is the covariance matrix resulting from the location procedure), and ΔX^2 is the value of the normal distribution at the required confidence level and degrees of freedom (tabulated on p. 692, Press, *et al.*, 1992).

In the **analyst** module, locations are computed with the depth constrained to the free surface and with depth a free parameter. A score is given dependent on the value of $\sigma_s - \sigma_f$, where σ_s and σ_f are the standard deviations of the residuals when depth is constrained and when it is free, respectively. A score of 1 indicates the event is earthquake-like (deep) and that there was good data for the location (there was an adequate number of stations used in the location and σ_s was sufficiently small). Higher score values (up to 5) indicate shallower depths and/or poorer data.

Depth by pP

AFTAC has developed a score which indicates depth using pP travel time stepout. For small values of the average difference in observed pP travel time t_{pP} and P travel time t_P (or if the data are poor), a high score (shallow event) is given. For large values of the stepout, the maximum $t_{pP} - t_p$ minus the minimum $t_{pP} - t_p$, low scores are given.

$M_s:m_b$

The values of M_s and m_b for events recorded at teleseismic distances are written to the arrivals bulletin by **synwav** and examine by **analyst**. We use a procedure similar to AFTAC's for scoring events according to their ratio of M_s to m_b, which uses values of the quantity

$$c_r = \frac{\Delta_{min} - \Delta M}{\sigma_d}$$

where Δ_{min} is a prescribed quantity (typically near one),

$$\Delta M = \overline{m_b} - \overline{M_s}$$

(overbar indicates network average), and

$$\sigma_d = 0.3 \left(\frac{1}{\overline{m_b}} + \frac{1}{\overline{M_s}} \right)^{1/2} .$$

A low score indicates good data and large values of c_r, which result from earthquake-like $M_s:m_b$ values.

Regional Phase Spectral Slopes

The scores discussed above pertain to teleseismic events (where depth phases or M_s can be observed). We describe here a means for scoring based on discriminants proposed for regional phases. We begin with the spectral slope discriminant, which is based on observations that the spectral slope (at least for Lg) is generally least for earthquakes, steeper for normally buried explosions, steeper still for overburied explosions and steepest for quarry blasts (Barker, *et al.*, 1994). The score for a particular phase is computed from

$$S = 1 + INT \left[\frac{s - d(m_b)}{\sigma} \right]$$

where INT indicates that the integer value is to be taken, σ is the standard deviation in the estimates of magnitude for the phase,

$$s = m_{b_{lo}} - m_{b_{hi}}$$

and $d(m_b)$ is the value of the decision line in spectral slope vs m_b space. W e use the term m_b here to refer to values of log spectral amplitude corrected for attenuation according to regional propagation relations (see Appendix XX). The quantities $m_{b_{lo}}$ and $m_{b_{hi}}$ are m_b's at low and high frequencies,

respectively. In XNICE, we use values averaged over the bands from 1 to 2 Hz for the $m_{b_{lo}}$ and the band from 6 to 8 Hz for $m_{b_{hi}}$. The decision line is described by the linear relation $d = a - b\, m_b$, where a and b are proscribed values. Thus, this test compares the change in value of the spectrum $\left(m_{b_{lo}} - m_{b_{hi}}\right)$ with the change predicted by the decision line.

Lg/P Spectral Ratios

This discriminant is based on observations that the spectral ratio of Lg/P is greatest for earthquakes. The score is obtained from

$$S = INT\left[\frac{1 - \left(m_{b_{Lg}} - m_{b_P}\right)}{\sigma}\right]$$

where we use m_b in the same sense as we used it above with spectral values taken at 1 Hz, P means the larger of Pn (if present) and Pg, and σ is the standard deviation in the estimate of network Lg magnitude,

$M_L{:}M_0$

This discriminant is based on observations that the ratio of the local magnitude M_L to the scalar moment M_0 is least for earthquakes. The score is obtained from

$$S = INT\left[\frac{3 + M(M_0) - M_L}{\sigma}\right]$$

where

$$M(M_0) = -5.6 + \frac{2}{3}\log(M_0)$$

and σ is the standard deviation in the estimate of network M_L.

Methods for Estimating Thresholds

XNICE is a Monte Carlo scheme that computes the properties of populations of events. It is useful to compute a threshold of signal level at which the events meet specified conditions. In the following, we describe the method for doing this.

The underlying assumption is that the probability of detection or identification can be represented by a Normal (Gaussian) distribution. The threshold is then the magnitude at which a specified probability of detection or identification is achieved. If events have the distribution B(W), where W is source strength, then the cumulative number of events with strength less than or equal to W is

$$N_{cum}(W) = \int_{-\infty}^{W} B(\chi,\mu,\sigma)dx$$

$$P(W,\mu,\sigma) = \int_{-\infty}^{W} p(t,\mu,\sigma)dt$$

where $p(t,\mu,\sigma)$ is the Normal probability density with mean μ and standard deviation σ. In XNICE, the source strength is log moment for earthquakes and log yield for the other sources. The corresponding incremental distribution is

$$N_{inc}(W) = B(W)P(W,\mu,\sigma).$$

The strategy is the compute realizations of each source strength (the realizations are of the distributions of station noise, propagation noise, etc.) and infer the values of μ and σ that fit the computed $N_{inc}(W)$ (this is done with a non-linear least-squares search). The distribution B(W) is found from the events bulletin. We typically run **events** such that B(W) is constant (equal to the number of realizations), with the values of W chosen so that there are no detections at the smallest values and full detection at the largest values. The calibration plots are useful for determining the range of source strengths. Then, the threshold for source strength is the value W_T for which $P(W_T, \mu, \sigma)$ equals a requested value, typically 0.9.

The procedure outlined above yields a threshold with respect to source strength, whereas a threshold with respect to a measured amplitude or magnitude m_T is more often used. To relate the magnitude to source strength, we perform a linear regression on values of magnitude versus W (from the events and discrimination bulletins), and calculate m_T from the linear relation.

Appendix C
Program Manual

analyst

NAME

analyst - create discrimination bulletin

SYNOPSIS

analyst run_parameter_file

DESCRIPTION

The **analyst** module reads the events bulletin created by **synwav** and generates a discrimination bulletin. Calculational methods are discussed in Appendix B. File descriptions are in Appendix A.

DATA READ FROM RUN PARAMETERS FILE

keyword	description
network	network station list file name
discrim	discrimination catalog file name
arrivals	arrivals catalog file name
str	structure file name
rgnldir	regional wave propagation parameter directory
properr	propagation errors list
magrels	magnitude relations file name

FILES

see files in run description file above

SEE ALSO

evswan

events

NAME

events - generate events bulletin

SYNOPSIS

events run_parameter_file

DESCRIPTION

The **events** module extracts file information from the run parameters file and seismicity information from seismicity files and generates an events bulletin. Details of file formats used by **events** are found in Appendix A. The **events** module operates in one of two modes (specified by the grid flag in the run parameters file). Events can be located on a grid for making map views of identification properties or can be located in an area. The properties of the seismicity and how **events** uses them are described in the seismicity parameter file, while grid properties are described in the events grid file. The input files can be generated by the XNICE user's interface or by a file editor.

DATA READ FROM RUN PARAMETERS FILE

keyword	description
events	events bulletin file name
grid	This entry indicates whether the event locations are specified by a seismicity or grid file
year	years in which events occur (used only if natural seismicity is specified).
nevmax	maximum number of events (used only if natural seismicity is specified). (events)
area	area (seismicity or event grid file) name

FILES

RUNPARDIR/run_parameter_file - input run parameter file
SEISDIR/area - input seismicity file
EVGRIDDIR/area - input grid parameter file
EVENTSDIR/events_bulletin - output events bulletin

SEE ALSO

evswan

evswan

NAME

evswan - events, synwav and analyst modules combined into one

SYNOPSIS

evswan run_parameters_file

DESCRIPTION

The **evswan** combines the **events, synwav** and **analyst** modules into one module. This combination eliminates considerable overhead and duplication and greatly reduces input/output operations. It thus requires much less computer time than running the three modules separately. For large simulations, **evswan** is recommended. The data files used are the same as the composite modules.

FILES

see file requirements in manual pages for events, synwav and analyst

SEE ALSO

events, synwav and analyst

synwav

NAME

synwav - synthetic seismogram module (generate arrivals bulletin)

SYNOPSIS

synwav file

DESCRIPTION

The **synwav** module reads the events bulletin created by **events** and generates arrivals at stations in a specified network. Calculational methods are discussed in Appendix B. File descriptions are in Appendix A.

DATA READ FROM RUN PARAMETERS FILE

keyword	description
network	network station list file name
events	events catalog file name
arrivals	arrivals catalog file name
lpinst	long period instrument response file name
spinst	short period instrument response file name
path	surface wave eigenfunction and dispersion file name
str	structure file name
bwdir	body wave travel time and amplitude directory
refdir	body wave reference amplitude directory
rgnldir	regional wave propagation parameter directory
properr	propagation errors list
freq	frequencies at which regional amplitude spectra are computed
magrels	magnitude relations file name
bwmeth	body wave calculation method (convolution or magnitude)
swmeth	surface wave calculation method (synsrf or magnitude). If magnitude is specified, the magnitude relation and tectonic type must follow
pmdfil	path medium description file name
pgrfil	path grid file name

FILES

see files in run description file above

SEE ALSO

evswan

XNICE

NAME

XNICE - X user's interface

SYNOPSIS

XNICE

DESCRIPTION

The XNICE user's interface can be used to construct parameter files to run the **events, synwav** and **analyst** modules, to examine the discrimination bulletins and to plot the results. There are also pop-up windows to browse various files.

SETTING UP XNICE RUNS (the "Functions" menu)

Choosing the run name

The run name is used as the default value for the run parameter file and the events, arrivals and discrimination bulletins. In general, this provides a good means for organizing a run, and the run parameter file is a record of the files used. By selecting "Set Run Name" under the "Functions" menu, a window with an editable text window and a "Select" button will appear (Figure C.1). The "Select" button allows the user to browse the run parameters directory with a file selection menu.

Setting up the run parameters file

If the "Set Propagation Parameters" is selected under the "Functions" menu, a window appears that allows the user to enter and edit parameters. The choices are the entries in the run parameters file (see run parameters file description, Appendix A). For each parameter, there is an editable text window and a "Select" pushbutton, as shown in Figure C.2. Pushing 'Select" with mouse button 1 brings up a file selection or a directory selection window, or in the case of the regional frequency list and the regional propagation errors list, a window which can be more easily edited.

Setting up the source parameters file

The source parameters can be chosen for the various source types by selecting "Set Source Parameters" under the "Functions" menu. The first step is to indicate whether this will be a grid calculation or an area calculation by pressing the toggle button "Grid" or "Area" (Figure C.3). This sets a flag in the
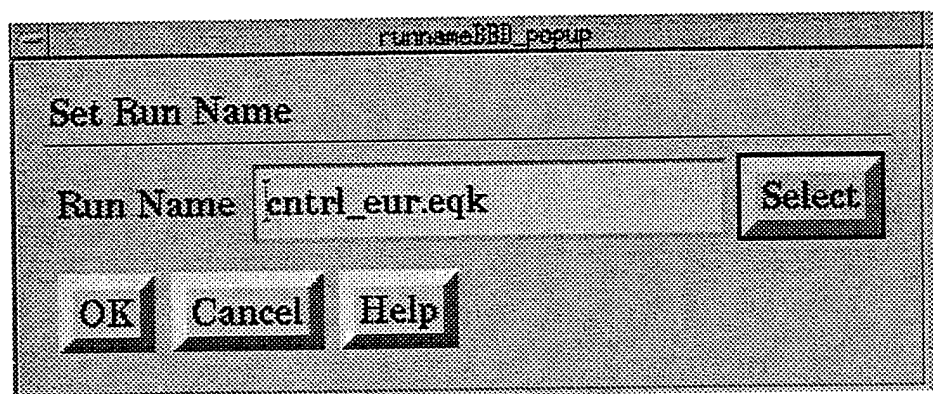
Figure C.1   Pop-up window for selecting run name. Clicking on "Select" causes a dialog to appear which shows existing run names (discrimination bulletins).

Run Parameters Selection

Area/Seismicity Bulletin	eus.test01	Select
Network File	hsn.30	Select
Structure File	ekz	Select
Surface Wave Eigenfunctions	ekz	Select
Long Period Instrument	kono.lpz	Select
Short Period Instrument	kono.spz	Select
Amplitude Table Directory	nrc	Select
Amplitude Reference Directory	nrc	Select
Regional Directory	eus.test	Select
Regional Frequencies	1.0 1.5 2.0 3.0 4.0 5.0 6.0 6.5 7.0 7.5 8.0 10.	Select
Regional Propagation Errors	Lg 0.28 S 0.19 Sn 0.19 P 0.26 Pn 0.26 Pg 0.25	Select

OK Cancel Help

Figure C.2 Pop-up window for selecting run (propagation) parameters. Clicking on "Select" causes the appropriate selection dialog to appear.
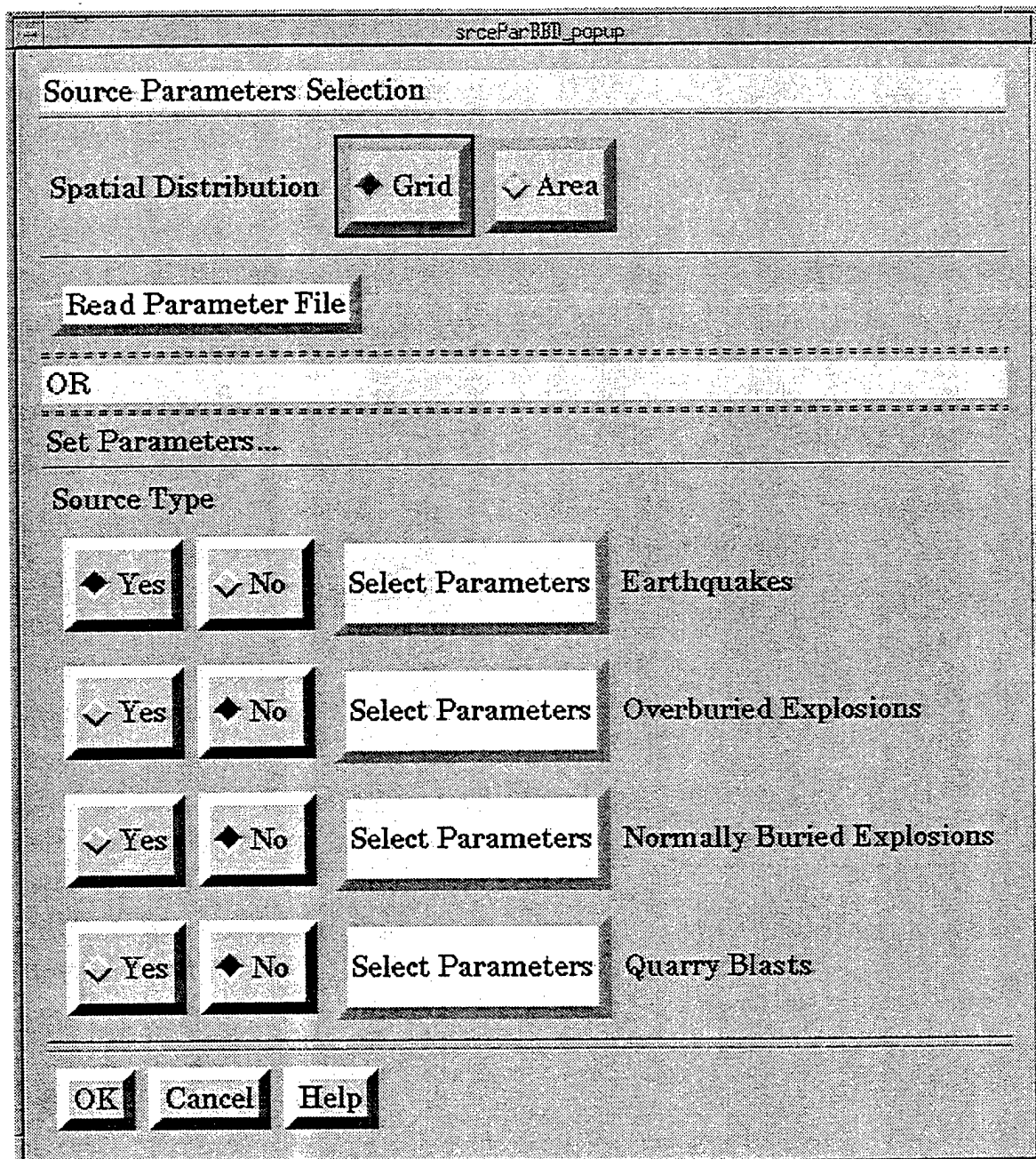
Figure C.3   Pop-up window for selecting source parameters. "Grid" and "Area" buttons are toggles for selection of spatial mode. Clicking on "Read Parameters File" brings up a dialog to select an Events Bulletin and reads the source parameters from that file. For each source type, the "Yes" and "No" buttons indicate whether that source is included in the simulation, and "Select Parameters" allows further selection.

file program which influences subsequent choices. To read an existing run parameter file to use as a template, press the "Read Parameters File" button, which brings up a selection menu. For each source type, there is a "Yes" and "No" toggle to indicate which source types are to be included in the run, and "Set Parameters" button, which will cause windows to appear that are specific to the source type. If a run parameters file has been read, the toggles will be set according the source types specified in the file. Figure C.4 shows parameters selection windows resulting from pressing the "Set Parameters" button for earthquakes and overburied explosions. The fault orientation and stress drop can be entered for earthquakes, and "Select" buttons bring up windows to choose the moment distribution and spatial distribution. The "Moment Distribution" select has a pulldown menu which has two choices: a "b-value" (Poisson recurrence rate) choice or a uniform choice. In the first case events are distributed according to (see Appendix A, the seismicity file description)

$$logN(M_0) = a=b \ log(M_0), \ M_0 > minM_0 \ ,$$

while in the second case they are distributed uniformly in log moment. The pulldown choices under "Moment Distribution" allow one to specify the appropriate parameters. The "Spatial Distribution" select button puts up a window to set either grid parameters or area parameters, depending on the state of the "Grid" or "Area" toggle buttons. For the overburied explosion, the log yield bounds and increment can be specified as well as the material type and number of realizations of each state. The "Spatial Distribution" can be selected and the parameters associated with a "Grid" or "Area" specification can be set. The parameter choices for normally buried explosions and quarry blasts are similar.

Starting NICE runs

After the run name, propagation parameters and source parameters are set as described above, one can spawn one of the XNICE modules or a sequence of them. The choices and the Unix command that is made are:

Menu Item	Unix Command
Events	events run_name
Arrivals	synwav run_name
Discrimination Analysis	analyst run_name
Arrivals > Discrimination Analysis	synwav run_name l analyst run_name
Events > Arrivals > Discrimination Analysis	evswan run_name

112

srcePar BB1 popup

Overburied Explosion

Minimum Log Yield -2.700000

Maximum Log Yield 0.700000

Log Yield Increment 0.100000

Material tuff

Number of Relizations 10

Spatial Distribution Select

OK Cancel Help

---

eqkBB1 popup

Earthquake Parameters

Fault Orientation

Value Sigma

Strike 28.000000 0.000000

Value Sigma

Dip 34.000000 0.000000

Value Sigma

Rake -80.000000 0.000000

Stress Drop

Value 1.00e+07 Sigma 1.00e+06

Moment Distribution Select

Spatial Distribution Select

OK Cancel Help

Figure C.4 Pop-up window for selecting earthquake source parameters. The "Select" buttons bring up windows in which further selections can be made.

MAKING PLOTS (the "Plot" menu)

Events Plots

With this selection, one can make plots of source parameters to inspect the events bulletin, Figure C.5 shows the window which appears when "Select Events Plot" is chosen from the "Plot" menu. One or more source types can be chosen from the toggle buttons near the top of the window. The events bulletin can be typed in the text area or by pressing "Select", which brings up a file selection window. The plot variables can be chosen from the boxes on the center of the window: the y-axis from the choices on the right versus the x-axis from the choices on the left. The "Current Plot Choice" shows which plot has been chosen (and changes when plot variables are chosen).

Calibration Plots

Calibration plots are used to plot values in the discrimination bulletin against other values in that bulletin or against source parameters in the events bulletin. The primary purpose is to verify that source and propagation parameters match observations. Figure C.6 shows the selection window for calibration plots (this comes up when "Calibration Plots" is chosen from the "Plot" menu). The discrimination bulletin is chosen by typing in the text area or from the file selection menu that appears when "Select" is chosen. The events bulletin used to synwav/analyst run is assumed to have the same name as the discrimination bulletin. The "Current Plot Choice" is a status window that shows the summarizes the latest plot settings. There are several basic plot type choices, made with the buttons under the "Plot Type Choice" heading:

1. Discrimination vs Source Parameter: with this choice, plots of variables in the discrimination bulletin (e.g. $m_b(Lg)$, M_s) can be plotted against source variables (e.g. log moment or yield). The variables are chosen with the "Select" buttons on the right side by the "Discrimination y Variable" and "Source Variable" labels. The text areas by the labels show the current choice.

2. Discrimination vs Discrimination Parameter: with this choice, plots of variables in the discrimination bulletin can be plotted against another discrimination variable (e.g. M_s vs m_b). The variables are chosen with the "Select" buttons on the right side by the "Discrimination y Variable" and "Discrimination x Variable" labels. The text areas by the labels show the current choice.

Figure C.5 Pop-up window for selecting events plot parameters. The source type(s) plotted are chosen with the buttons at the top. The events bulletin can be selected with the editable window or with the "Select" button, which allows one to browse the current files.

Calibration Plot Parameters Selection

Discrimination Bulletin aur.50x5.unf | Select |

Current Plot Choice | mb(Lg) versus Log_Moment for eqks |

Plot Type Choice

♦ Discrimination vs Source Parameter

◇ Discrimination vs Discrimination Parameter

◇ Cumulative Number vs Discrim. Variable

◇ Incremental Number vs Discrim. Variable

Source Choice

♦ Earthquakes

◇ Quarry Blasts

◇ Normally Buried Explosions

◇ Overburied Explosions

Discrimination x Variable | mb(Lg) | | Select |

Discrimination y Variable | mb(Lg) | | Select |

Source Variable | Log_Moment | | Select |

GMT Plot? | ∨ Yes ♦ No |

| OK | Apply | Cancel | Help |

Figure C.6   Pop-up window for selecting calibration plot parameters. The discrimination bulletin can be selected with the editable window or with the "Select" button, which allows one to browse the current files. One of four plot types can be chosen under the "Plot Type Choice". The "Select" buttons on the right side bring up menus of possible variable types. A single source type is chosen with the buttons under "Source Choice".

116

3. Cumulative Number vs Discrimination Variable: with this choice, plots of cumulative number occurring in the discrimination bulletin can be plotted. The variable is chosen with the "Select" buttons on the right side by the "Discrimination x Variable" label.

4. Incremental Number vs Discrimination Variable: with this choice, plots of incremental number occurring in the discrimination bulletin can be plotted. The variable is chosen with the "Select" buttons on the right side by the "Discrimination x Variable" label. If m_b is chosen as a discrimination variable, an auxiliary window will appear that requests the teleseismic or regional m_b that is to be used.

We show in Figure C.7 a sample calibration plot. In addition to the plot on the XNICE main window, the program writes a script for the GMT plot package and spawns the GMT plotter in the "Yes" toggle is pressed by the "GMT plot?" label. As an aid to checking calibration levels, an additional window is shown (see Figure C.7) with the results of a linear regression on the plotted data.

Discrimination Analysis Plots

Two types of plots can be made of data in the discrimination bulletin, chosen with the pulldown menu beside "Select Discrimination Analysis Plots": "xy plot" or "contour". In both these cases, plot data and GMT scripts are written to files and a GMT plot is executed (if requested). For xy plots, a plot is also made on the main XNICE window. Figure C.8 shows the plot selection window if "xy plot" is chosen. Pulldown menus offer the choices of incremental and cumulative numbers and fractions, spectral ratios, horizontal and vertical ellipses and Lg/P ratios for the y-axis and m_b, M_s and depth for the x-axis. If m_b is chosen as a discrimination variable, an auxiliary window will appear that requests the teleseismic or regional phase(s) from which the m_b measurement was made (to the right of the main window in Figure C.8).

The program plots data which meet a set of conditions (called the "A conditions") contingent upon a second set of conditions (the "B conditions"), that is, plots the occurrence A given B. The conditions are either limits on the source parameters, on the identification class or the discriminant responsible for the class. The term "identification class" describes how well an identification or detection was made. The conditions are set by pressing the 'Select" buttons under the "A Conditions" or "B Conditions" headings. Figure C.9 shows the window for selecting class and discriminant. There are 10 choices of class. Classes 1 through 7 are based on combinations of discrimination scores in the bulletin, with Class 1 being events that are best identified as earthquakes (see the description of the analyst module in
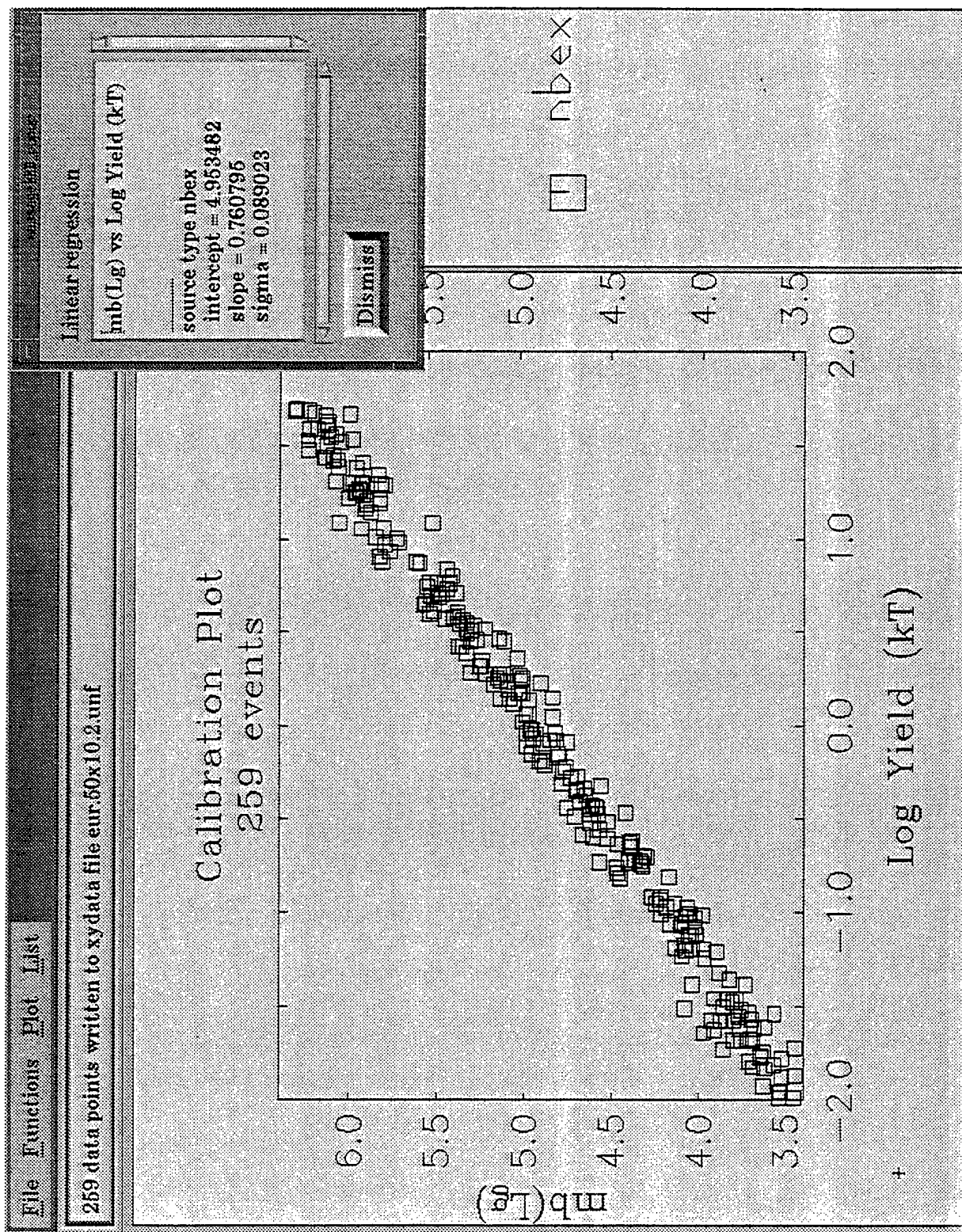
117

Figure C.7 Example of a calibration plot, showing $m_b(Lg)$ versus log yield for a suite of normally buried explosions. The pop-up window in the upper right shows the results of a linear regression.

Figure C.8   Pop-up window for selecting discrimination xy plot parameters. The discrimination bulletin can be selected with the editable window or with the "Select" button, which allows one to browse the current files. Clicking on the "Select" buttons by the "x" and "y variable" labels causes a pull-down menu to appear from which choices can be made. The phase selection pop-up on the right appears when appropriate (e.g. when "mb" is chosen as a plot variable). One or more source types can be chosen. Conditions on the events chosen can be made with the "Select" buttons under "A" and "B Conditions".

119

Set A conditions

Classes

◇ c1 one or more 1s

◇ c2 two or more 2s

◇ c3 one 2

◇ c4 one 3

◇ c5 one 4 or two or more 3s

◇ c6 two or more 4s

◇ c7 one or more 5s

◇ c8 1's by spec'd discriminant

◇ c9 2s by spec'd discriminant

◇ c10 3's by spec'd discriminant

◇ c11 2 or higher by spec'd discriminant

◇ c12 high frequency regional detection

◇ c13 regional GSE detection

◇ c14 GSE detection

◇ c15 observed

◇ c16 occurring

Discriminants

☐ Depth from P travel times

☐ Depth from pP

☐ Ms:mb

☐ Lg spectral ratio

☐ Pg spectral ratio

☐ Pn spectral ratio

☐ Lg/Pg spectral ratio

☐ Lg/Pg at one Hz

☐ M1:M6

OK Apply Cancel

Figure C.9 Pop-up window for selecting classes (choose one) and discriminants (one or more).

120

Appendix B for a discussion of discrimination scores). Class 9 is events with a score of 2 and Class 10 is events with a score of 3. Class 11 is those events with a score of 2 or higher (not earthquake-like to explosion-like). Class 12 is events for which high frequency measurements were possible (exceeded the signal-to-noise). Class 13 is events which passed the GSE detection criteria based solely on regional phases. Class 14 consists of those events which meet the current GSE event detection criteria. Class 15 is events for which any magnitude is reported. Class 16 is simply all the events in the bulletin.

The "Discriminant" buttons on the right side of the window on Figure C.9 allows the user to specify one or more discriminants that contributed to the class. For example, if Class 1 and the M_s:m_b and Depth from pP discriminants are chosen, then only those events that have one or more scores of 1 from either the M_s:m_b or pP scores are extracted from the file.

The user can also specify the depth and magnitude ranges, the origin years and the area names of the data that are to be extracted, as shown in Figure C.10. Other items on the plot menu for xy plots (Figure C.11), are the bulletin selection (edit the text window or press "Select" for a file selection dialog) and the source type (one or more).

The discrimination contour plot has a format similar to the xy plot, as seen in Figure C.11. The conditions have the same meaning. Choices for contour variables are: number and fraction detecting, horizontal and vertical error ellipses, and m_b and M_s thresholds. For the number and fraction detecting and the error ellipses, the user is asked to specify whether the values are at the threshold or at a specified m_b, and from what phase the m_b measurement is made. The phase is also requested if the m_b threshold are to be contoured. The contour data are written to file specified by the "Contour File" text or the file selection that is available from the "Select" button (see the file description for contour data in Appendix A).

Changing Plot Limits

The limits of a current plot can be changed with the "Set Plot Limits for Current Plot" button under the "Function" menu. When a new plot is generated by the plot commands above, the limits are reset to the minima and maxima on the plot.

LISTING FILES (the "List" menu)

This option allows the user to view a file with a window with scroll bars. The events and discrimination bulletin, the run parameter and source parameter files and the network files can be browsed in this manner.

Figure C.10 Pop-up window for selecting areas, ranges of m_b, M_s and depth, years and location conditions.

Figure C.11 Pop-up window for selecting discrimination contour plot parameters. The discrimination bulletin can be selected with the editable window or with the "Select" button, which allows one to browse the current files. Clicking on the "Select" buttons by the "x" and "y variable" labels causes a pull-down menu to appear from which choices can be made. The phase selection pop-up on the right appears when appropriate (e.g. when "m$_b$thresh" is chosen as a plot variable). One or more source types can be chosen. Conditions on the events chosen can be made with the "Select" buttons under "A" and "B Conditions".

123

THOMAS AHRENS
SEISMOLOGICAL LABORATORY 252-21
CALIFORNIA INSTITUTE OF TECHNOLOGY
PASADENA, CA 91125

RALPH ALEWINE
NTPO
1901 N. MOORE STREET, SUITE 609
ARLINGTON, VA 22209

SHELTON ALEXANDER
PENNSYLVANIA STATE UNIVERSITY
DEPARTMENT OF GEOSCIENCES
537 DEIKE BUILDING
UNIVERSITY PARK, PA 16801

MUAWIA BARAZANGI
INSTITUTE FOR THE STUDY OF THE CONTINENTS
3126 SNEE HALL
CORNELL UNIVERSITY
ITHACA, NY 14853

RICHARD BARDZELL
ACIS
DCI/ACIS
WASHINGTON, DC 20505

T.G. BARKER
MAXWELL TECHNOLOGIES
P.O. BOX 23558
SAN DIEGO, CA 92123

DOUGLAS BAUMGARDT
ENSCO INC.
5400 PORT ROYAL ROAD
SPRINGFIELD, VA 22151

THERON J. BENNETT
MAXWELL TECHNOLOGIES
11800 SUNRISE VALLEY DRIVE SUITE 1212
RESTON, VA 22091

WILLIAM BENSON
NAS/COS
ROOM HA372
2001 WISCONSIN AVE. NW
WASHINGTON, DC 20007

JONATHAN BERGER
UNIVERSITY OF CA, SAN DIEGO
SCRIPPS INSTITUTION OF OCEANOGRAPHY IGPP, 0225
9500 GILMAN DRIVE
LA JOLLA, CA 92093-0225

ROBERT BLANDFORD
AFTAC
1300 N. 17TH STREET
SUITE 1450
ARLINGTON, VA 22209-2308

STEVEN BRATT
NTPO
1901 N. MOORE STREET, SUITE 609
ARLINGTON, VA 22209

RHETT BUTLER
IRIS
1616 N. FORT MEYER DRIVE
SUITE 1050
ARLINGTON, VA 22209

LESLIE A. CASEY
DOE
1000 INDEPENDENCE AVE. SW
NN-40
WASHINGTON, DC 20585-0420

CATHERINE DE GROOT-HEDLIN
SCRIPPS INSTITUTION OF OCEANOGRAPHY
UNIVERSITY OF CALIFORNIA, SAN DIEGO
INSTITUTE OF GEOPHYSICS AND PLANETARY PHYSICS
LA JOLLA, CA 92093

STANLEY DICKINSON
AFOSR
110 DUNCAN AVENUE, SUITE B115
BOLLING AFB
WASHINGTON, D.C. 20332-001

SEAN DORAN
ACIS
DCI/ACIS
WASHINGTON , DC 20505

DIANE I. DOSER
DEPARTMENT OF GEOLOGICAL SCIENCES
THE UNIVERSITY OF TEXAS AT EL PASO
EL PASO, TX 79968

RICHARD J. FANTEL
BUREAU OF MINES
DEPT OF INTERIOR, BLDG 20
DENVER FEDERAL CENTER
DENVER, CO 80225

JOHN FILSON
ACIS/TMG/NTT
ROOM 6T11 NHB
WASHINGTON, DC 20505

MARK D. FISK
MISSION RESEARCH CORPORATION
735 STATE STREET
P.O. DRAWER 719
SANTA BARBARA, CA 93102-0719

LORI GRANT
MULTIMAX, INC.
311C FOREST AVE. SUITE 3
PACIFIC GROVE, CA 93950

I. N. GUPTA
MULTIMAX, INC.
1441 MCCORMICK DRIVE
LARGO, MD 20774

JAMES HAYES
NSF
4201 WILSON BLVD., ROOM 785
ARLINGTON, VA 22230

MICHAEL HEDLIN
UNIVERSITY OF CALIFORNIA, SAN DIEGO
SCRIPPS INSTITUTION OF OCEANOGRAPHY IGPP, 0225
9500 GILMAN DRIVE
LA JOLLA, CA 92093-0225

EUGENE HERRIN
SOUTHERN METHODIST UNIVERSITY
DEPARTMENT OF GEOLOGICAL SCIENCES
DALLAS, TX 75275-0395

VINDELL HSU
HQ/AFTAC/TTR
1030 S. HIGHWAY A1A
PATRICK AFB, FL 32925-3002

RONG-SONG JIH
PHILLIPS LABORATORY
EARTH SCIENCES DIVISION
29 RANDOLPH ROAD
HANSCOM AFB, MA 01731-3010

LAWRENCE LIVERMORE NATIONAL LABORATORY
ATTN: TECHNICAL STAFF (PLS ROUTE)
PO BOX 808, MS L-200
LIVERMORE, CA 94551

LAWRENCE LIVERMORE NATIONAL LABORATORY
ATTN: TECHNICAL STAFF (PLS ROUTE)
PO BOX 808, MS L-221
LIVERMORE, CA 94551

ROBERT GEIL
DOE
PALAIS DES NATIONS, RM D615
GENEVA 10, SWITZERLAND

HENRY GRAY
SMU STATISTICS DEPARTMENT
P.O. BOX 750302
DALLAS, TX 75275-0302

DAVID HARKRIDER
PHILLIPS LABORATORY
EARTH SCIENCES DIVISION
29 RANDOLPH ROAD
HANSCOM AFB, MA 01731-3010

THOMAS HEARN
NEW MEXICO STATE UNIVERSITY
DEPARTMENT OF PHYSICS
LAS CRUCES, NM 88003

DONALD HELMBERGER
CALIFORNIA INSTITUTE OF TECHNOLOGY
DIVISION OF GEOLOGICAL & PLANETARY SCIENCES
SEISMOLOGICAL LABORATORY
PASADENA, CA 91125

ROBERT HERRMANN
ST. LOUIS UNIVERSITY
DEPARTMENT OF EARTH & ATMOSPHERIC SCIENCES
3507 LACLEDE AVENUE
ST. LOUIS, MO 63103

ANTHONY IANNACCHIONE
BUREAU OF MINES
COCHRANE MILL ROAD
PO BOX 18070
PITTSBURGH, PA 15236-9986

THOMAS JORDAN
MASSACHUSETTS INSTITUTE OF TECHNOLOGY
EARTH, ATMOSPHERIC & PLANETARY SCIENCES
77 MASSACHUSETTS AVENUE, 54-918
CAMBRIDGE, MA 02139

LAWRENCE LIVERMORE NATIONAL LABORATORY
ATTN: TECHNICAL STAFF (PLS ROUTE)
PO BOX 808, MS L-207
LIVERMORE, CA 94551

LAWRENCE LIVERMORE NATIONAL LABORATORY
ATTN: TECHNICAL STAFF (PLS ROUTE)
LLNL
PO BOX 808, MS L-175
LIVERMORE, CA 94551

LAWRENCE LIVERMORE NATIONAL LABORATORY
ATTN: TECHNICAL STAFF (PLS ROUTE)
PO BOX 808, MS L-208
LIVERMORE, CA 94551

LAWRENCE LIVERMORE NATIONAL LABORATORY
ATTN: TECHNICAL STAFF (PLS ROUTE)
PO BOX 808, MS L-202
LIVERMORE, CA 94551

LAWRENCE LIVERMORE NATIONAL LABORATORY
ATTN: TECHNICAL STAFF (PLS ROUTE)
PO BOX 808, MS L-195
LIVERMORE, CA 94551

LAWRENCE LIVERMORE NATIONAL LABORATORY
ATTN: TECHNICAL STAFF (PLS ROUTE)
PO BOX 808, MS L-205
LIVERMORE, CA 94551

THORNE LAY
UNIVERSITY OF CALIFORNIA, SANTA CRUZ
EARTH SCIENCES DEPARTMENT
EARTH & MARINE SCIENCE BUILDING
SANTA CRUZ, CA 95064

ANATOLI L. LEVSHIN
DEPARTMENT OF PHYSICS
UNIVERSITY OF COLORADO
CAMPUS BOX 390
BOULDER, CO 80309-0309

DONALD A. LINGER
DNA
6801 TELEGRAPH ROAD
ALEXANDRIA, VA 22310

LOS ALAMOS NATIONAL LABORATORY
ATTN: TECHNICAL STAFF (PLS ROUTE)
PO BOX 1663, MS F659
LOS ALAMOS, NM 87545

LOS ALAMOS NATIONAL LABORATORY
ATTN: TECHNICAL STAFF (PLS ROUTE)
PO BOX 1663, MS F665
LOS ALAMOS, NM 87545

LOS ALAMOS NATIONAL LABORATORY
ATTN: TECHNICAL STAFF (PLS ROUTE)
PO BOX 1663, MS D460
LOS ALAMOS, NM 87545

LOS ALAMOS NATIONAL LABORATORY
ATTN: TECHNICAL STAFF (PLS ROUTE)
PO BOX 1663, MS C335
LOS ALAMOS, NM 87545

GARY MCCARTOR
SOUTHERN METHODIST UNIVERSITY
DEPARTMENT OF PHYSICS
DALLAS, TX 75275-0395

KEITH MCLAUGHLIN
MAXWELL TECHNOLOGIES
P.O. BOX 23558
SAN DIEGO, CA 92123

BRIAN MITCHELL
DEPARTMENT OF EARTH & ATMOSPHERIC SCIENCES
ST. LOUIS UNIVERSITY
3507 LACLEDE AVENUE
ST. LOUIS, MO 63103

RICHARD MORROW
USACDA/IVI
320 21ST STREET, N.W.
WASHINGTON, DC 20451

JOHN MURPHY
MAXWELL TECHNOLOGIES
11800 SUNRISE VALLEY DRIVE SUITE 1212
RESTON, VA 22091

JAMES NI
NEW MEXICO STATE UNIVERSITY
DEPARTMENT OF PHYSICS
LAS CRUCES, NM 88003

JOHN ORCUTT
INSTITUTE OF GEOPHYSICS AND PLANETARY PHYSICS
UNIVERSITY OF CALIFORNIA, SAN DIEGO
LA JOLLA, CA 92093

PACIFIC NORTHWEST NATIONAL LABORATORY
ATTN: TECHNICAL STAFF (PLS ROUTE)
PO BOX 999, MS K6-48
RICHLAND, WA 99352

PACIFIC NORTHWEST NATIONAL LABORATORY
ATTN: TECHNICAL STAFF (PLS ROUTE)
PO BOX 999, MS K7-34
RICHLAND, WA 99352

PACIFIC NORTHWEST NATIONAL LABORATORY
ATTN: TECHNICAL STAFF (PLS ROUTE)
PO BOX 999, MS K6-40
RICHLAND, WA 99352

PACIFIC NORTHWEST NATIONAL LABORATORY
ATTN: TECHNICAL STAFF (PLS ROUTE)
PO BOX 999, MS K7-22
RICHLAND, WA 99352

PACIFIC NORTHWEST NATIONAL LABORATORY
ATTN: TECHNICAL STAFF (PLS ROUTE)
PO BOX 999, MS K5-72
RICHLAND, WA 99352

PACIFIC NORTHWEST NATIONAL LABORATORY
ATTN: TECHNICAL STAFF (PLS ROUTE)
PO BOX 999, MS K6-84
RICHLAND, WA 99352

PACIFIC NORTHWEST NATIONAL LABORATORY
ATTN: TECHNICAL STAFF (PLS ROUTE)
PO BOX 999, MS K5-12
RICHLAND, WA 99352

FRANK PILOTTE
HQ/AFTAC/TT
1030 S. HIGHWAY A1A
PATRICK AFB, FL 32925-3002

KEITH PRIESTLEY
DEPARTMENT OF EARTH SCIENCES
UNIVERSITY OF CAMBRIDGE
MADINGLEY RISE, MADINGLEY ROAD
CAMBRIDGE, CB3 OEZ UK

JAY PULLI
RADIX SYSTEMS, INC.
6 TAFT COURT
ROCKVILLE, MD 20850

PAUL RICHARDS
COLUMBIA UNIVERSITY
LAMONT-DOHERTY EARTH OBSERVATORY
PALISADES, NY 10964

DAVID RUSSELL
HQ AFTAC/TTR
1030 SOUTH HIGHWAY A1A
PATRICK AFB, FL 32925-3002

CHANDAN SAIKIA
WOOODWARD-CLYDE FEDERAL SERVICES
566 EL DORADO ST., SUITE 100
PASADENA, CA 91101-2560

SANDIA NATIONAL LABORATORY
ATTN: TECHNICAL STAFF (PLS ROUTE)
DEPT. 5704
MS 0979, PO BOX 5800
ALBUQUERQUE, NM 87185-0979

SANDIA NATIONAL LABORATORY
ATTN: TECHNICAL STAFF (PLS ROUTE)
DEPT. 6116
MS 0750, PO BOX 5800
ALBUQUERQUE, NM 87185-0750

SANDIA NATIONAL LABORATORY
ATTN: TECHNICAL STAFF (PLS ROUTE)
DEPT. 5791
MS 0567, PO BOX 5800
ALBUQUERQUE, NM 87185-0567

SANDIA NATIONAL LABORATORY
ATTN: TECHNICAL STAFF (PLS ROUTE)
DEPT. 9311
MS 1159, PO BOX 5800
ALBUQUERQUE, NM 87185-1159

SANDIA NATIONAL LABORATORY
ATTN: TECHNICAL STAFF (PLS ROUTE)
DEPT. 5704
MS 0655, PO BOX 5800
ALBUQUERQUE, NM 87185-0655

SANDIA NATIONAL LABORATORY
ATTN: TECHNICAL STAFF (PLS ROUTE)
DEPT. 5736
MS 0655, PO BOX 5800
ALBUQUERQUE, NM 87185-0655

SANDIA NATIONAL LABORATORY
ATTN: TECHNICAL STAFF (PLS ROUTE)
DEPT. 6116
MS 0750, PO BOX 5800
ALBUQUERQUE, NM 87185-0750

THOMAS SERENO JR.
SCIENCE APPLICATIONS INTERNATIONAL
CORPORATION
10260 CAMPUS POINT DRIVE
SAN DIEGO, CA 92121

4

AVI SHAPIRA
SEISMOLOGY DIVISION
THE INSTITUTE FOR PETROLEUM RESEARCH AND
GEOPHYSICS
P.O.B. 2286, NOLON 58122 ISRAEL

ROBERT SHUMWAY
410 MRAK HALL
DIVISION OF STATISTICS
UNIVERSITY OF CALIFORNIA
DAVIS, CA 95616-8671

DAVID SIMPSON
IRIS
1616 N. FORT MEYER DRIVE
SUITE 1050
ARLINGTON, VA 22209

BRIAN SULLIVAN
BOSTON COLLEGE
INSITUTE FOR SPACE RESEARCH
140 COMMONWEALTH AVENUE
CHESTNUT HILL, MA 02167

NAFI TOKSOZ
EARTH RESOURCES LABORATORY, M.I.T.
42 CARLTON STREET, E34-440
CAMBRIDGE, MA 02142

GREG VAN DER VINK
IRIS
1616 N. FORT MEYER DRIVE
SUITE 1050
ARLINGTON, VA 22209

TERRY WALLACE
UNIVERSITY OF ARIZONA
DEPARTMENT OF GEOSCIENCES
BUILDING #77
TUCSON, AZ 85721

JAMES WHITCOMB
NSF
NSF/ISC OPERATIONS/EAR-785
4201 WILSON BLVD., ROOM785
ARLINGTON, VA 22230

JIAKANG XIE
COLUMBIA UNIVERSITY
LAMONT DOHERTY EARTH OBSERVATORY
ROUTE 9W
PALISADES, NY 10964

OFFICE OF THE SECRETARY OF DEFENSE
DDR&E
WASHINGTON, DC 20330

TACTEC
BATTELLE MEMORIAL INSTITUTE
505 KING AVENUE
COLUMBUS, OH 43201 (FINAL REPORT)

MATTHEW SIBOL
ENSCO, INC.
445 PINEDA COURT
MELBOURNE, FL 32940

JEFFRY STEVENS
MAXWELL TECHNOLOGIES
P.O. BOX 23558
SAN DIEGO, CA 92123

DAVID THOMAS
ISEE
29100 AURORA ROAD
CLEVELAND, OH 44139

LAWRENCE TURNBULL
ACIS
DCI/ACIS
WASHINGTON, DC 20505

FRANK VERNON
UNIVERSITY OF CALIFORNIA, SAN DIEGO
SCRIPPS INSTITUTION OF OCEANOGRAPHY IGPP, 0225
9500 GILMAN DRIVE
LA JOLLA, CA 92093-0225

DANIEL WEILL
NSF
EAR-785
4201 WILSON BLVD., ROOM 785
ARLINGTON, VA 22230

RU SHAN WU
UNIVERSITY OF CALIFORNIA SANTA CRUZ
EARTH SCIENCES DEPT.
1156 HIGH STREET
SANTA CRUZ, CA 95064

JAMES E. ZOLLWEG
BOISE STATE UNIVERSITY
GEOSCIENCES DEPT.
1910 UNIVERSITY DRIVE
BOISE, ID 83725

DEFENSE TECHNICAL INFORMATION CENTER
8725 JOHN J. KINGMAN ROAD
FT BELVOIR, VA 22060-6218 (2 COPIES)

PHILLIPS LABORATORY
ATTN: XPG
29 RANDOLPH ROAD
HANSCOM AFB, MA 01731-3010

PHILLIPS LABORATORY
ATTN: GPE
29 RANDOLPH ROAD
HANSCOM AFB, MA 01731-3010

PHILLIPS LABORATORY
ATTN: TSML
5 WRIGHT STREET
HANSCOM AFB, MA 01731-3004

PHILLIPS LABORATORY
ATTN: PL/SUL
3550 ABERDEEN AVE SE
KIRTLAND, NM 87117-5776 (2 COPIES)